

F.W. Klaiber, T.J. Wipf, J.R. Reid, M.J. Peterson

**Investigation of Two Bridge  
Alternatives for Low Volume Roads  
Volume 2 of 2**

**Concept 2:  
Beam In Slab Bridge**

Sponsored by the  
Iowa Department of Transportation  
Project Development Division and the  
Iowa Highway Research Board

April 1997



**Iowa Department  
of Transportation**

Iowa DOT Project HR-382  
ISU-ERI-Ames-97405

**report**  
FINAL  
**College of  
Engineering  
Iowa State University**

The opinions, findings, and conclusions expressed  
in this publication are those of the authors and not  
necessarily those of the Iowa Department of Transportation

F.W. Klaiber, T.J. Wipf, J.R. Reid, M.J. Peterson

**Investigation of Two Bridge  
Alternatives for Low Volume Roads  
Volume 2 of 2**

**Concept 2:  
Beam In Slab Bridge**

Sponsored by the  
Iowa Department of Transportation  
Project Development Division and the  
Iowa Highway Research Board

Iowa DOT Project HR-382  
ISU-ERI-Ames-97405



**engineering  
research institute**

**iowa state university**

## ABSTRACT

Recent reports have indicated that 23.5 percent of the nation's highway bridges are structurally deficient and 17.7 percent are functionally obsolete. A significant number of these bridges are on the Iowa secondary road system where over 86 percent of the rural bridge management responsibilities are assigned to the counties. Some of the bridges can be strengthened or otherwise rehabilitated, but many more are in need of immediate replacement.

In a recent investigation, HR-365 "Evaluation of Bridge Replacement Alternatives for the County Bridge System," several types of replacement bridges that are currently being used on low volume roads were identified. It was also determined that a large number of counties (69 percent) have the ability and are interested in utilizing their own forces in the design and construct of short span bridges. After reviewing the results from HR-365, the research team developed one "new" bridge replacement concept and a modification of a replacement system currently being used.

Both of these bridge replacement alternatives were investigated in this study, the results of which are presented in two volumes. This volume (Volume 2) presents the results of Concept 2 - Modification of the Beam-in-Slab Bridge, while Concept 1 - Steel Beam Precast Units is presented in Volume 1. Concept 2 involves various laboratory tests of the Beam-in-Slab bridge (BISB) currently being used by Benton County and several other Iowa counties. In this investigation, the behavior and strength of the BISB were determined; a new method of obtaining composite action between the steel beams and concrete was also tested. Since the Concept 2 bridge is primarily intended for use on low-volume roads, the system can be constructed with new or used beams.

In the experimental part of the investigation, there were three types of laboratory tests: push-out tests, service and ultimate load tests of models of the BISB, and composite beam tests utilizing the newly developed shear connection. In addition to the laboratory tests, there was a field test in which an existing BISB was service load tested. An equation was developed for predicting the strength of the shear connection investigated; in addition, a finite element model for analyzing the BISB was also developed.

Push-out tests were completed to determine the strength of the recently developed shear connector. A total of 36 specimens were tested, with variables such as hole diameter, hole spacing, presence of reinforcement, etc. being investigated.

In the model tests of the BISB, two and four beam specimens ( $L = 9,140$  mm (30 ft)) were service load tested for behavior and load distribution data. Upon completion of these tests, both specimens were loaded to failure.

In the composite beam tests, four beams, one with standard shear studs and three using the shear connection developed, were tested. Upon completion of the service load tests, all four beams were loaded to failure. The strength and behavior of the beams with the new shear connection were found to be essentially the same as that of the specimen with standard shear studs.

In this investigation, the existing BISB ( $L = 15,240$  mm (50 ft)) was determined to be extremely stiff in both the longitudinal and transverse directions, deflecting approximately 6 mm (1/4 in.) when subjected to 445 kN (100 kips). To date, Concept 2 has successfully passed all laboratory tests. Prior to implementing a modification to the BISB in the field, a limited amount of laboratory testing remains to be completed.

## TABLE OF CONTENTS

	<u>Page</u>
ABSTRACT .....	iii
List of Figures .....	ix
List of Tables .....	xiii
<b>1. INTRODUCTION AND LITERATURE REVIEW .....</b>	<b>1</b>
1.1 Background .....	1
1.2 Objective and Scope .....	2
1.3 Research Approach .....	3
1.3.1 Push-out Tests .....	3
1.3.2 BISB Laboratory Tests .....	3
1.3.2.1 Two-Beam Specimen .....	3
1.3.2.2 Four-Beam Specimen .....	4
1.3.3 Composite Specimens .....	4
1.3.4 BISB Field Tests .....	4
1.4 Benton County Bridge .....	5
1.5 Literature Review .....	9
1.5.1 Leonhardt, et al. - The Pioneers .....	9
1.5.2 Veldanda, Oguejiofor, and Hosain - Canadian Studies .....	14
1.5.3 Roberts and Heywood - Australian Studies .....	17
<b>2. SPECIMEN DETAILS .....</b>	<b>21</b>
2.1 Push-out Test Specimens .....	21
2.2 BISB Laboratory Specimens .....	25
2.3 Composite Beam Specimens .....	26
2.3.1 Inverted T-Beam .....	26
2.3.2 Imbedded I-Beam .....	30
2.3.3 Standard Composite Beam .....	34
2.4 BISB Field Bridge .....	34

	<u>Page</u>
3. TESTING PROGRAM .....	41
3.1 Push-out Tests .....	41
3.2 BISB Laboratory Tests .....	43
3.2.1 Two-Beam Specimen .....	43
3.2.2 Four-Beam Specimen .....	47
3.3 Composite Beam Tests .....	53
3.3.1 Service Load Tests .....	53
3.3.2 Ultimate Load Tests .....	53
3.4 BISB Field Tests .....	57
4. BEAM-IN-SLAB BRIDGE GRILLAGE ANALYSIS .....	65
4.1 Element Types .....	65
4.1.1 BEAM4 Element .....	65
4.1.2 BEAM44 3-D Tapered Unsymmetric Beam Element .....	65
4.2 Grillage Analogy Model .....	66
5. EXPERIMENTAL AND ANALYTICAL RESULTS .....	73
5.1 Push-out Test Results and Theoretical Analysis .....	73
5.1.1 Experimental Results .....	73
5.1.2 Analysis of Experimental Results and Development of Strength Equation ....	80
5.1.3 Sensitivity Study of Theoretical Strength Equation .....	84
5.2 BISB Laboratory Test Results and Analysis .....	87
5.2.1 Two-Beam Specimen .....	87
5.2.2 Four-Beam Specimen .....	93
5.2.2.1 Experimental Results .....	93
5.2.2.2 Comparison of Experimental and Analytical Results .....	101
5.3 Composite Beam Test Results .....	104
5.4 Field Bridge Test Results and Analysis .....	112
5.4.1 Field Bridge Results .....	112

5.4.2 Comparison of Experimental and Analytical Results .....	124
6. SUMMARY AND CONCLUSIONS .....	131
7. RECOMMENDED RESEARCH .....	135
8. ACKNOWLEDGEMENTS .....	138
9. REFERENCES .....	139

## LIST OF FIGURES

	<u>Page</u>
Fig. 1.1. Beam-in-slab bridge .....	6
Fig. 1.2. Photographs of BISB applications .....	7
Fig. 1.3. BISB abutment details .....	8
Fig. 1.4. Leonhardt's Perfobond Rib Connector .....	10
Fig. 1.5. Internal forces in a composite beam associated with the Perfobond Rib Shear Connector .....	12
Fig. 1.6. Inverted steel T-section with perforbond rib shear connectors .....	19
Fig. 1.7. Roberts and Heywood's shearbox test .....	19
Fig. 2.1. Push-out specimens .....	22
Fig. 2.2. Description of the hole arrangements used in the push-out tests .....	23
Fig. 2.3. Cross section of BISB four-beam specimen .....	27
Fig. 2.4. Composite beam specimen: T-section (Specimen 1) .....	28
Fig. 2.5. T-section fabrication cutting schedule .....	31
Fig. 2.6. Composite beam specimen: Imbedded I-beam (Specimens 2 and 3) .....	32
Fig. 2.7. Composite beam specimen: Welded studs (Specimen 4) .....	35
Fig. 2.8. Description of field bridge .....	37
Fig. 2.9. Photograph of BISB bridge tested .....	39
Fig. 3.1. Location of instrumentation used in the push-out tests .....	42
Fig. 3.2. Loading apparatus used for testing the BISB two-beam specimen .....	44
Fig. 3.3. Instrumentation for the two-beam specimen .....	46
Fig. 3.4. Location of strain gages on four-beam specimen .....	48
Fig. 3.5. Location of strain gaged cross sections on four-beam specimen .....	49
Fig. 3.6. Location of loading points for service level load testing the four-beam specimen ...	50
Fig. 3.7. Locations of load points for ultimate load test of the four-beam specimen .....	52
Fig. 3.8. Location of strain gages on composite beam specimens .....	54
Fig. 3.9. Location of deflection instrumentation in composite beam tests .....	55
Fig. 3.10. Composite beam test setup .....	56



	<u>Page</u>
Fig. 3.11. Location of instrumentation - field bridge .....	58
Fig. 3.12. Wheel configuration and weight distribution of test vehicles .....	60
Fig. 3.13. Location of test vehicles .....	61
Fig. 3.14. Photographs of test vehicles on bridge .....	62
Fig. 4.1. Geometry of BEAM4 element .....	66
Fig. 4.2. Geometry of BEAM44 element .....	66
Fig. 4.3. Basic grillage model of BISB system .....	68
Fig. 4.4. Sensitivity study results for basic parameters .....	70
Fig. 4.5. Sensitivity studies for beam properties .....	72
Fig. 5.1. Load slip curves for various test sequences .....	77
Fig. 5.2. Illustration of equation variables .....	82
Fig. 5.3. Shear strength vs. hole area .....	86
Fig. 5.4. Shear strength vs. area of reinforcing steel through shear hole .....	86
Fig. 5.5. Shear strength vs. area of transverse reinforcement .....	88
Fig. 5.6. Shear strength vs. number of shear holes .....	88
Fig. 5.7. Strain response for two-beam BISB during load testing .....	90
Fig. 5.8. Strain profile for two-beam BISB during load testing .....	91
Fig. 5.9. Average end slip during load testing .....	92
Fig. 5.10. Theoretical and experimental midspan deflection .....	92
Fig. 5.11. Test A1 results: deflections and strains at centerline .....	95
Fig. 5.12. Deflection of beams due to 20 kips load applied at Section 1 .....	96
Fig. 5.13. Deflection of beams due to 20 kips load applied at Section 2 .....	97
Fig. 5.14. Deflection of beams due to 20 kips load applied at Section 3 .....	98
Fig. 5.15. Deflections during BISB ultimate load test .....	99
Fig. 5.16. Strains during ultimate load test .....	100
Fig. 5.17. Comparison of experimental and analytical results for BISB Test A1 .....	102
Fig. 5.18. Comparison of experimental and analytical results for BISB Test C3 .....	103

	<u>Page</u>
Fig. 5.19. Specimen 1 service test results .....	105
Fig. 5.20. Specimen 2 service test results .....	106
Fig. 5.21. Comparison of service test results of Specimens 2 and 3 .....	108
Fig. 5.22. Specimen 3 service test results .....	109
Fig. 5.23. Specimen 4 service test results .....	110
Fig. 5.24. Comparison of the composite beam deflection at the centerline .....	111
Fig. 5.25. Ultimate load deflections .....	113
Fig. 5.26. Deflection and moment fraction data for Test 1 .....	114
Fig. 5.27. Deflection and moment fraction data for Test 2 .....	115
Fig. 5.28. Deflection and moment fraction data for Test 3 .....	116
Fig. 5.29. Deflection and moment fraction data for Test 4 .....	117
Fig. 5.30. Deflection and moment fraction data for Test 5 .....	118
Fig. 5.31. Deflection and moment fraction data for Test 6 .....	119
Fig. 5.32. Deflection and moment fraction data for Test 7 .....	120
Fig. 5.33. Deflection and moment fraction data for Test 8 .....	121
Fig. 5.34. Symmetry determination on field bridge .....	123
Fig. 5.35. Field bridge grillage analogy .....	125
Fig. 5.36. Comparison of theoretical and experimental deflections at midspan: Test 1 .....	126
Fig. 5.37. Comparison of theoretical and experimental deflections at midspan: Test 2 .....	126
Fig. 5.38. Comparison of theoretical and experimental deflections at midspan: Test 3 .....	127
Fig. 5.39. Comparison of theoretical and experimental deflections at midspan: Test 4 .....	127
Fig. 5.40. Comparison of theoretical and experimental deflections at midspan: Test 5 .....	128
Fig. 5.41. Comparison of theoretical and experimental deflections at midspan: Test 7 .....	128
Fig. 5.42. Comparison of theoretical and experimental deflections at midspan: Test 8 .....	129
Fig. 5.43 Comparison of theoretical and experimental moment fractions at midspan:	
Test 2, truck at midspan .....	129
Fig. 5.44 Comparison of theoretical and experimental moment fractions at midspan:	
Test 7, truck at midspan .....	130

**LIST OF TABLES**

	<b><u>Page</u></b>
Table 2.1. Beam spacing in field bridge .....	38
Table 2.2. Field bridge abutment measurements .....	38
Table 3.1. Test designations for BISB field tests .....	63
Table 5.1. Push-out test results .....	75
Table 5.2. Theoretical strengths vs. experimental strengths .....	84
Table 5.3. Results of sensitivity investigation .....	85

## **1. INTRODUCTION AND LITERATURE REVIEW**

### **1.1 Background**

Recent reports have indicated that 23.5 percent of the nation's highway bridges are structurally deficient and 17.7 percent are functionally obsolete (1). Unfortunately, a significant number of these bridges are on the Iowa county road system. According to a 1989 report (2), 86.4 percent of rural bridge maintenance responsibilities are assigned to the county. Some of the bridges can be strengthened and rehabilitated, but many are in need of replacement. A recent questionnaire sent to all of the county engineers in Iowa asked about the need of and interest in a study to review and evaluate replacement bridges. Over 76 percent of the respondents replied that such a study would be beneficial or very beneficial.

Such a study was recently completed in research project: HR-365 "Evaluation of Bridge Replacement Alternatives for the County Bridge System" (3). In this investigation, several replacement bridges currently being used on the county road system in Iowa and surrounding states were identified and evaluated. This investigation (HR-365) documented several unique replacement bridge types that are currently being used on low volume roads. It also determined that a large number of counties (69 percent) have the capability of and are interested in using their own forces to design and construct short span bridges, provided the construction procedures are relatively simple. To minimize the initial cost of replacement and subsequent maintenance costs, it is important to select the right type of replacement bridge for a particular site. Cost can obviously be minimized by selecting bridges that can be designed and constructed by local work forces.

From the evaluation of the questionnaire responses from the Iowa counties and investigation of the various bridge replacement concepts currently in use, the research team developed one "new" bridge replacement concept and a modification of a replacement system currently being used. To determine if there was interest in these two concepts, the researchers contacted several county and city engineers to obtain their input on the two bridge concepts. Each county engineer contacted thought both concepts had

merit, and would be interested in participating in a demonstration project involving the replacement systems if the research went that far.

For discussion purposes the “new” idea, steel beam precast units, will be identified as Concept 1. The portion of the project that involves the modification of a current replacement system, beam-in-slab bridge (BISB), will be referenced as Concept 2. The results from this investigation have been published in two volumes. Concept 1 is presented in Volume 1 while Concept 2 is presented in this volume (Volume 2).

Concept 2 involved the testing of the BISB system and modifications to it to obtain strength and behavior data. The BISB system is a combination of steel beams and unreinforced concrete; concrete is placed between the closely spaced steel beams with the top surface at the same elevation as the top flanges of the steel beams. Modifications of the system involved removing the top flanges of the steel beams and “tension” concrete. With these modifications, the riding surface should be improved and the dead load reduced, which should permit the system to span longer distances.

## **1.2 Objective and Scope**

In this project, research was directed at evaluating the best method for developing shear resistance for composite action between the steel beams and concrete deck typically used in bridges. The intent of these tests was to establish an effective modification of the current BISB system. Push-out tests (11 series) were performed to determine the best possible shear connection in terms of load carrying capacity and ability to maintain such loads at high deformations. Tests were also performed on a two-beam specimen and a four-beam specimen, which simulated the BISB system to determine the strength and behavioral characteristics of the system under service and ultimate loads. A field test was also performed on a BISB in Benton County to obtain strength and behavior data from an actual bridge. Finally, tests were performed on several different composite beam specimens to determine an effective modification of the steel beams currently used in the BISB system.

### 1.3 Research Approach

This study is comprised of four distinct phases: push-out tests, laboratory BISB specimen tests, composite beam tests, and BISB field tests. Following is a summary of the tasks performed in each phase.

#### 1.3.1 Push-out Tests

Based upon the research initially performed by Leonhardt et al. (4), eleven series of push-out specimens were tested to determine the load carrying capacity and the ability of the connection to maintain that load over large displacements. Typically, in composite construction, some type of shear connection on the top flange of the beam is used to ensure the load is properly transferred from the concrete to the steel. In this investigation, holes were drilled in the steel web (in beams without a top flange) to provide the necessary shear connection; this type of shear connection will be referred to as an alternate shear connector (ASC) in this report. Five variables were evaluated to determine the best arrangement of those holes in the ASC:

- Size of holes
- Spacing of holes
- Alignment of holes
- Inclusion of reinforcing steel in holes
- Effects of “sloppy” craftsmanship

The results from these tests were used in designing the ASC, which was in turn used in the composite beam tests that were subsequently performed.

#### 1.3.2 BISB Laboratory Tests

##### 1.3.2.1 Two-Beam Specimen

Tests were performed on a two-beam section modeled after the BISB to obtain data on its strength and behavior. These tests were completed to determine the following:

- Load carrying capacity
- Reserve strength after overloading
- Deflections, strains, and slip data during service and ultimate loading

#### 1.3.2.2 *Four-Beam Specimen*

Tests were performed also on a four-beam model of the BISB. The bridge model was instrumented so that strains and deflections could be determined at critical locations. The tests were undertaken to determine the following:

- Load distribution in the system
- Behavior under service loads
- Load carrying capacity
- Reserve strength after overloading
- Strains, slip data, and deflections during service and ultimate loading

#### 1.3.3 Composite Specimens

The ASC developed and tested in the push-out tests was used in composite beam tests. Four composite beams were tested; one had standard shear studs, and the other three had different variations of the ASC. The composite beams were instrumented so that strains and deflections could be determined at critical locations. Tests on the composite beams were completed to determine the amount of composite action, the behavior under service loads, the ultimate strength, and the type of failure that would occur when overloaded.

#### 1.3.4 BISB Field Tests

To obtain strength and behavior data from an existing bridge, a BISB in Benton County was instrumented and tested. The BISB tested was 15,240 mm (50 ft) in length, had W12 sections, and had no guardrails or gravel cover. Stream conditions, height above stream, and road conditions were considered in the selection of the test bridge.

Two standard tandem-axle county trucks, with approximate total weights of 222.5 kN (50 kips) each, were used in the testing of the bridge. The trucks were positioned at critical locations on the bridge to produce maximum strains and deflections. These data were then compared to theoretical data to determine the amount of composite action and load distribution in the bridge.

## 1.4 Benton County Bridge

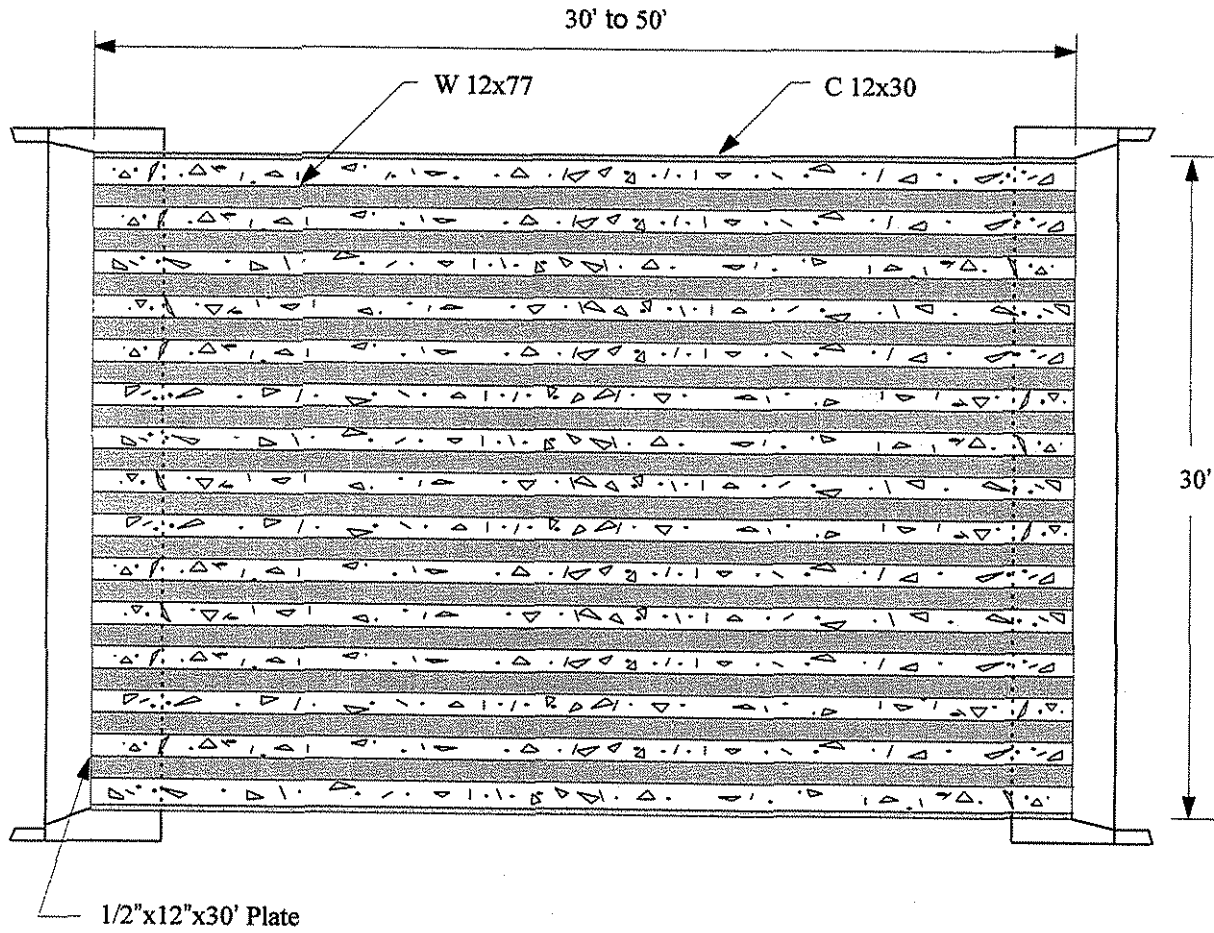
The BISB is a bridge system (see Fig. 1.1) consisting of a series of W shape steel beams generally spaced at 610 mm (2 ft). These structures are used for spans between 6,100 and 15,200 mm (20 and 50 ft). In general, this system is used on low volume roads. When it is used as a low water stream crossing (see Fig. 1.2a), no guardrails are used. At sites where there are long distances from the bridge deck to the stream, guardrails are added (see Fig. 1.2b).

Typically, nine steel piles are driven on 1,220 mm (4 ft) centers in each face of the two bridge abutments. As shown in Fig. 1.3a, wing walls of the desired height are connected with reinforcement to each of the abutments. Dowels (see Fig. 1.3b) are provided for connection of the superstructure to the abutment.

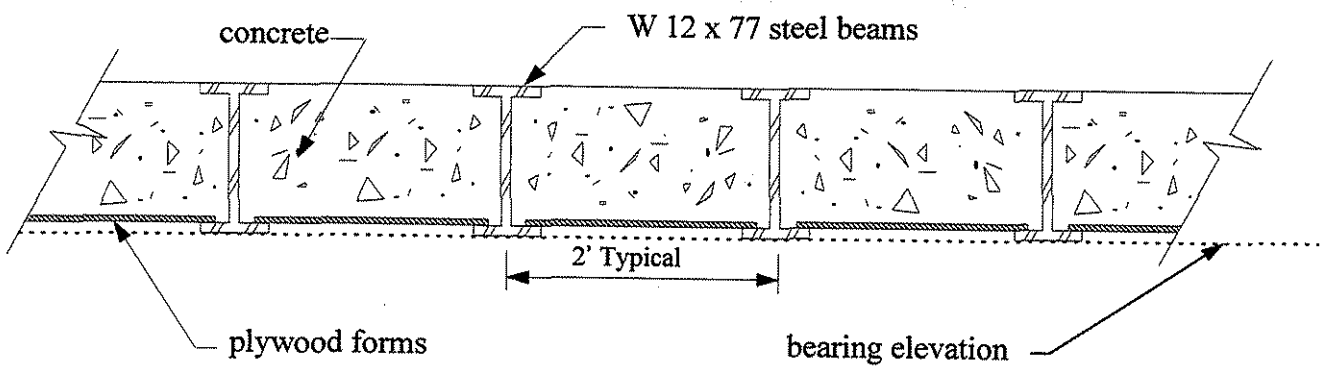
The superstructure consists of a series of W sections (usually W 12X79) positioned adjacent to each other on 610 mm (2 ft) centers. The exterior beam is either a channel section (generally C12X30) of the same height as the W sections, or another W section. Plywood 16 mm or 19 mm (5/8 in. or 3/4 in.) thick is then placed between the adjacent beams. The plywood is cut to a width of 460 mm (18 in.) so that when concrete is placed, it is in contact with the top surface of the bottom flange. Therefore, even after the formwork has deteriorated, there will still be bearing between the concrete and steel (see Fig. 1.1b). To ensure no movement of the beams during the placement of the concrete, 6 mm (1/4 in.) steel straps are welded across the bottom of the flanges at third points (see Fig. 1.3b). Concrete is poured flush with the top flange of the beams. Note, there is no reinforcement in the concrete. Guardrails may be added by welding posts (MC 8X22.8) to the exterior channel sections.

In general, as the BISB span length decreases, the cost per square ft. increases. In 1993, a low water stream crossing, spanning 10,400 mm (34 ft) with a width of 9,150 mm (30 ft), was constructed in Blackhawk County at a cost of \$35 per square ft. This cost included guardrails, steel, labor, and equipment rental. Similarly, a 7,600 mm (25 ft) span bridge without guardrail had a unit cost of \$35 per square ft, a 6,400 mm (21 ft) span cost \$42.50 per square ft, and a 12,200 mm (40 ft) bridge was estimated at \$32 per square ft.





a. Plan view



b. Cross section

Fig. 1.1. Beam-in-slab bridge.

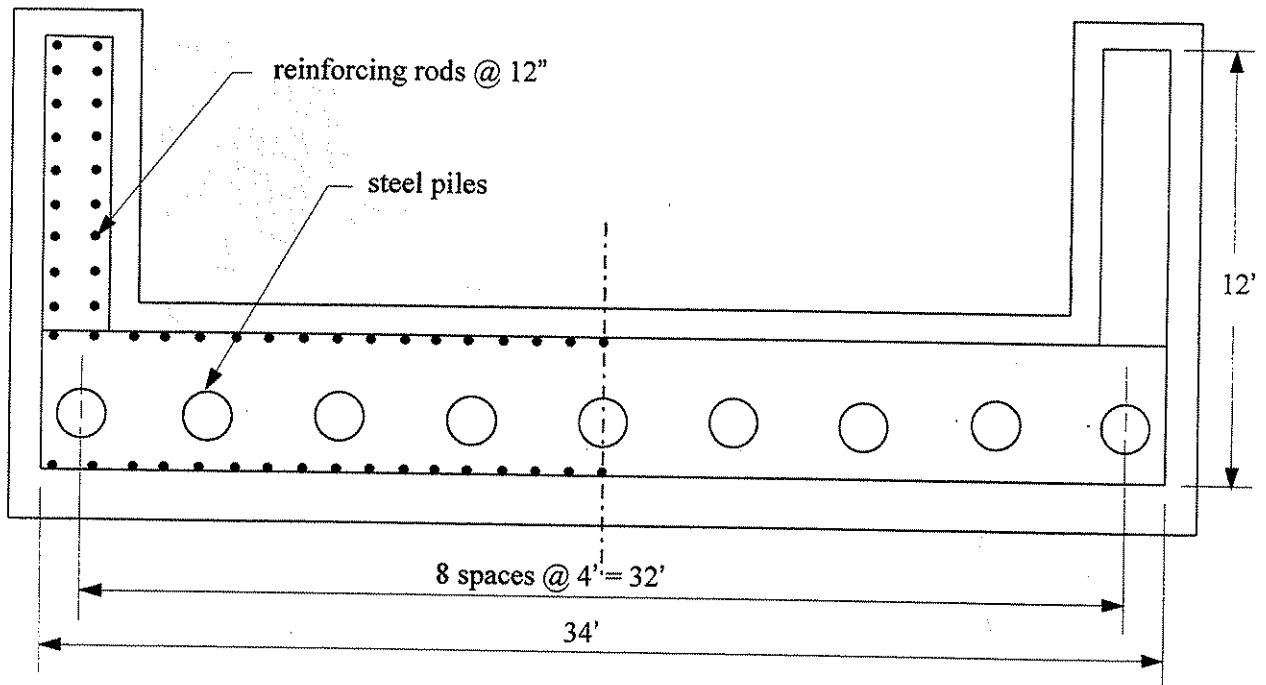


a. Low water stream crossing--no guardrails

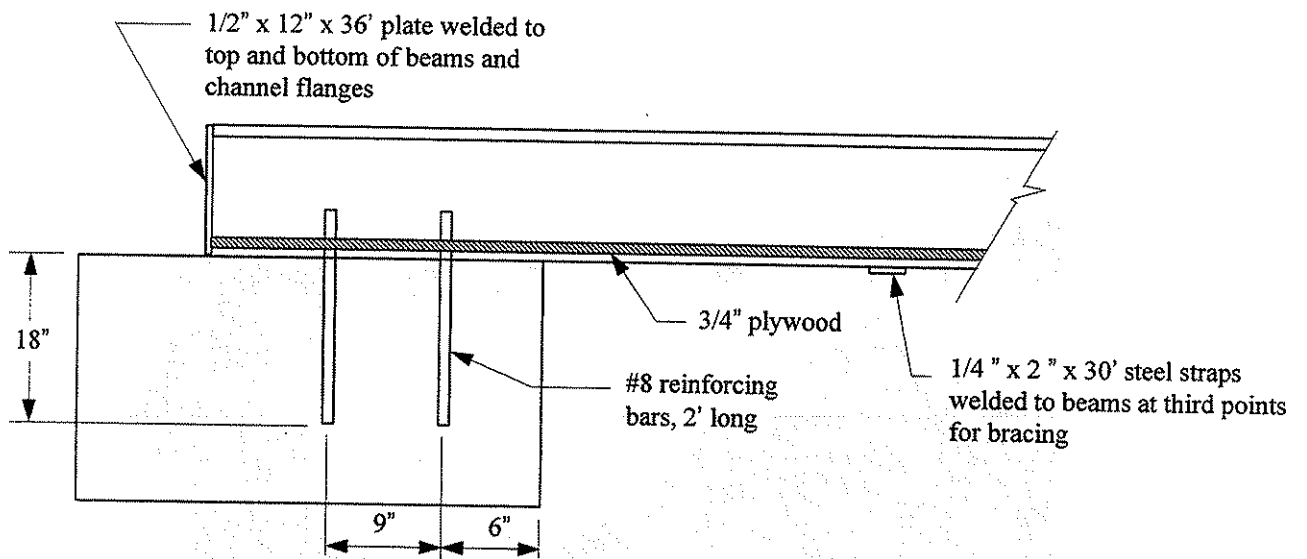


b. Bridge application--with guardrails

Fig. 1.2. Photographs of BISB applications.



a. Plan view of abutment



b. Connection of superstructure to abutment

Fig. 1.3. BISB abutment details.

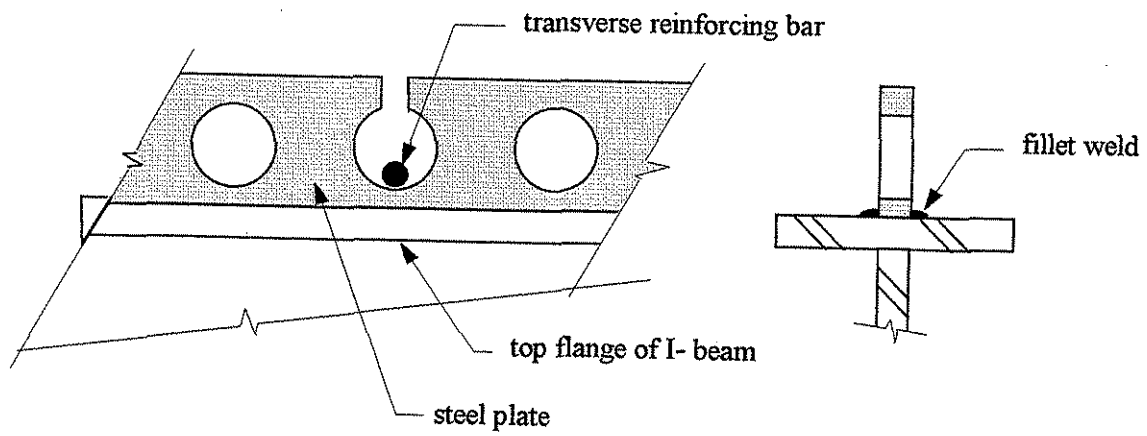
## 1.5 Literature Review

To the authors' knowledge, the BISB is unique to Iowa. Although several literature searches (Transportation Research Information Service through the Iowa Department of Transportation, Geodex System in the ISU Bridge Engineering Center Library, and several computerized literature searches through the ISU Library) were made, no information was found on the BISB. Literature review in this investigation focused on a new means of obtaining shear connection between concrete and steel, known as the Perfobond Rib Connector. Research has been performed on the Perfobond Rib Connector in West Germany, Australia, and Canada; however, the literature search uncovered no research on this type of connector in the United States. In the following sections, research on this connection undertaken in these three countries is briefly summarized.

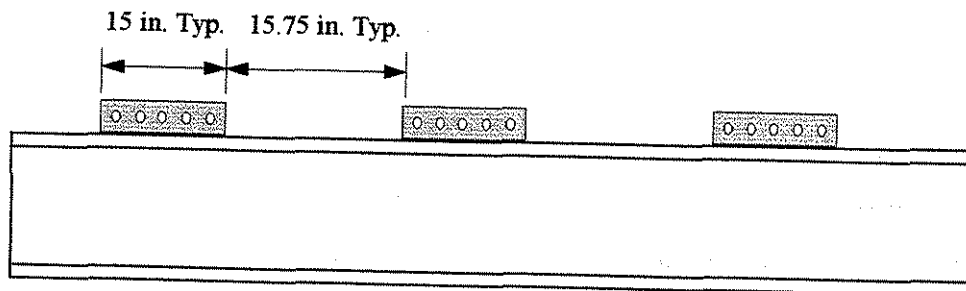
### 1.5.1 Leonhardt et al. - The Pioneers

Most composite bridges utilize shear studs as the mechanism for transferring shear from the concrete to the steel beams. Research over the past 30 years has determined that over time, due to large local pressures at the foot of the stud, loosening may occur. This may lead to progressive slippage, resulting in the stresses moving upward from the foot of the stud. This in turn increases the flexural stress in the stud, which may result in a flexural failure of the stud. The progressive slippage that starts this cycle is often the result of fatigue problems. Thus, a shear connector that will be virtually slip-free is needed, eliminating the possibility for fatigue problems, and involving only elastic deformations under service loading conditions.

In hopes of overcoming these potential fatigue problems in designing the Third Caroni Bridge in Venezuela, the consulting firm of Leonhardt, Andrea, and Partners utilized a new type of shear connector, the Perfobond Rib (see Fig. 1.4). The Perfobond Rib is a flat rectangular steel plate perforated with a series of holes. The rib is then welded onto the top flange of a steel beam. The holes are spaced closely, and the diameter of the holes is greater than the maximum diameter of the coarse aggregate used in the concrete. This allows the aggregate to penetrate the holes and form a series of



a. Perfobond Rib detail



b. Perfobond Rib placement on steel beam

Figure 1.4. Leonhardt's Perfobond Rib Connector.

concrete dowels which act in shear. Steel reinforcement may or may not be included in the holes depending on the required strength.

With the Perfobond Rib Connector, three types of failure were noted by Leonhardt et al. There may be a shearing of the steel strip between the Perfobond holes, a bearing failure of the concrete dowels within the holes, or a shearing failure of the concrete dowels themselves. Perfobond Ribs are designed to ensure that the concrete dowels fail in shear. Designating a minimum hole spacing prevents shearing of the steel; specifying a minimum thickness of steel and minimum amount of transverse reinforcement ensures the confinement of the concrete, thus preventing a bearing failure. The transverse reinforcement is needed to confine the concrete around the rib and to ensure that the concrete in the hole is confined in three dimensions. A strut-tie analogy, shown in Fig. 1.5, was later used by Roberts and Heywood (5) to explain how the transverse reinforcement confines the concrete in three dimensions. Without the transverse reinforcement, the concrete in the holes would tend to "pop out" at relatively low loads. Transverse reinforcement creates a tensile force that confines the concrete in the holes, thereby preventing "pop out" failures.

Thus, with proper transverse reinforcement, spacing of the holes, and rib thickness, stresses in the dowels are below the elastic limit, and a rigid, generally slip-free connection is maintained throughout service level conditions. With increased loading, the concrete dowel will incur greater shearing stresses, until it fails in shear along the steel-concrete interface; however, a significant amount of strength will be maintained due to high levels of friction between the concrete and steel. Failures are therefore gradual, and in most situations are noticed and can most likely be repaired before severe damage or failure occurs.

Leonhardt et al. performed a series of three push-out tests, including static and dynamic loading. Results from these tests led Leonhardt and his colleagues to conclude the following:

- Low amounts of flexible plastic slip occur between the concrete and steel during static loading.

- There is practically no increase in slip resulting from applying dynamic loading rather than static loading.
- After shear failure of the concrete dowels occurred, there was no sudden decrease in load.
- The most efficient combination of variables tested included holes 35 mm (1.4 in.) in diameter, on 50 mm (2 in.) centers, with a plate thickness of 12 mm (0.5 in.).

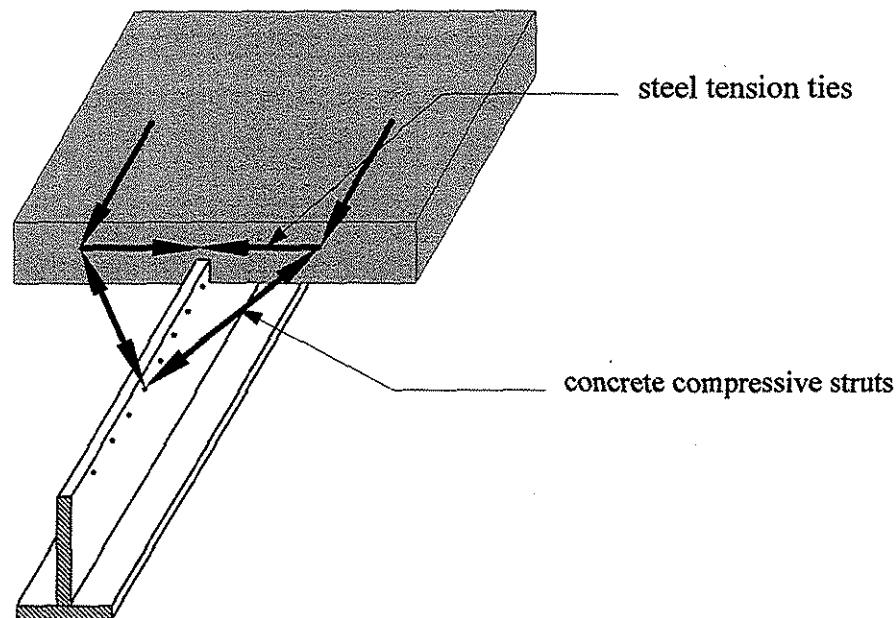


Fig. 1.5. Internal forces in a composite beam associated with the Perfobond Rib Shear Connector.

The Perfobond Ribs performed as expected; there was virtually no deformation under static or service loading, no fatigue problems due to dynamic loading, and after failure, the load was adequately maintained. Based on the test results, design equations were developed to determine the hole size, spacing, thickness, and amount of transverse reinforcement necessary for adequate strength.

As previously noted, three potential failure modes were determined by Leonhardt, et. al.; details on these three follow. Note that the original equations utilized concrete cube strength; the following equations were modified to convert the cubic concrete strength to the more conventional cylinder strength. In addition to the three equations for

determining the ultimate shear,  $V_u$ , associated with the three potential types of failure, an equation was developed for determining the amount of reinforcing steel required to insure the concrete inside the hole is confined in three dimensions.

1. Failure of the concrete dowels

$$V_u = 2 \times \frac{\pi D^2}{4} \times 1.625 f_c' \quad (1.1)$$

where:

$V_u$  = ultimate shear strength for one dowel with two shear planes, kN.

$D$  = hole diameter, mm.

$f_c'$  = concrete cylinder strength, kPa.

2. Bearing failure of the concrete dowels in the holes

$$V_u = D \times t \times 10.71 f_c' \quad (1.2)$$

where:

$t$  = thickness of the steel plate, mm.

3. Shearing of the steel strip between the holes

$$V_u = A_s \times \frac{f_{sy}}{\sqrt{3}} \times \pi \quad (1.3)$$

where:

$A_s$  = area of steel in between adjacent holes,  $\text{mm}^2$ .

$f_{sy}$  = yield stress of the steel plate, kPa.

4. Transverse reinforcing requirements

$$A_{st} \geq \frac{.56 V_u}{f_{sy}} \quad (1.4)$$

where:

$A_{st}$  = Area of transverse steel required per hole,  $\text{mm}^2$ .

As previously noted, the desired failure mode is shearing of the concrete dowels; therefore, Eqn. 1.1 is the equation of most interest. The 'two' in Eqn. 1.1 is due to two shearing planes, one on each side of the dowel. The area of the hole is then multiplied,



along with a factor, times the concrete strength. This factor in the paper by Leonhardt et al. (4) (based on laboratory tests) was 1.3; however, the 1.625 takes into account the conversion from cubic strength to cylinder strength. It must be noted that this design equation is valid only for a steel plate thickness of 12 mm (0.5 in.). Likewise, the equation is based on pushout tests utilizing only 35 and 40 mm (1.4 and 1.6 in.) holes on 50 mm (2 in.) centers. Furthermore, the equation fails to incorporate the friction or cohesion between the concrete and the steel plate. Therefore, this design equation is limited in its application, and cannot be used for significantly different hole spacings and plate thicknesses.

#### 1.5.2 Veldanda, Oguejiofor, and Hosain - Canadian Studies

Although Leonhardt's research was completed in 1987, additional research was not performed until the early 1990's. At that time, researchers at the University of Saskatchewan began a comprehensive, three phase research program to determine the feasibility of using the Perfobond Rib Connectors in composite floor systems. Preliminary investigation by Antunes (6) involved the testing of eight push-out specimens, and resulted in the recommendation that the height of the Perfobond Rib Connectors be maximized to obtain the maximum load carrying capacity.

From this preliminary data, Veldanda and Hosain (7) performed a series of 56 push-out tests on various types of Perfobond Ribs. These tests resulted in the following observations:

- Failure was triggered by the longitudinal splitting of the concrete slab, followed by the crushing of concrete in front of the Perfobond Rib.
- A considerable amount of load was retained over a large slip after the maximum load was attained.
- After failure of the dowels and crushing of the concrete, friction between the cracked concrete surfaces continued to provide shear resistance.
- The capacity of one Perfobond hole, 35 mm (1.4 in.) diameter, is equivalent to approximately five 16 mm x 75 mm (0.6 in. x 3 in.) studs.

- An appreciable improvement in the shear capacity of the connection was observed with the addition of steel reinforcement through the Perfobond Rib holes (approximately, a 50% increase in strength).
- The Perfobond Rib Connectors exhibited greater stiffness under service loads than conventional headed studs.
- A significant portion of the ultimate shear resistance of a Perfobond Rib Connector is provided by the concrete dowels.
- "Shallow" Perfobond Rib Connectors ( $< 60$  mm (2.35 in.) in height) are relatively ineffective.
- Perfobond Rib Connectors can be effectively used in composite beams with or without ribbed decks placed parallel to the steel beams.

Phase two of this project involved the verification of the findings from the push-out tests. Oguejiofor and Hosain (8) tested six full-sized composite beams. Three of the specimens had headed studs, whereas the other three had Perfobond Rib Connectors. In addition to verifying the push-out test results, the influence of the slab and deck on the performance of the beams was determined. The span length was held constant, while the concrete slab width and deck type were varied. Although reinforcing bars were used in many of the push-out tests, the full size tests utilized only the Perfobond Rib Connectors. Results of the investigation follow:

- The failure mode observed was longitudinal splitting of the concrete, followed by concrete crushing in front of the Perfobond Rib Connectors.
- More Perfobond Rib Connectors of smaller size result in a delay of the concrete crushing and a higher ultimate load.
- All specimens showed excellent ductile behavior.
- The predicted ultimate strength based on push-out tests compared reasonably well with the experimental values.

The overall conclusion from these papers was that the Perfobond Rib Connector was a viable alternative to the headed studs currently used in composite bridge

construction. Subsequently, the final phase of the study was to investigate the properties of the Perfobond Rib Connector to establish design guidelines for calculating its capacity (9). This involved the testing of 42 push-out specimens with variances in reinforcing, positioning of the Perfobond holes, number of Perfobond holes, and concrete strength. From these results, an empirical design equation was developed incorporating all the pertinent terms relating to the strength of the connection. Results of the extensive push-out tests were as follows:

- Failure was initiated by longitudinal splitting of the concrete slab while the Perfobond Rib Connectors and weld metal remained completely intact.
- Failure occurred in both slabs of the specimens with reinforcing bars.
- An increase in strength was noted for an increase in hole spacing up to approximately two times the hole size diameter.
- Four holes within a 375 mm (14.75 in) length did not perform as well as three holes within the length. This is likely due to the overlapping of the stress fields as the hole spacing decreases.

From these observations, and from a base equation presented by Davies in 1969 (10) developed through studying the shear capacity of a stud connector with a similar failure mechanism, an empirical relationship was developed using the shear area of the concrete, the area of transverse reinforcement, and the Perfobond hole area.

The design equation (Eqn. 1.5) presented by Oguejiofor and Hosain is based on an application for beams using 375 mm (14.75 in.) long strips. End bearing of the steel strip on the concrete thus occurred. Also, as is typical of building applications, a lighter transverse reinforcing was used as compared to Leonhardt, et. al.

$$V_u = 0.6348A_{cc}\sqrt{f'_c} + 1.1673A_{tr}f_y + 1.6396A_{hs}\sqrt{f'_c} \quad (1.5)$$

Where:

$V_u$  = shear capacity per Perfobond Rib Connector, kN.

$A_{cc}$  = area of the concrete in the plane of the connector, mm<sup>2</sup>.

$A_{rt}$  = area of transverse reinforcement,  $\text{mm}^2$ .

$f_y$  = yield strength of transverse reinforcement, kPa.

$A_{hs}$  = total area of the dowels in shear,  $\text{mm}^2$ .

$f'_c$  = concrete compressive cylinder strength, kPa.

The first term relates to the splitting of the concrete upon failure. The second term corresponds to the degree of confinement provided by the transverse reinforcement, and the last term denotes the shear strength of the actual concrete dowel. Due to the difference in transverse reinforcement used, the failure modes differed, which explains why Leonhardt, et. al. used the concrete strength while Oguejiofor and Hosain used the square root of the concrete strength.

To verify the applicability of the empirical relationship to full size beams, five full size composite beams were also tested. Earlier research has determined that, in general, results from push-out specimens are conservative compared to those obtained from beam tests. Slutter and Driscoll (11) attributed the difference to the eccentricity of loading that often occurs in push-out specimen. In addition, a greater amount of reinforcement is required for the push-out specimens to obtain similar ultimate strength of connections than would be required in a beam. Whatever the case, it has been shown many times that the results from a push-out test can be used as a conservative estimate of the results of a similar beam test. Therefore, by comparing the empirical relationship derived from the push-out results to the data from the beam tests, the empirical relationship can be verified. Results of that comparison yielded values generally 5%-10% lower than predicted values; thus, the empirical relationship was assumed to be an accurate strength estimate for composite beams.

### 1.5.3 Roberts and Heywood - Australian Studies

Around the same time that researchers at the University of Saskatchewan began investigating Perfobond Rib Connectors, researchers at the Queensland University of Technology initiated a similar program to evaluate the use of Perfobond Rib Connectors in bridges. However, Roberts and Heywood (12) took the existing research to a new

level with the idea of removing the top flange of the beam and drilling the holes directly into the web, creating an inverted steel T-section as shown in Fig. 1.6.

The main purpose of the top flange when the Perfobond Rib Connection is used is to provide an area on which to weld the steel plate. In terms of strength, the top flange contributes very little to the composite section due to its close proximity to the neutral axis. The removal of the top flange not only saves money in material costs, but also decreases the overall dead weight of the structure, thus allowing the system to resist larger design moments. With this in mind, Roberts and Heywood performed a series of push-out tests to determine the behavior of the Perfobond Rib Connectors without a top flange. Conclusions from their tests follow:

- The Perfobond Rib Connectors remain functional without the top flange. The initial stiffness is similar; however, there is some reduction in the ultimate load due to the confining of the concrete around the Perfobond strip by the top flange.
- Generally, as holes are spaced closer, the load decreases.
- Equations developed by Leonhardt et al., and Oguejiofor and Hosain do not adequately consider the effect of friction between the steel plate and concrete.

To determine the extent to which friction between the steel plate and the concrete contributed to the strength of the shear connection, Roberts and Heywood developed a shear box test shown in Fig. 1.7. The 12 mm (0.5 in.) thick steel plates which contain holes were subjected to a confining force, and then sheared along one interface between the plate and concrete. Sixty specimens were tested using varying hole diameter and the confining force. Results from these tests indicated that there was a cohesion effect caused by the bond between the concrete and steel plate. This cohesion effect is included in the design equation developed by Roberts and Heywood. The following equation is only valid for hole sizes between 30 and 40 mm (1.2 and 1.6 in.) at any spacing.

$$V_u = \sqrt{f'_c} [ A_p (0.046 + 0.15\sigma_n) + A_h \{ (2.1 - 0.00055 A_h) + (-0.079 + 0.00029 A_h) \sigma_n \} ] \quad (1.6)$$

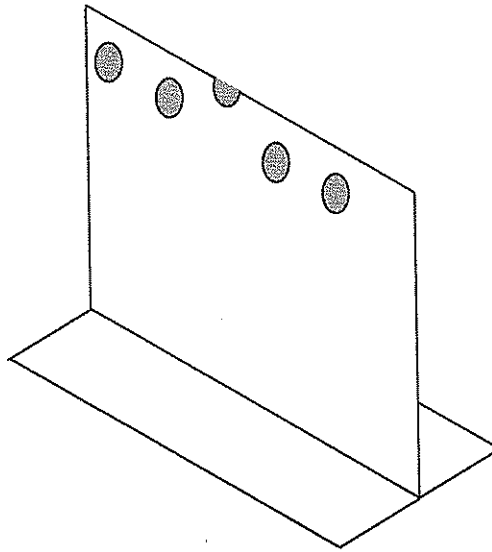


Fig. 1.6. Inverted steel T-section with perfobond rib shear connectors.

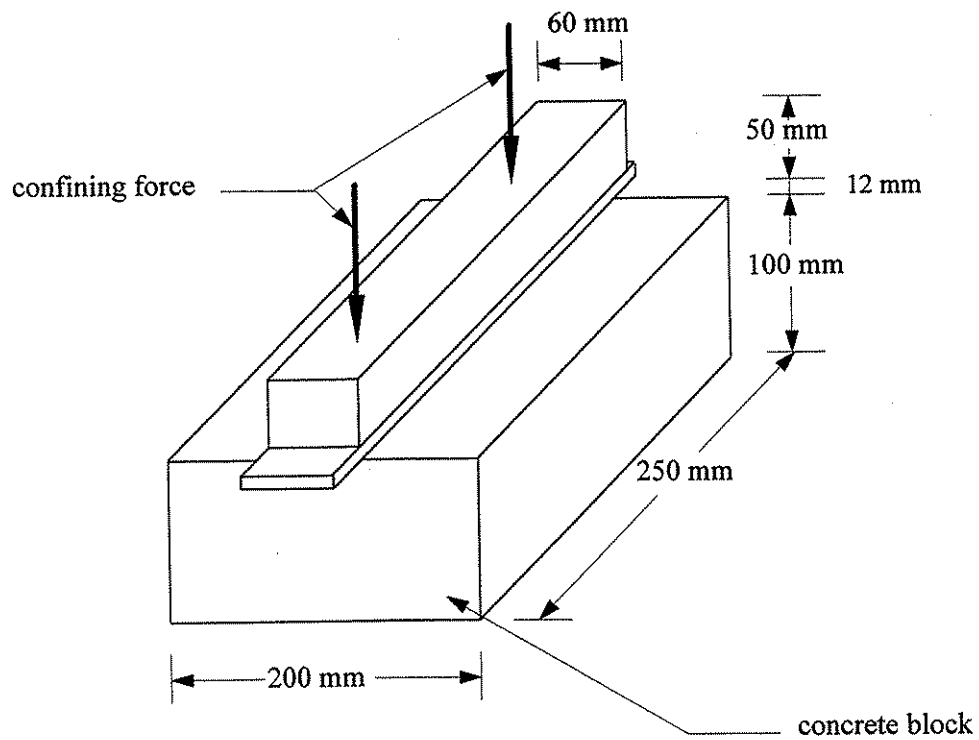


Fig. 1.7. Roberts and Heywood's shearbox test.

Where:

$V_u$  = Shear force per shear plane, N.

$A_h$  = the hole area, mm.

$A_p$  = the plate area in contact with the concrete less the hole area, mm.

$\sigma_n$  = the stress normal to the plate, MPa.

$f'_c$  = the concrete strength, MPa.

For determining the stress normal to the plate ( $\sigma_n$ ), strain gages were placed on the transverse reinforcement, and the average strain was measured. This average strain was used to calculate the stress normal to the connector, which is in turn used in the above equation to calculate failure loads.

In all applications, the shearbox equation slightly underestimated the failure load. Thus, if the stress normal to the plate ( $\sigma_n$ ) is a known variable, then this equation appears to be accurate. However, in the design of a given structure, this stress will not be known; thus, the hole area ( $A_h$ ) and the contact area ( $A_p$ ) can not be determined using this equation. Therefore, an equation is needed that can accurately determine the effect of friction and cohesion based upon the dimensions of the steel plate and amount of transverse reinforcement present.

In addition to push-out tests, a full-scale bridge was designed and constructed with one section utilizing the inverted steel T-section with Perfobond holes. The bridge was subjected to 500,000 cycles of loading equivalent to a T44 design truck plus impact (AUSTROADS requirements). In addition, an ultimate load was applied to the slab to investigate the transfer of load from the slab to the web of the T-section. There were no measurable signs of deterioration during the fatigue testing, and no relative displacement between the slab and T-section during the ultimate load test. Thus, the conclusion was made that this type of design could be used as an economical alternative to existing prestressed concrete designs.

## 2. SPECIMEN DETAILS

### 2.1 Push-out Test Specimens

Dimensions of the push-out tests are presented in Fig 2.1. Each specimen consisted of a stiffened steel plate 9.5 mm (3/8 in.) x 510 mm (20 in.) x 380 mm (15 in.) partially encased in two concrete slabs 210 mm (8 1/4 in.) x 530 mm (21 in.) x 510 mm (20 in.). The plate thickness was chosen to simulate the smallest web thickness that may be encountered in the field. The contact area in each slab (430 mm (17 in.) x 64 mm (2 1/2 in.)) between the concrete and steel was held constant, and was based on the configuration of Series 1 shown in Fig. 2.2. Load was applied to a steel plate welded to the stiffened plate as was previously described, which in turn transferred the load to the concrete slabs via the shear connection.

A total of 36 push-out specimens (11 series), were tested with variables as follows:

- Size of shear holes.
- Spacing of shear holes.
- Alignment of shear holes.
- Inclusion of steel reinforcement through a shear hole.
- Size of steel reinforcement through shear hole.
- Effects of "sloppy" craftsmanship.

A sketch of the hole arrangement used in each of the 11 series is presented in Fig.

2.2. Series 7 tests, which involved a steel plate without holes, are not illustrated; this series provided a basis for determining the frictional effect between the steel plate and the concrete. To determine the effects of each of the test variables, series were compared as follows:

- Series 1 vs. Series 2 - to determine the effect of hole spacing.
- Series 2 vs. Series 3 - to determine the effect of hole size.
- Series 1 vs. Series 10, Series 3 vs. Series 6, Series 7 vs. Series 11 - to determine the effect of including reinforcement through a shear hole.



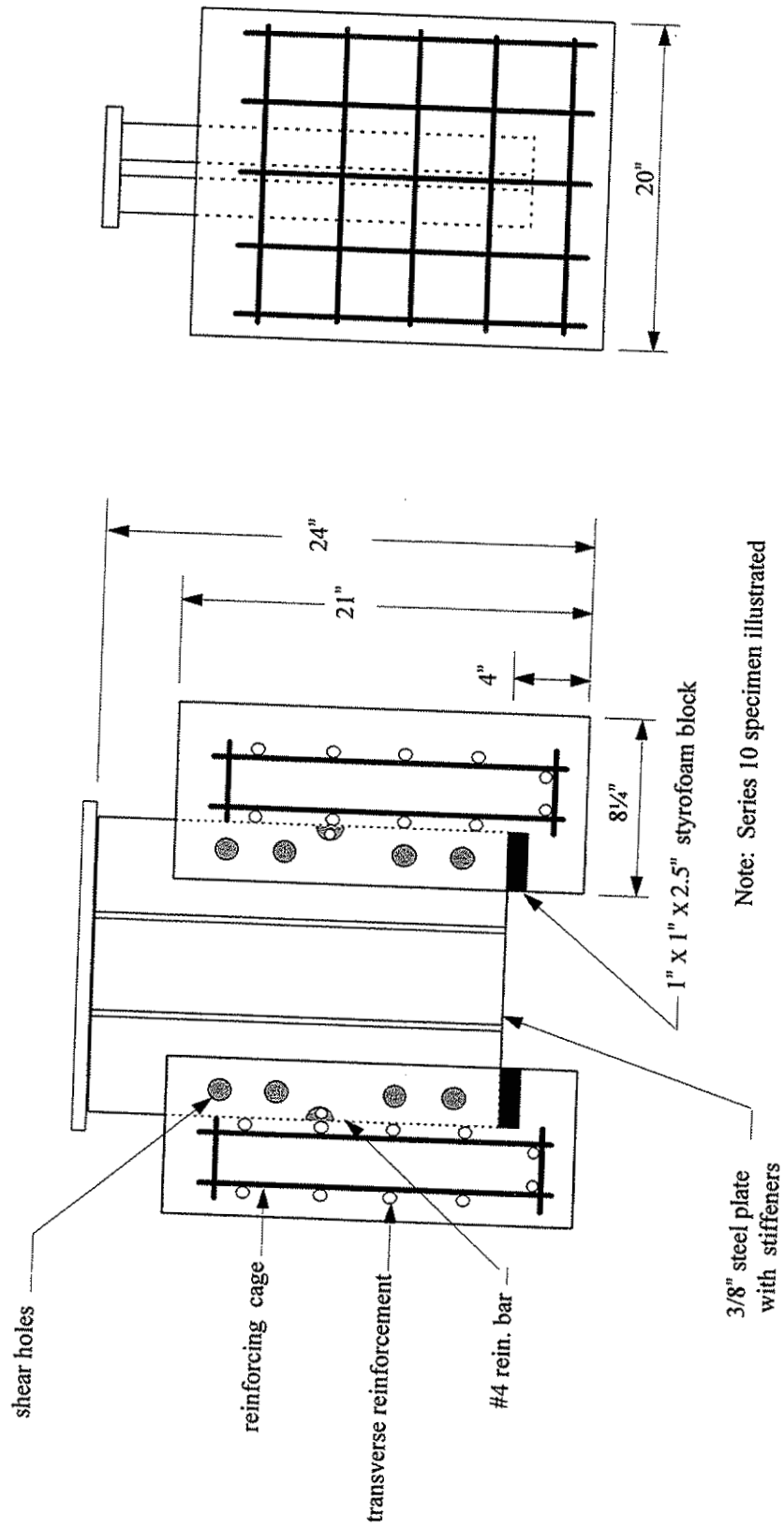
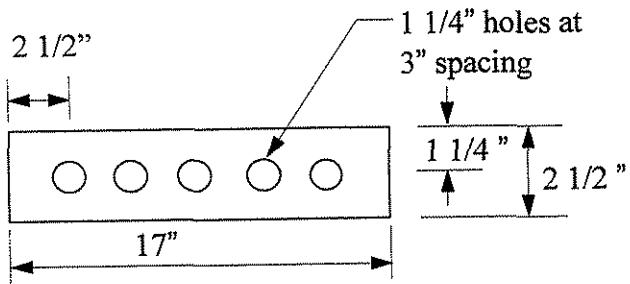
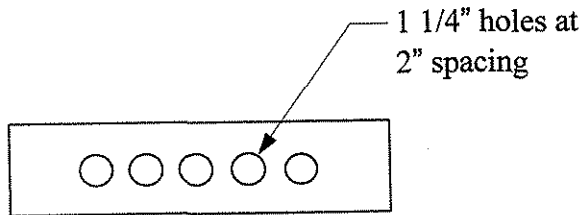


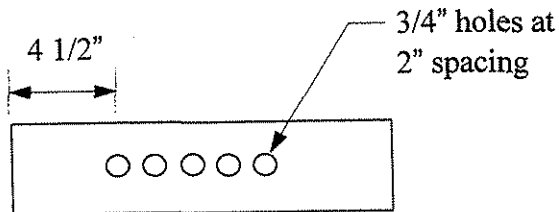
Fig. 2.1. Push-out specimens.



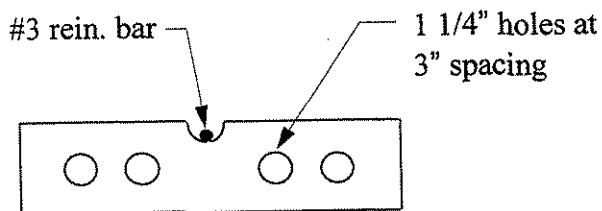
a. Series 1



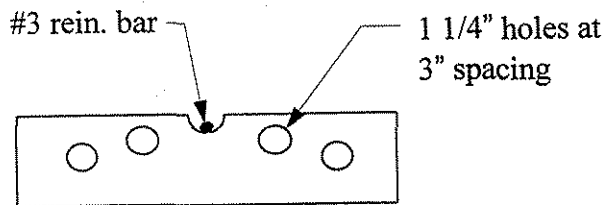
b. Series 2



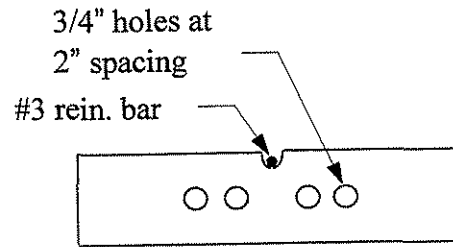
c. Series 3



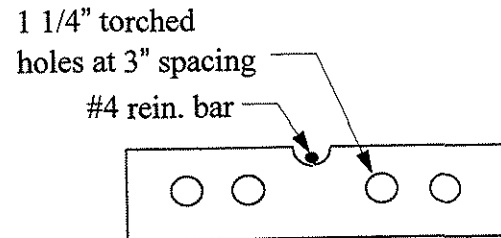
d. Series 4



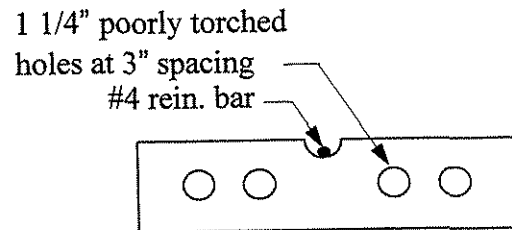
e. Series 5



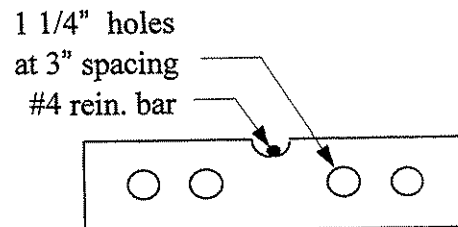
f. Series 6



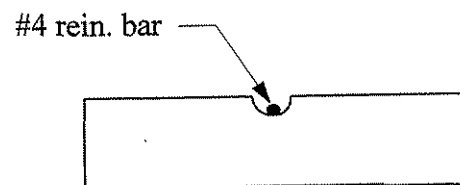
g. Series 8



h. Series 9



i. Series 10



j. Series 11

Fig. 2.2. Description of the hole arrangements used in the push-out tests.

- Series 4 vs. Series 5 - to determine the effect of shear hole alignment.
- Series 10 vs. Series 8 and Series 9 - to determine the effect of drilled holes vs. torched holes and “sloppy” craftsmanship.
- Series 4 vs. Series 8 - to determine the effect of size of reinforcement through the shear hole

Additionally, Series 7 and Series 11 were used to determine an expression to account for the strength associated with excluding the shear holes. Data from all series were used in the development of an expression for determining the shear strength of the ASC.

Transverse reinforcement in each of the concrete slabs was held constant for each specimen, and was calculated based on recommendations presented by Leonhardt, et al. [4]. The equation relating transverse reinforcement to reinforcement yield strength and ultimate shear force is as follows:

$$A_{st} \geq \frac{.56 V_u}{f_{sy}} \quad (2.1)$$

Where:

$V_u$  = Ultimate shear strength per hole, kN.

$A_{st}$  = Area of transverse steel required per hole, mm<sup>2</sup>.

$f_{sy}$  = Yield strength of the reinforcing steel, kPa.

The largest anticipated ultimate strength was used to determine that two #4 reinforcing bars per shear hole were required for transverse reinforcement; this slab reinforcement is shown in Fig. 2.1.

The first step in fabricating the push-out test specimens involved manufacturing the shear holes in the 9.5 mm (3/8 in.) steel plate. This was accomplished by either drilling the holes with a magnetic drill or torching the holes. To fasten the lateral stiffeners, 19 mm (3/4 in.) holes were drilled in the steel plate at the same time as the shear holes. Voids were created in the concrete at the end of the steel plates by epoxying styrofoam to the edge of the steel plates. This styrofoam was removed prior to testing to create an unobstructed slip path for the steel plate (see Fig. 2.1).

To expedite the casting process, forms were fabricated so that three specimens could be cast simultaneously. The steel plates were placed in the forms, followed by the pre-fabricated reinforcing steel cages, being sure to restrict movement of the steel cages in the forms. The concrete slabs were cast vertically so that both sides of the push-out specimens could be poured at the same time, ensuring that the concrete strength would be consistent in the slabs. A total of six specimens were cast per pour, using concrete from a local ready-mix plant. The concrete was placed in three lifts and vibrated after each lift to eliminate voids. Samples were taken throughout the casting to ensure slump and air were within Iowa DOT standards, and to ensure that the concrete was consistent throughout the pour.

In addition to the push-out specimens, fifteen 152 mm x 305 mm (6 in. x 12 in.) standard ASTM concrete test cylinders and two 152 mm x 152 mm x 1,524 mm (6 in. x 6 in. x 5 ft) modulus of rupture beams were cast for each series. The push-out specimens, cylinders, and beams were then covered with wet burlap and plastic and allowed to moist cure for seven days. Formwork was removed after seven days and the specimens were allowed to air cure until tested. All of the specimens were tested within two to three days of the desired 28-day curing period.

## **2.2 BISB Laboratory Specimens**

To obtain strength and behavior information on the original BISB, two specimens which simulated a portion of the BISB were fabricated and tested in the laboratory. One specimen had two steel beams and the other had four steel beams. Since the only difference in the two specimens was the number of steel beams, only information concerning the fabrication of the two beam specimen is presented in this report. In the fabrication of the two-beam specimen, two 9,150 mm (30 ft) long 12W79 steel beams were used, approximating the 12W77 beams used in most of the county BISB's. The beams were positioned so the webs were 610 mm (2 ft) apart; steel straps (6.4 mm x 102 mm (1/4 in. x 4 in.)) were then welded at the third points to ensure the beams would remain in position throughout the placing of the concrete.

Next, 1,220 mm (4 ft) plywood sections measuring 19 mm x 457 mm (3/4 in. x 18 in.) were placed on the bottom flanges of the two beams and glued to the steel using

PL400 structural adhesive. Approximately 63 mm (2 1/2 in.) gaps were left between the web and the edge of the plywood so that concrete would be in contact with the bottom flange (similar to that shown in Fig. 1.1b). Plywood sections were also used for the ends of the specimens. These sections were bolted to the beams using fasteners that had been previously welded to the steel beams. Like the original BISB, no reinforcing steel was included in the structure. Lastly, all joints were sealed with caulk and allowed to cure before concrete was poured.

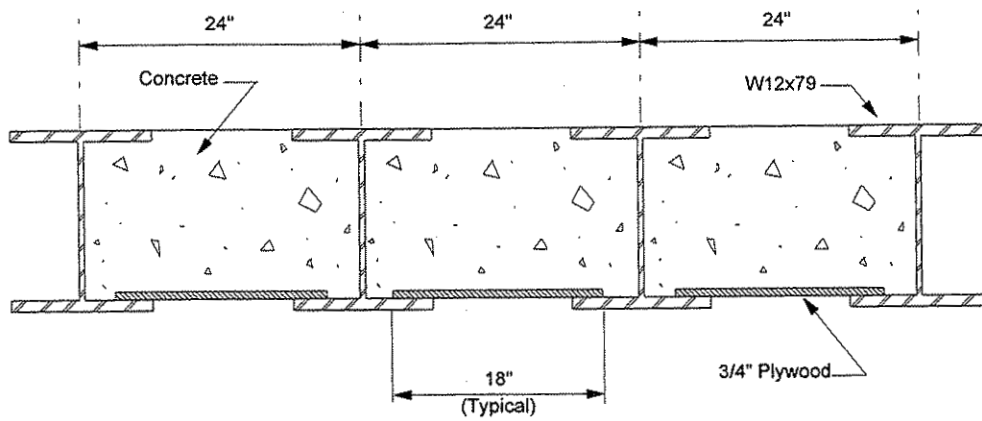
A standard Iowa DOT bridge mix was obtained from a local ready-mix plant. The concrete was placed in two lifts of approximately 152 mm (6 in.); the concrete was vibrated after each lift to ensure contact with the steel. Extra concrete was screeded off and the exposed concrete troweled to create a smooth, level surface for the strain gages that were added. Six 152 mm x 305 mm (6 in. x 12 in.) concrete test cylinders and one 152 mm x 152 mm x 1524 mm (6 in. x 6 in. x 5 ft) modulus of rupture beam were also made.

The four-beam BISB specimen is illustrated in Fig. 2.3. As previously noted, the same procedure was used in the fabrication of this specimen; the only difference between the two is the additional beams (i.e., four beams rather than two beams).

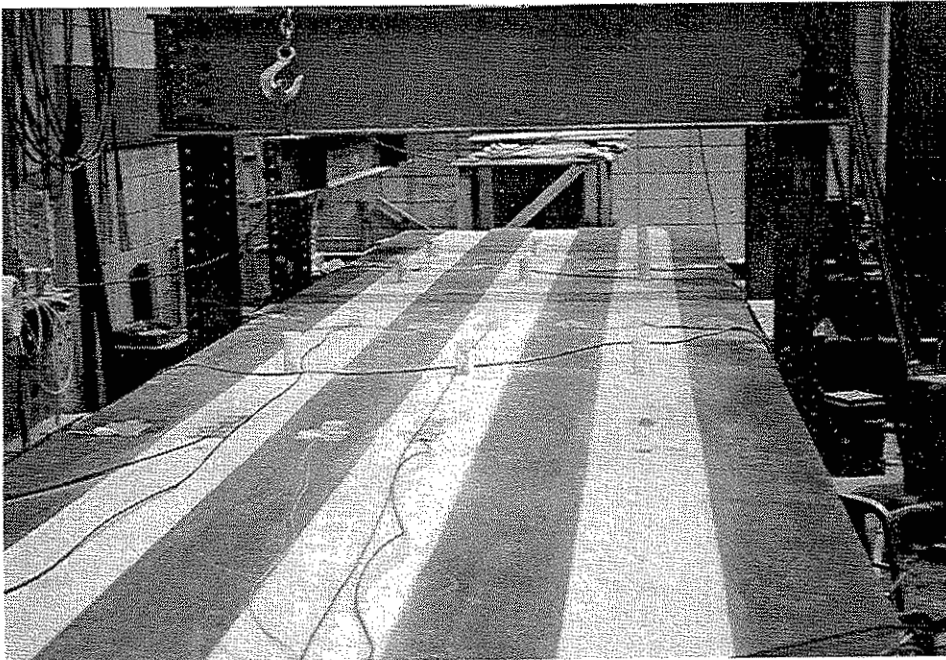
## **2.3 Composite Beam Specimens**

### **2.3.1 Inverted T-Beam**

Specimen 1, illustrated in Fig. 2.4, consisted of a W21x62 with its top flange and 25 mm (1 in.) of the web removed, giving it a depth of 492 mm (1 ft - 7 3/8 in.). Information on cutting off the top flange is given at the end of this section. Holes 27 mm (1 1/16 in.) in diameter on 102 mm (4 in.) centers and 457 mm (18 in.) from the top of the bottom flange were drilled in the web (see Fig. 2.4c). A 152 mm (6 in.) deep slab, 610 mm (24 in.) wide, was poured to form a specimen with a total depth of 584 mm (23 in.). Reinforcement was placed in every other hole. A second layer of reinforcement was placed in 13 mm (1/2 in.) grooves cut at the top of the T-section (see Fig. 2.4d). The second layer of reinforcement offset from the first layer by 102 mm (4 in.) was placed on 203 mm (8 in.) centers. A layer of longitudinal reinforcement was placed on top of the transverse reinforcement. This reinforcement consisted of two #4 reinforcing bars spaced

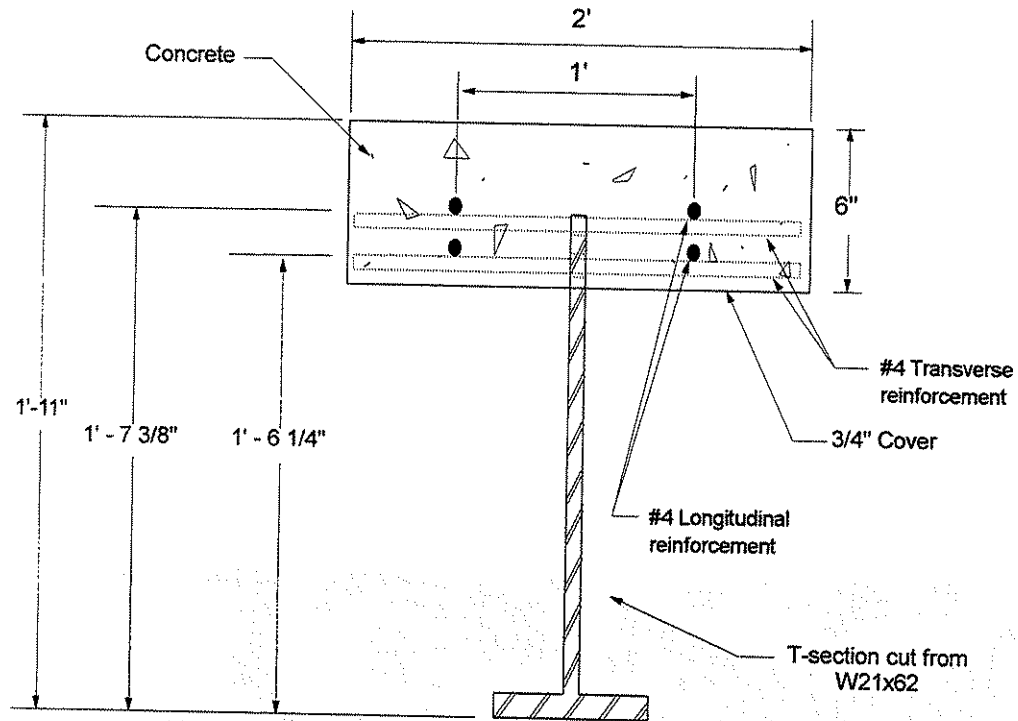


a. End view

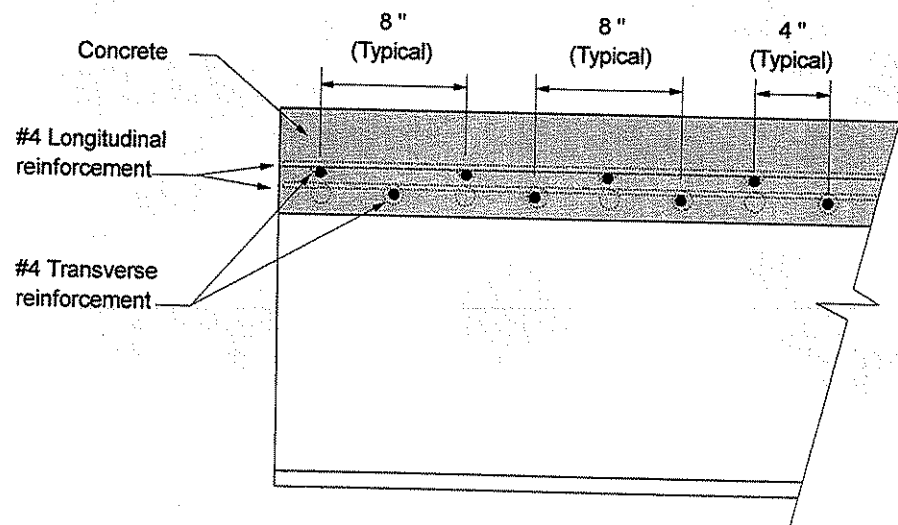


b. Photograph of BISB four-beam specimen

Fig. 2.3. Cross section of BISB four-beam specimen.

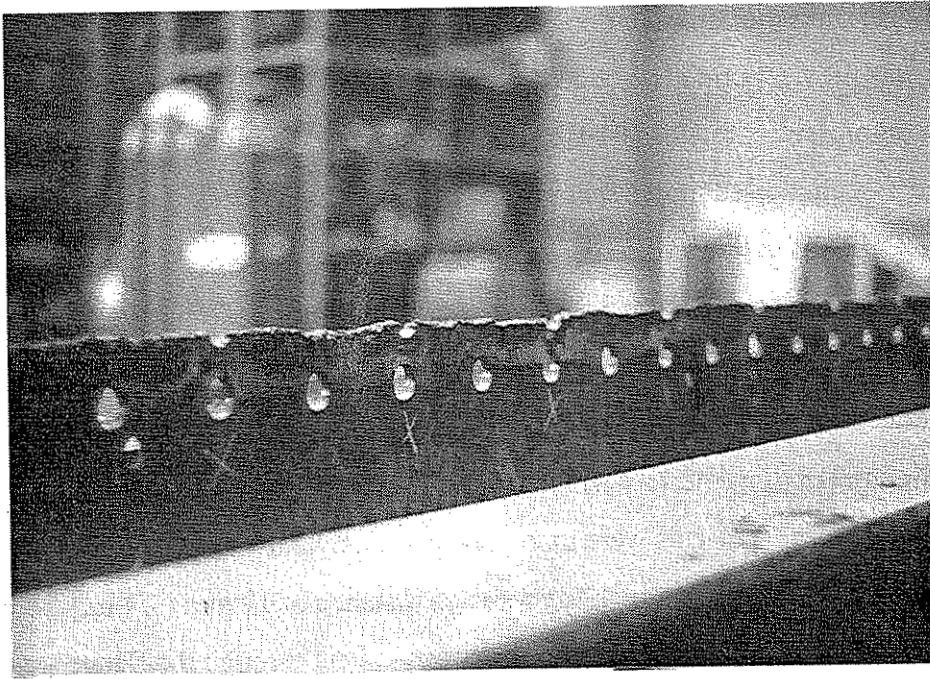


a. End view

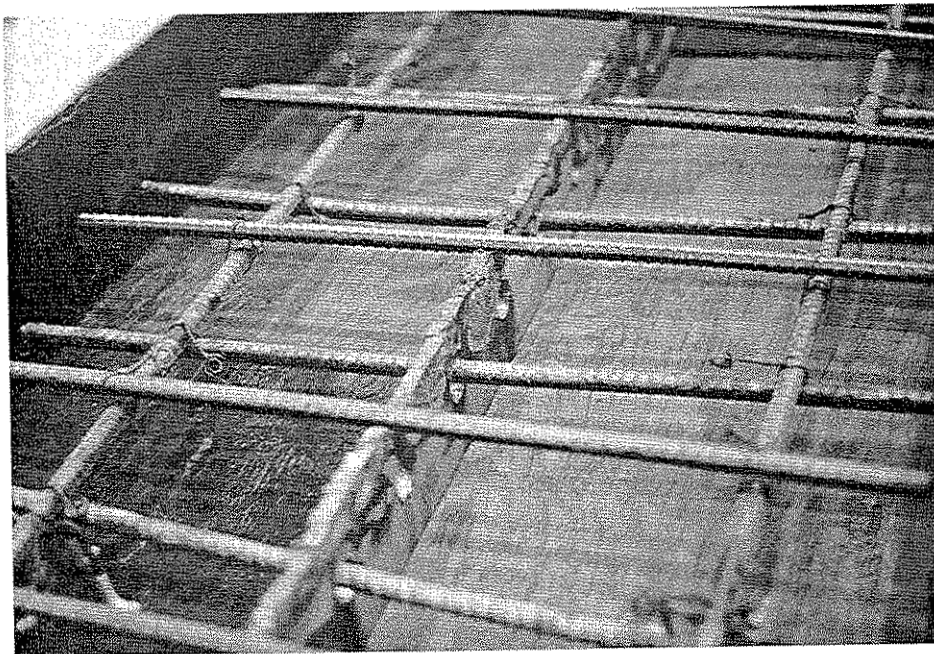


b. Side view

Fig. 2.4. Composite beam specimen: T-section (Specimen 1).



c. Photograph of holes in T-section



d. Photograph of transverse reinforcement in place

Fig. 2.4. Continued.



152 mm (6 in.) from the center of the T-section. During placement of the concrete, the formwork was fully supported. The formwork was then removed when the concrete reached a compressive strength of 10.7 MPa (3,000 psi).

The T-section used in this specimen was fabricated by cutting off the top flange and 25 mm (1 in.) of the web of a 10,360 mm (34 ft) long W21x62. To minimize possible out of plane bending, the beam was cut while supported on its bottom flange. In this position, it was simply supported on a clear span of 9,750 mm (32 ft). Due to safety concerns, it was decided that the beam would be cut in horizontal sections, each 305 mm to 915 mm (1 ft to 3 ft) long, with consecutive cuts alternating between each end of the beam. The cuts were made using an acetylene/oxygen torch. Each cut consisted of a horizontal cut through the web at a distance of 19 mm (3/4 in.) from the bottom of the top flange. Following this cut, a vertical cut through the flange was made separating the top flange from the original beam. The first two cuts were not followed by a vertical cut; only after the third and fourth cuts were vertical cuts made separating these pieces from the rest of the specimen. A total of 17 horizontal and 15 vertical cuts were made, as shown in Fig. 2.5. To simulate the worst case scenario for cutting the top flange of the specimen, an inexperienced individual was used to cut the specimen.

### 2.3.2 Imbedded I-Beam

Specimens 2 and 3, shown in Fig. 2.6, consisted of W21x62's with the top flange imbedded in a concrete slab. Like Specimen 1, the concrete slab was 610 mm (24 in.) wide and 152 mm (6 in.) in depth. Holes 27 mm (1 1/16 in.) in diameter were drilled 457 mm (18 in.) above the top of the bottom flange on 102 mm (4 in.) centers. For transverse reinforcement, #4 reinforcing bars were placed in every other hole. The slab was positioned so that the top flange of the imbedded beam had 51 mm (2 in.) of concrete cover. The total depth of the entire section was 584 mm (23 in.). Two specimens were constructed due to testing problems with Specimen 2; these problems are discussed in Ch. 5 where a comparison of results from the two specimens (Specimens 2 and 3) is presented.

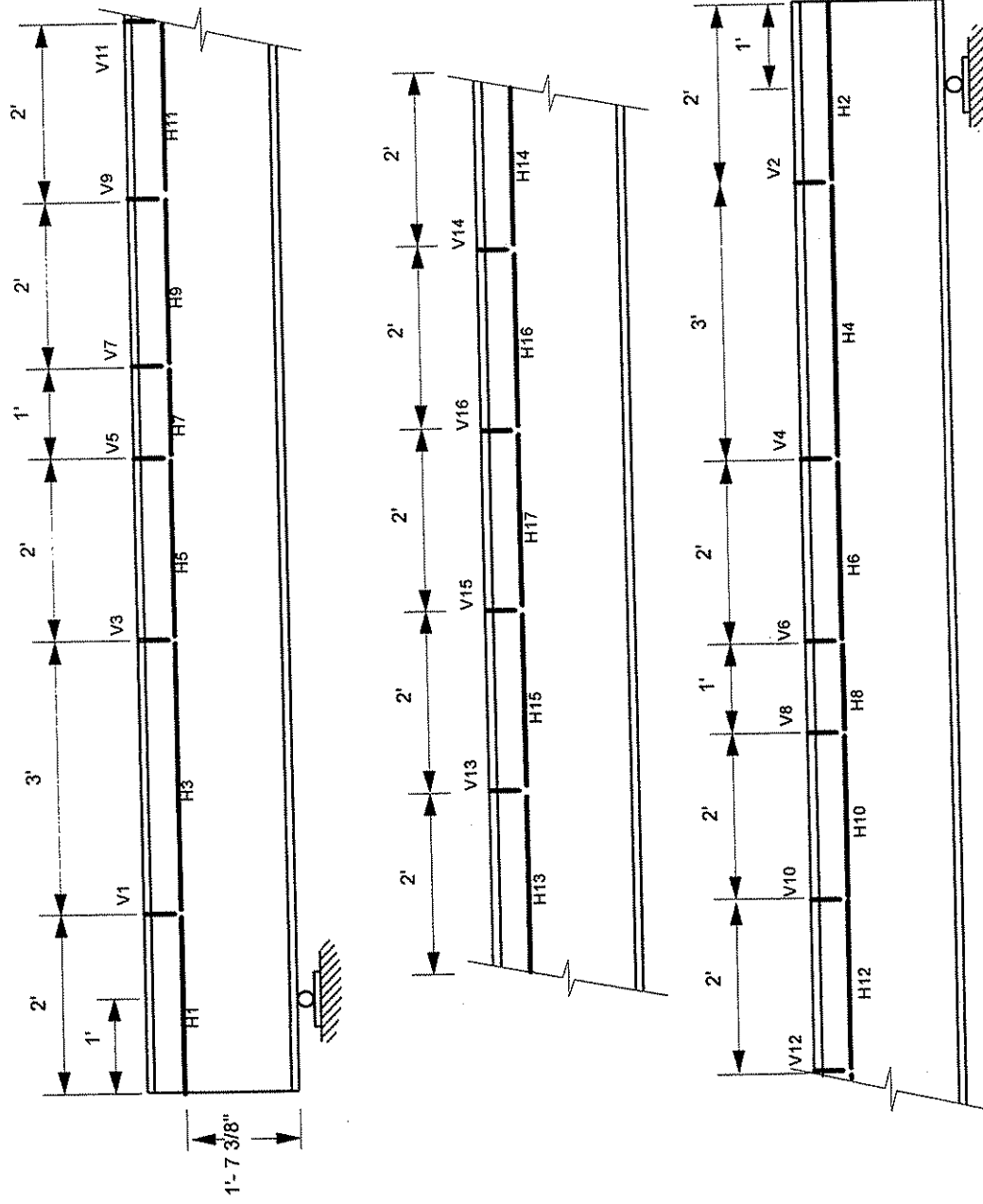


Fig. 2.5. T-section fabrication cutting schedule.

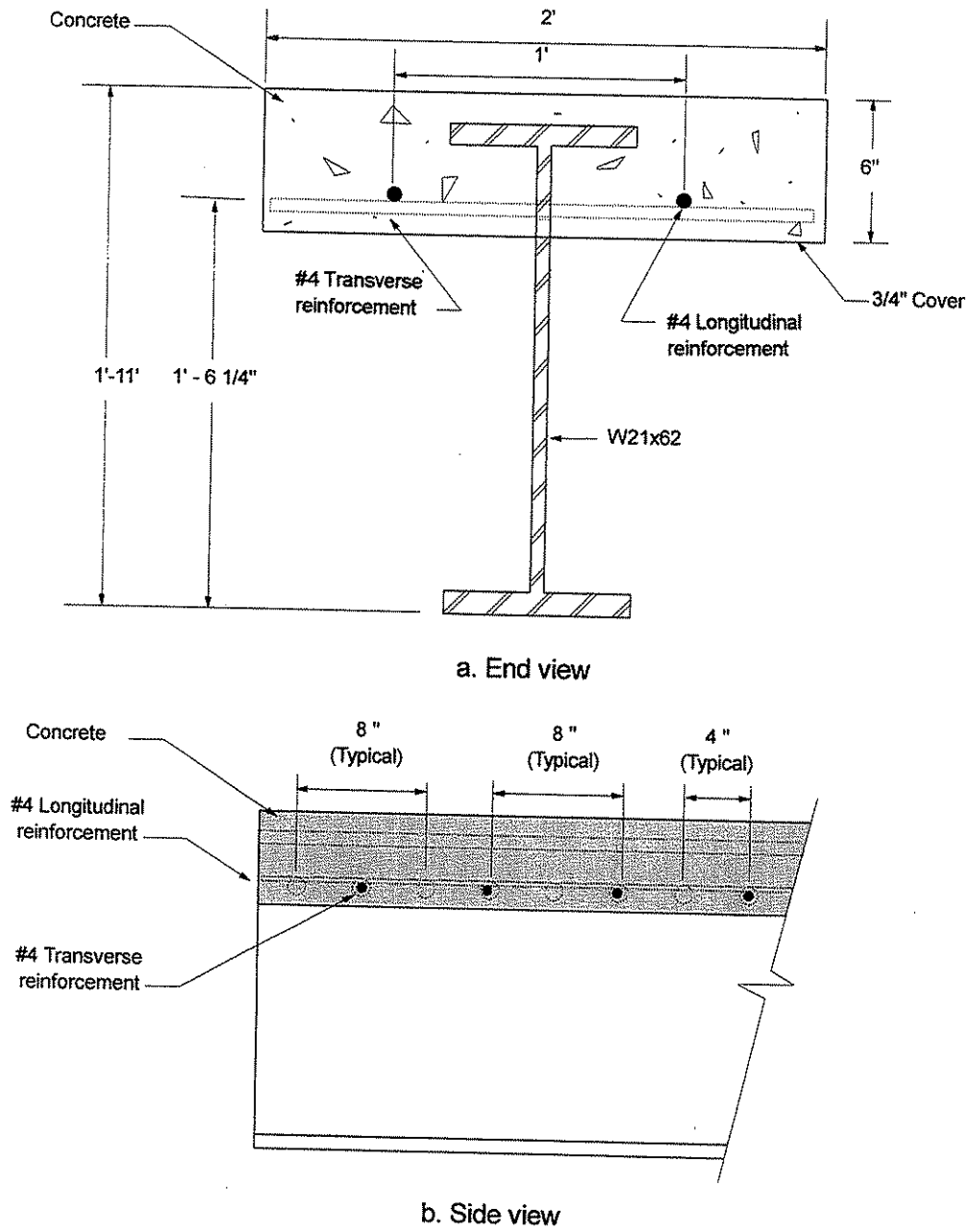
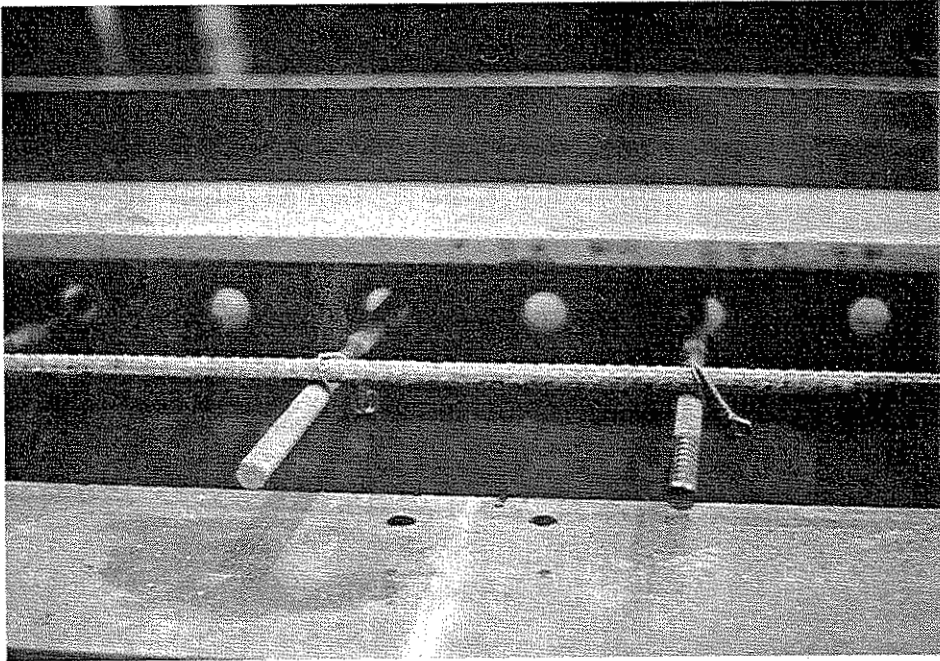
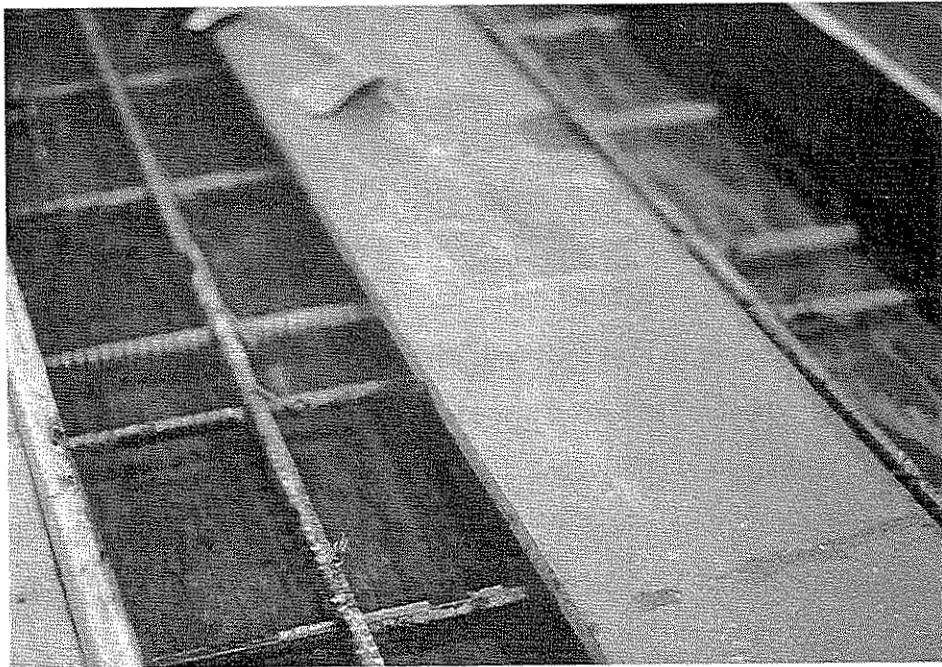


Fig. 2.6. Composite beam specimen: Imbedded I-beam (Specimens 2 and 3).



c. Side view of reinforcement in Specimen 2 and 3



d. Top view of reinforcement in Specimens 2 and 3

Fig. 2.6. Continued.

### 2.3.3 Standard Composite Beam

Specimen 4, shown in Fig. 2.7, consisted of a W21x62 with a 610 mm (24 in.) wide, 152 mm (6 in.) deep slab. Standard 102 mm (4 in.) shear studs, 13 mm (1/2 in.) in diameter, were placed on 305 mm (1 ft) centers along the entire length of the specimen, based on the ultimate load criteria in AASHTO Bridge Design Specification (13).

Reinforcement in the slab consisted of two layers of #4 reinforcing bars. The first layer was placed 25 mm (1 in.) above the top flange of the concrete and spaced every 203 mm (8 in.). The second layer of reinforcement was placed 102 mm (4 in.) above the top flange, also on 203 mm (8 in.) centers. Longitudinal reinforcement, consisting of #4 bars, was placed 152 mm (6 in.) from the center of the cross section (see Fig. 2.7c). The longitudinal reinforcement was placed directly upon the transverse reinforcement along the entire length of the span; thus, the longitudinal reinforcement layers were 38 mm (1 1/2 in.) and 114 mm (4 1/2 in.) above the top flange.

### 2.4 BISB Field Bridge

A representative BISB in Benton County was service load tested to obtain strength, deflection, and strain data. The road leading to the bridge was noted as a Level B service gravel road, often subject to flooding. Complete drawings and dimensions for the bridge are presented in Fig. 2.8 and Tables 2.1 and 2.2. Beams were typically spaced at 610 mm (24 in.), with bearings of 520 mm (20 1/2 in.) and 305 mm (12 in.) on the east and west ends, respectively. A photograph of the bridge tested is shown in Fig. 2.9.

Construction drawings indicated the bridge superstructure was attached to the abutment by 2 #8 reinforcing rods at each end, which extended into the bridge 152 mm (6 in.) (see Fig. 1.3). This reinforcement provided a certain rotational fixity at the end supports. The abutment, shown previously in Fig. 1.2, consisted of 9 steel piles on 1,220 mm (4 ft) centers in the abutment face, with wingwalls constructed to the desired height. Reinforcement on 305 mm (12 in.) centers was spaced around the outside of the entire abutment and wing walls.

Overall, the bridge was in very good condition. There was evidence of frequent flooding of the stream, causing minor corrosion problems on the lower flanges of the beams, and some erosion in the vicinity of the abutments. The plywood formwork was

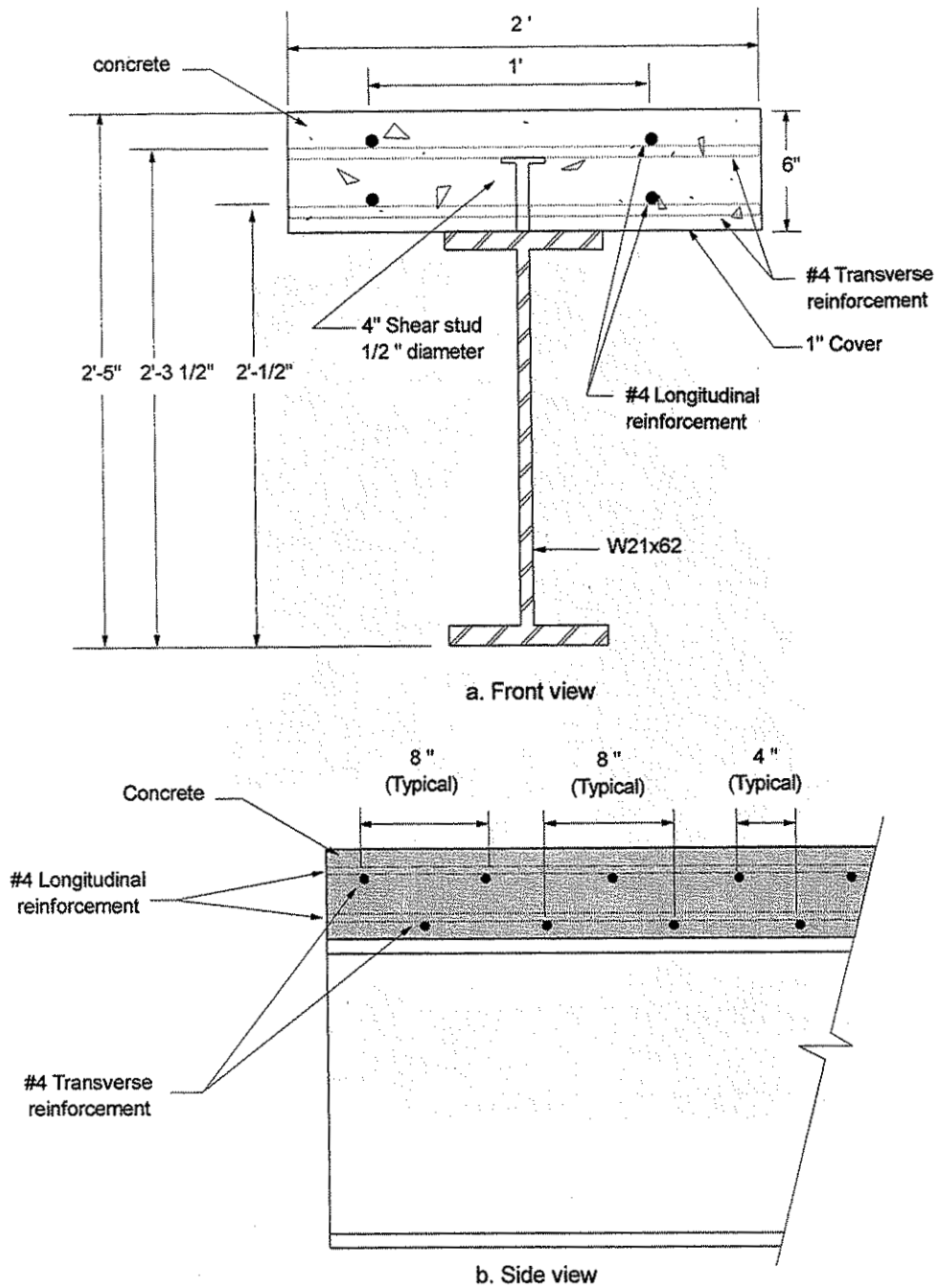
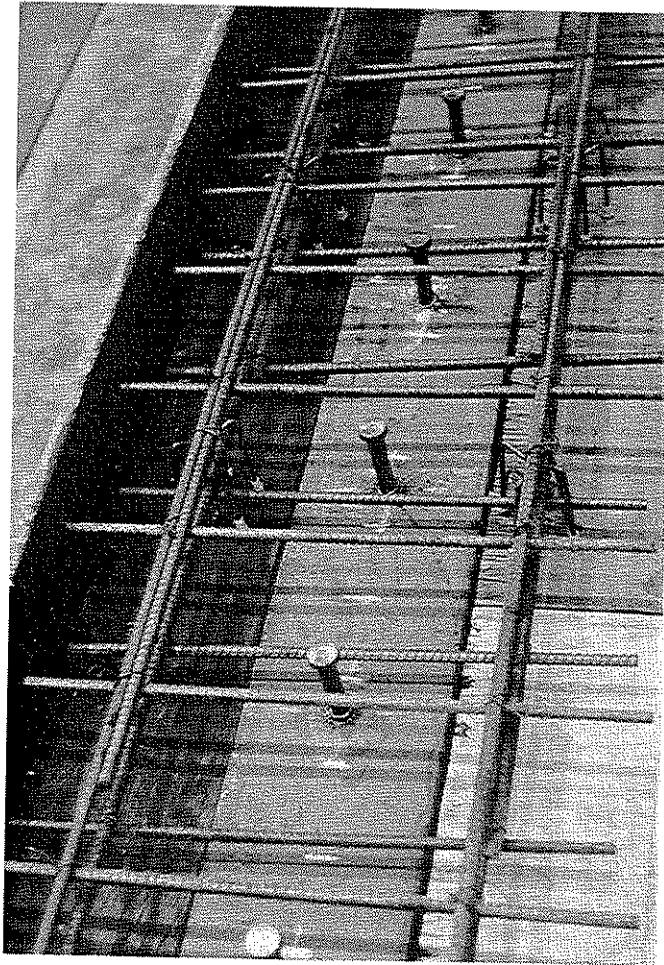


Fig. 2.7. Composite beam specimen: Welded studs (Specimen 4).



c. Photograph of shear studs and reinforcement in Specimen 4

Fig. 2.7. Continued.

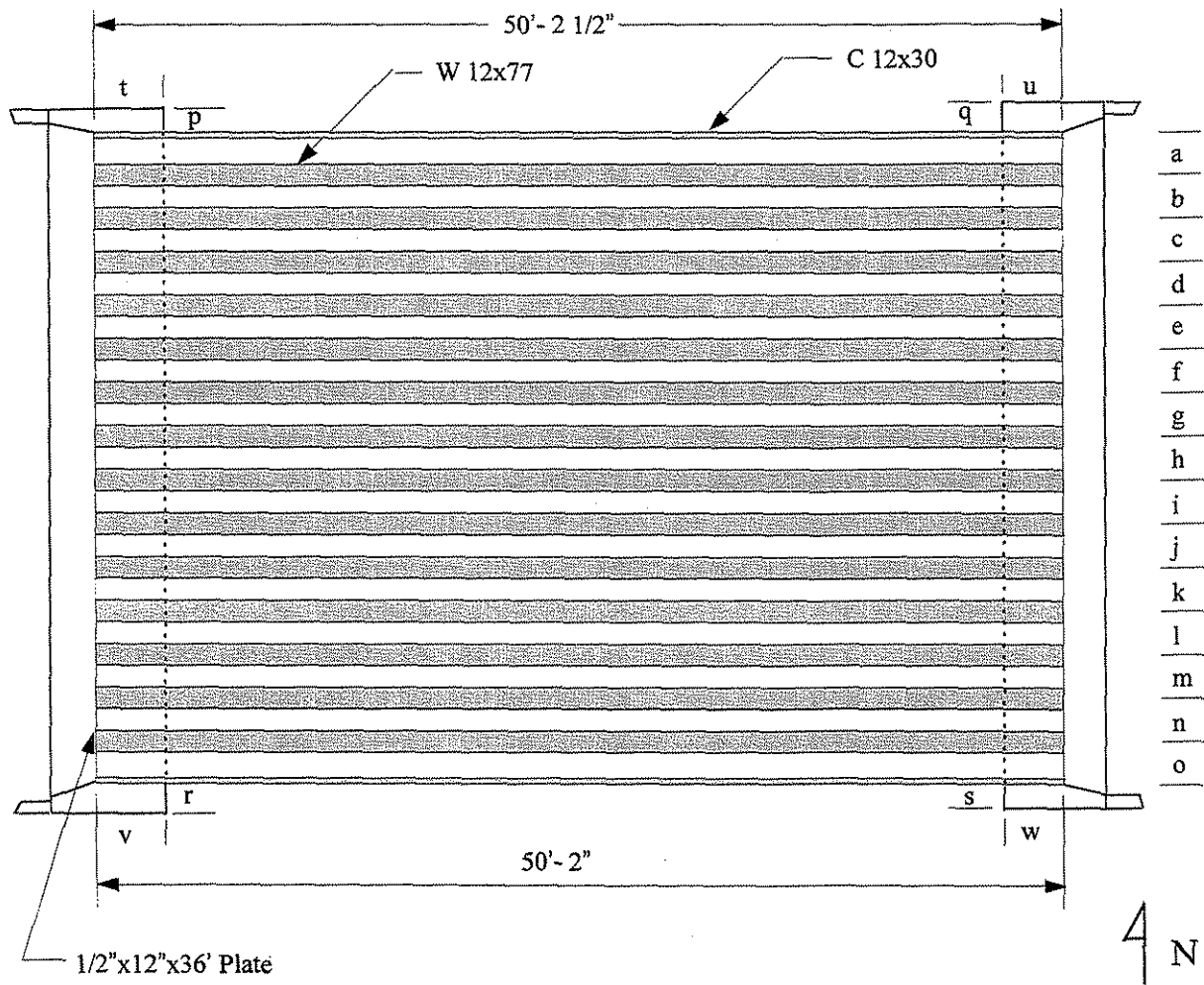


Fig. 2.8. Description of field bridge.



Table 2.1. Beam spacing in field bridge.

Beam Spacing	West Side (in.)	East Side (in.)
a	24 1/8	24 1/2
b	23 15/16	24 1/16
c	24 1/16	23 3/4
d	24	24 1/8
e	24 1/8	24 1/8
f	23 5/8	24 3/16
g	24 1/4	24
h	24 3/8	24 3/8
i	24 1/8	24
j	24 3/8	23 5/8
k	24 3/16	24 1/4
l	23 5/8	23 5/8
m	24	24 3/16
n	24	23 11/16
o	24 1/4	24 1/8

Table 2.2. Field bridge abutment measurements.

Abutment Dimension	Measurement (in.)
p	46 1/2
q	35
r	37
s	46
t	11 7/8
u	20 3/8
v	12 1/2
w	20 3/8



Fig. 2.9. Photograph of BISB bridge tested.

still in fairly good condition. There were only a few minor problems noticed in the bridge; some minor spalling and cracking of the abutment concrete directly under the beams and one noticeable crack on the southeast side of the east abutment have occurred. The top concrete surface was in excellent condition.

It was not possible to obtain material samples for determining the strength properties of the steel and concrete in the BISB tested. Therefore, it was assumed that the concrete strength was 45 MPa (6,500 psi), and the yield stress of the structural steel was conservatively assumed to be 250 MPa (36,000 psi). The concrete strength assumption was based on the assumption that Iowa DOT specifications were followed when the bridge was constructed. The assumption on the structural steel was based on the fact that A36 steel is a commonly used steel in bridge construction.

### 3. TESTING PROGRAM

The experimental portion of the investigation consisted of several different laboratory tests plus one field test. Details of these tests as well as the instrumentation used are presented in this chapter.

Instrumentation for the various tests included three different measuring devices. For measuring displacements (slip, deflection, and rotation), either direct current displacement transducers (DCDT's) or Celesco string potentiometers (Celescopes) were used. Strain data were obtained using electrical-resistance strain gages (strain gages).

The strain gages were attached to the base material (steel or concrete) using recommended surface preparations and adhesives. All strain gages were water proofed and covered to prevent moisture or mechanical damage. Lead wires were connected to the gages using a three-wire hook-up to minimize the effect of the long lead wires and temperature changes.

After installing the instrumentation, the lead wires were then connected to a computer controlled data acquisition system (DAS). With the DAS, deflections from the Celescopes and DCDT's, as well as strains from the strain gages, can be measured and recorded. All pertinent data were automatically stored on the computer hard drive, where it was later accessed and copied onto a computer disk.

#### 3.1 Push-out Tests

Slip and separation between the concrete slabs and the steel plate data were acquired on all push-out specimens (see Fig. 3.1). All 36 specimens were instrumented in the same manner, using seven DCDT's. Two of the DCDT's were fastened rigidly to the plate stiffeners for measuring slip between the concrete slabs and steel plate. The stems of the DCDT's were attached to wooden blocks that had been epoxied to the concrete slabs. Thus, the slip was measured relative to the centerline of the shear connectors.

Four of the DCDT's, used to measure separation between the concrete slabs and the steel shear plate, were rigidly attached to the base of the universal testing machine. Separation was measured at the top third point, and 76 mm (3 in.) below the bottom third point. It was assumed that if separation occurred, it would take place near the bottom of the slab; thus, the reason for placing the DCDT's lower than the bottom third point.

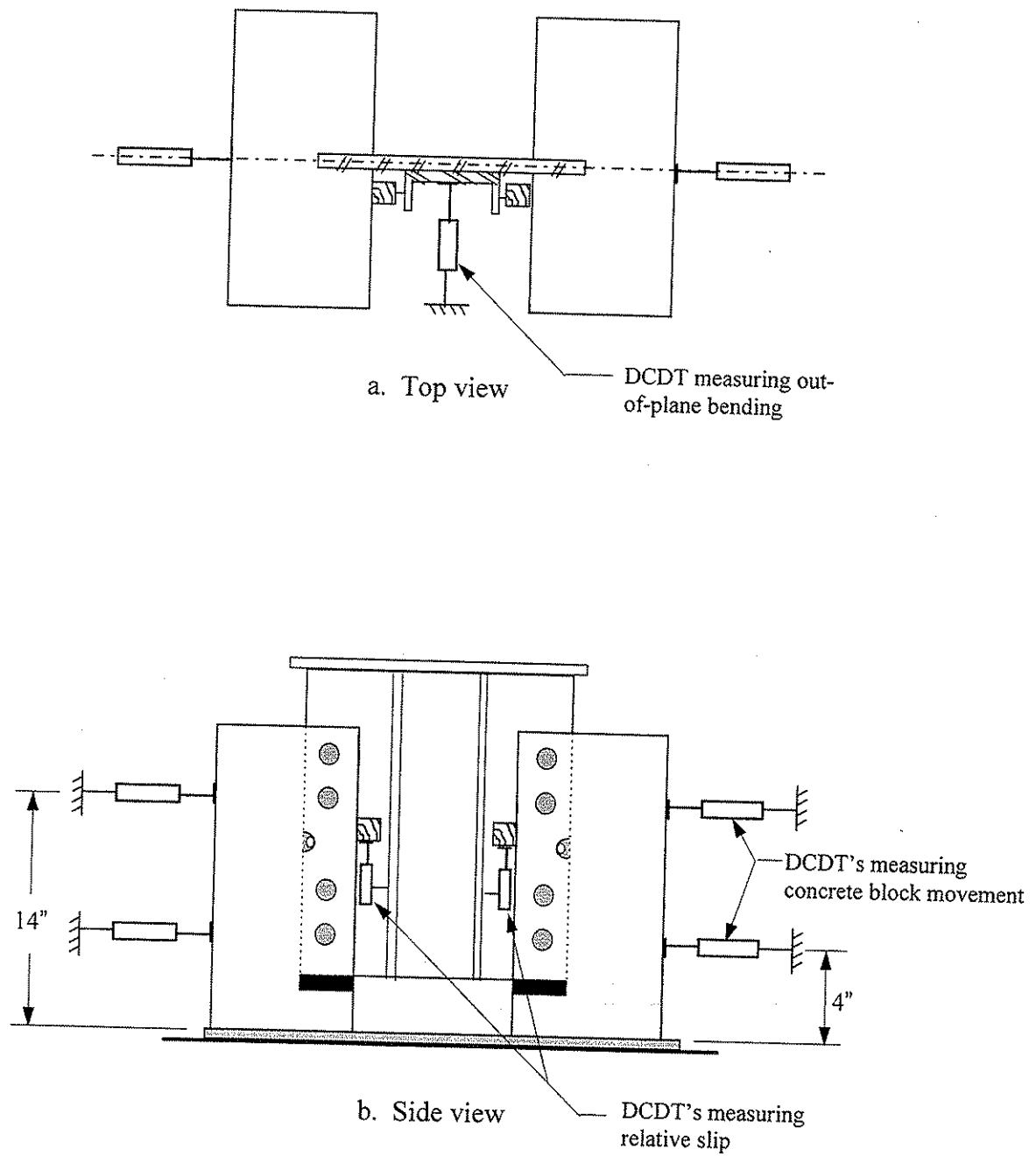


Fig. 3.1. Location of instrumentation used in the push-out tests.

The remaining DCDT was used to measure lateral deflection of the stiffened plate. It was initially a concern that large loads on the 9.5 mm (3/8 in.) thick steel shear plate might induce lateral buckling. Stiffeners were placed on the steel shear plate to prevent such buckling. The DCDT was used to monitor lateral displacements (i.e., out of plane bending).

To obtain uniform load distribution, 6.5 mm (1/4 in.) neoprene pads were placed under each of the concrete slabs. Load was applied to the top edge of the steel plate by the head of the testing machine through a 13 mm (1/2 in.) thick steel distribution plate, tack welded to the top of the steel shear plate. Care was taken prior to testing to level the top edge of the steel shear plate, which in turn ensured the welded distribution plate was level. Additionally, before loading, the position of each specimen was checked carefully to ensure it was "centered" in the testing machine so that load would be distributed equally to the two slabs.

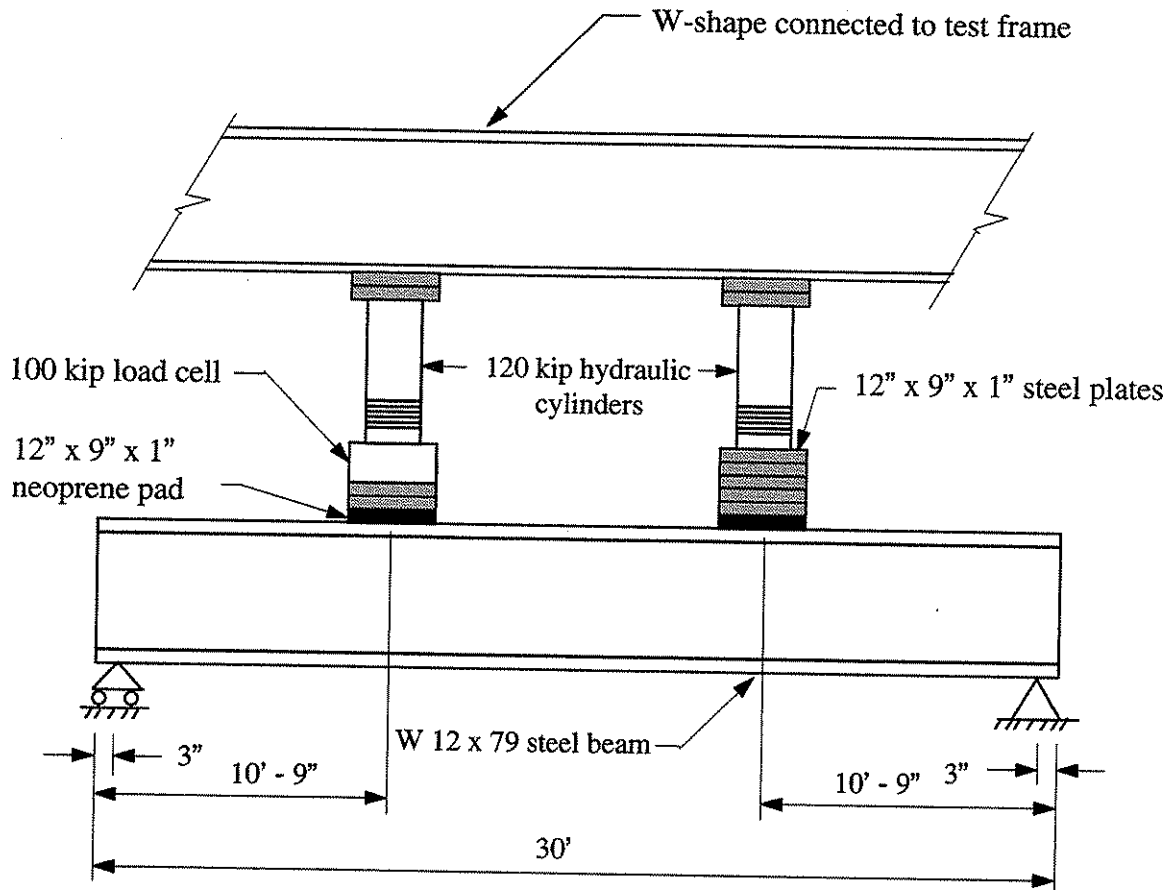
Testing began with an initial load of approximately 1.8 kN (400 lbs). The initial load was applied to make sure the deflection and slip instrumentation was operating correctly, and to ensure an even distribution of force through the distribution plate on the edge of the steel shear plate.

It has been reported by Slutter and Driscoll (11) that shrinkage of the concrete is sufficient enough to destroy the bond between the concrete and the steel shear plate. By destroying this bond, the entire load will be carried by the connection, thus inducing consistent and duplicable results (Siess, Newmark, Viest, (14)). In addition, in 1970, Ollgard (15) noted that the load-slip curve would not be affected by unloading and reloading the specimen. According to this, the initial load would not affect the final results.

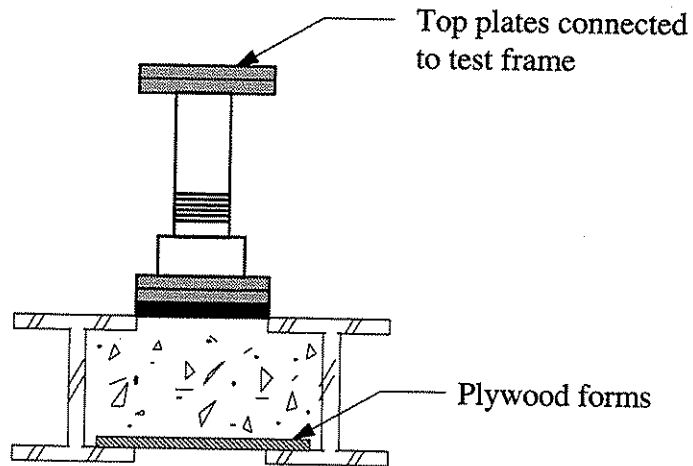
### **3.2 BISB Laboratory Tests**

#### **3.2.1 Two-Beam Specimen**

Using a test frame which was anchored to the structures laboratory floor, the load was applied to the composite beam specimen through two 534 kN (120 kip) hydraulic cylinders. The two-point loading system was used to create a constant moment region in the specimen. As shown in Fig. 3.2a, the loading points were located 3,300 mm (10.75



a. Profile view



b. End view

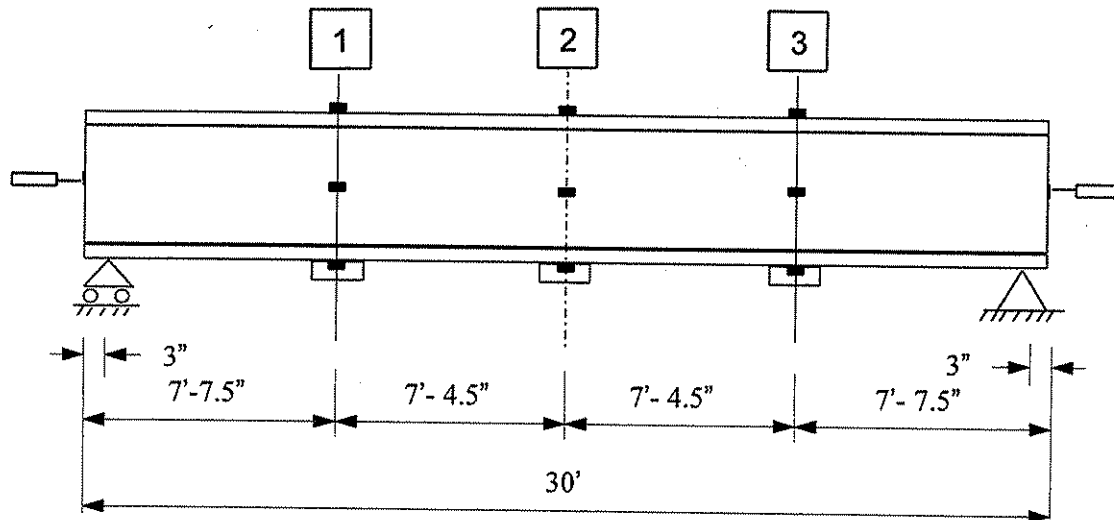
Fig. 3.2. Loading apparatus used for testing the BISB two-beam specimen.

ft) from the center line of the end supports, which provided a constant moment region of 2,440 mm (8 ft).

As in the push-out tests, neoprene pads were placed between the loading distribution plates and the concrete to transmit force uniformly to the concrete. The load was applied directly on the 305 mm (12 in.) concrete of the composite beam, between the two steel beams (see Fig. 3.2b). One 445 kN (100 kip) load cell placed under the left hydraulic cylinder was used to determine the load on the structure. Since one pump was used for both hydraulic cylinders, it can be assumed that the two hydraulic cylinders applied the same force. Magnitudes of applied load were recorded by the DAS, and were saved along with all other pertinent strain and deflection data.

Strain gages and Celescopes were installed on the steel beam prior to the pouring of the concrete to determine the amount of strain and deflection that occurred during placing of the concrete. DCDT's were later installed at the supports to measure the slip between the steel beams and the concrete. Location of strain gages, Celescopes, and DCDT's used in the tests are shown in Fig. 3.3. Strain gages were used to measure strains on the top, mid-height, and bottom of the steel beams, at 1/4, 1/2, and 3/4 of the span. The Celescopes were used to measure deflections at the same three locations. At Sections 1 and 2, the Celescopes were mounted on the bottom of each of the steel beams, as well as on the middle of the plywood. At Section 3, one Celesco was mounted in the middle of the plywood to check for symmetry along the span. A total of 18 strain gages, 4 DCDT's, and 7 Celescopes were used in testing the composite beam.

Two load tests were performed on the composite beam. In the first test, the load was applied in 2.22 kN (500 lbs) increments. After each load increment, strains, deflections, and slip measurements were taken and recorded using the DAS. The composite beam was loaded past yielding of the steel, to the 445 kN (100 kip) capacity of the load cell. Thus, a total load of 890 kN (200 kip) was applied to the specimen. The composite beam was then allowed to sit overnight to "relax." Measurements were taken throughout the night to determine the rate and extent to which the composite beam recovered. The following day, another load test was performed in the same manner to determine the reserve capacity of the composite specimen.



Symbols:

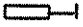


-  = DCDTs
-  = Strain gages
-  = Celescopes

Fig. 3.3. Instrumentation for the two-beam specimen.

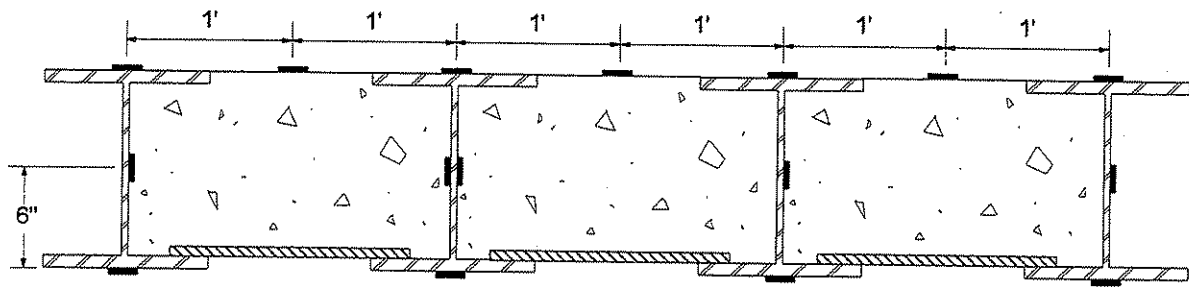


### 3.2.2 Four - Beam Specimen

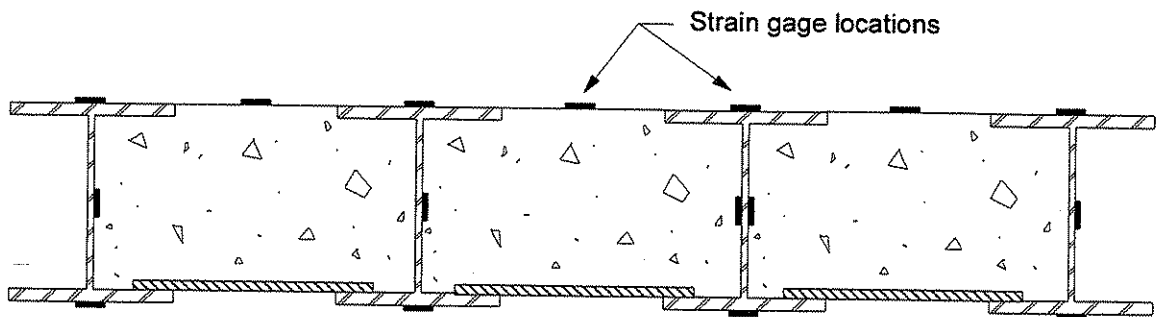
To determine the response of the bridge during load testing, the specimen was instrumented with 40 strain gages and 11 Celescopes. The strain gages were placed at three different sections along the span: the quarter point, the centerline, and three quarter point, as shown in Fig. 3.4. Strain gages located on steel beams were placed at the center of the top surface of the top flange, at mid-height of the web, and at the center of the bottom surface of the bottom flange. Concrete strain gages were placed on the top concrete surface midway between the steel beams. The primary purpose for installing strain gages at the three quarter point was to check for symmetry about the centerline of the specimen. The location of the three instrumented cross sections is shown in Fig. 3.5.

Figure 3.5 also shows the location of the Celescopes that were used to measure deflections. The Celescopes are located on each beam at the quarterpoint, three-eighths point, centerline, and three-quarter point. The two Celescopes at the three-quarter point were for determining if the specimen was responding symmetrically about its centerline.

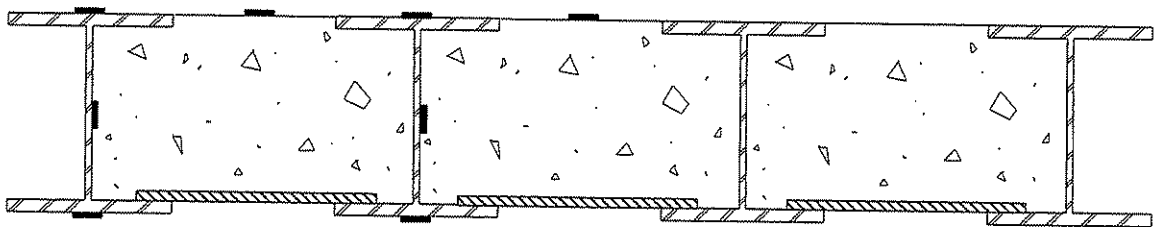
Testing of the four-beam specimen was different from the testing of the two-beam specimen, in that a single service load was applied at several locations so that the lateral load distribution in the system could be determined. The single point load had a surface contact area of 305 mm x 305 mm (1 ft x 1 ft). To insure that the specimen was not overstressed during the service level load tests, a maximum magnitude of 89 kN (20 kips) was used for the single point load. Calculations made prior to testing indicated that by limiting the applied load to this magnitude, stresses in the specimen would remain in the elastic range. As shown in Fig. 3.6, the load was positioned at the center of each steel beam or concrete section at distances of 1,500 mm, 2,720 mm, 3,940 mm, and 4,750 mm (4 ft - 11 in., 8 ft - 11 in., 12 ft - 11 in., and 15 ft - 7 in.) from the centerline of the pin support. As shown in this figure, load was applied at 25 different locations; for purposes of discussion, applying load at a given location is referred to as a "test." Thus, there were 25 service load tests. Each test is identified by an (x,y) notation which indicates the position of the load on the specimen. The x notation varies from A to G and indicates where the loading is located transversely; the y notation varies from 1 to 4 and indicates



a. Section at 1/4 span



b. Section at midspan



c. Section at 3/4 span

Fig. 3.4. Location of strain gages on four-beam specimen.

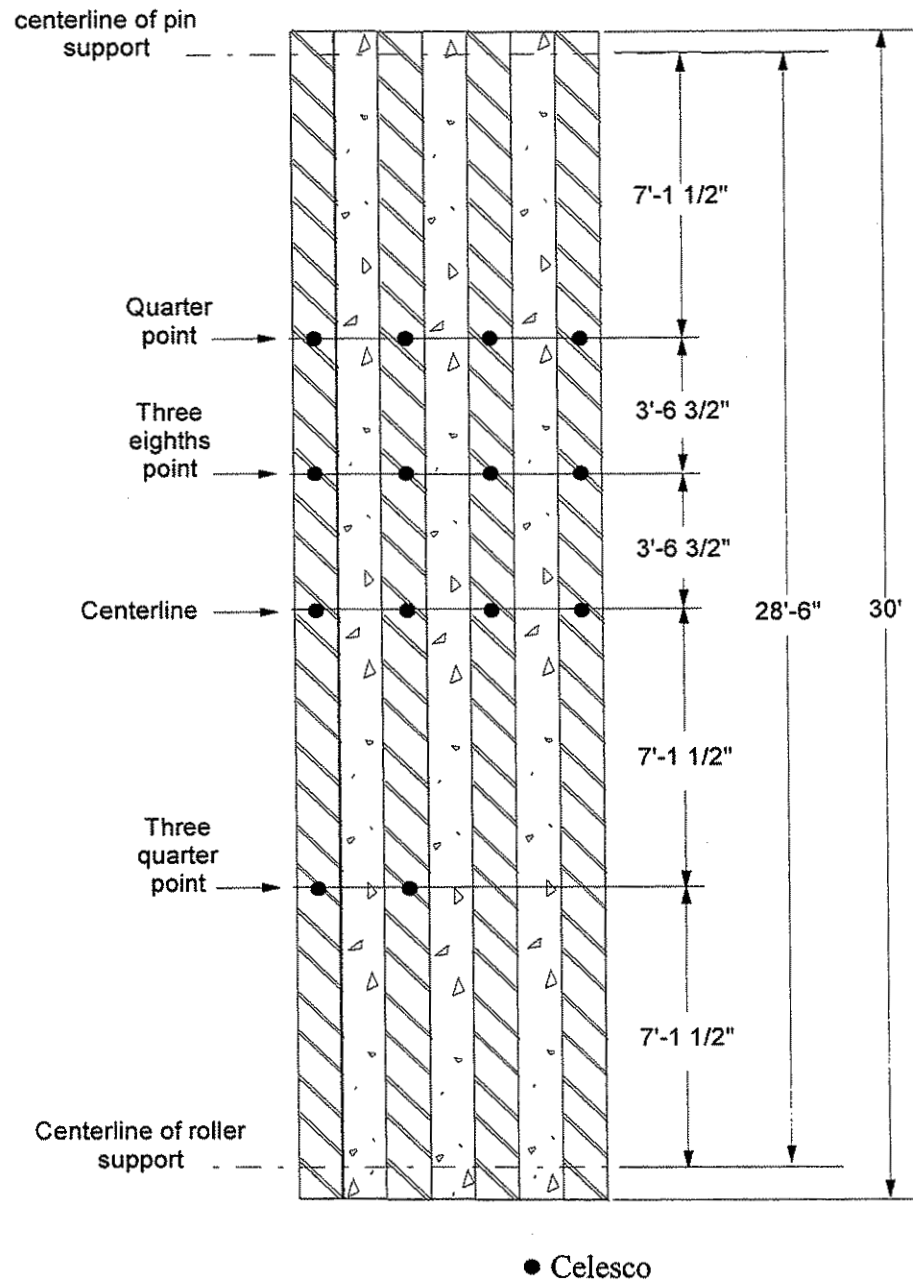


Fig. 3.5. Location of strain gaged cross sections on four-beam specimen.

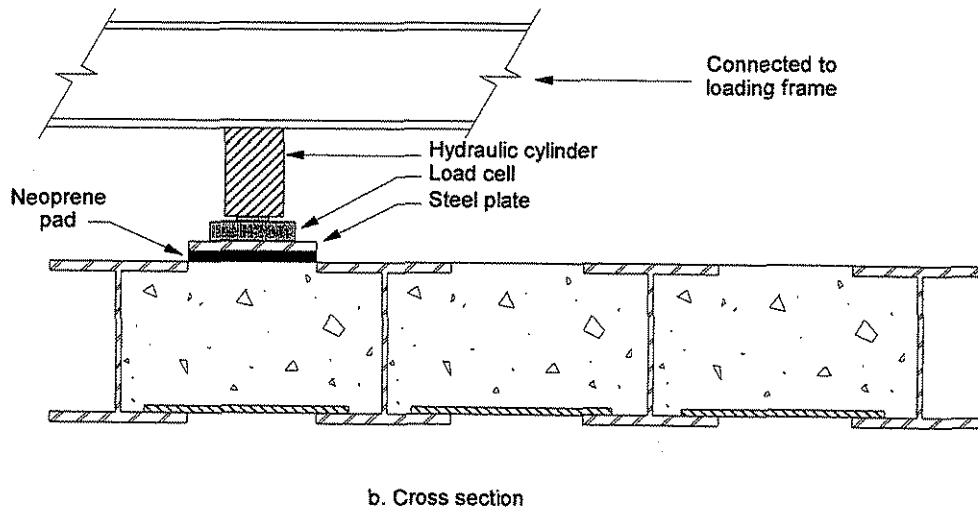
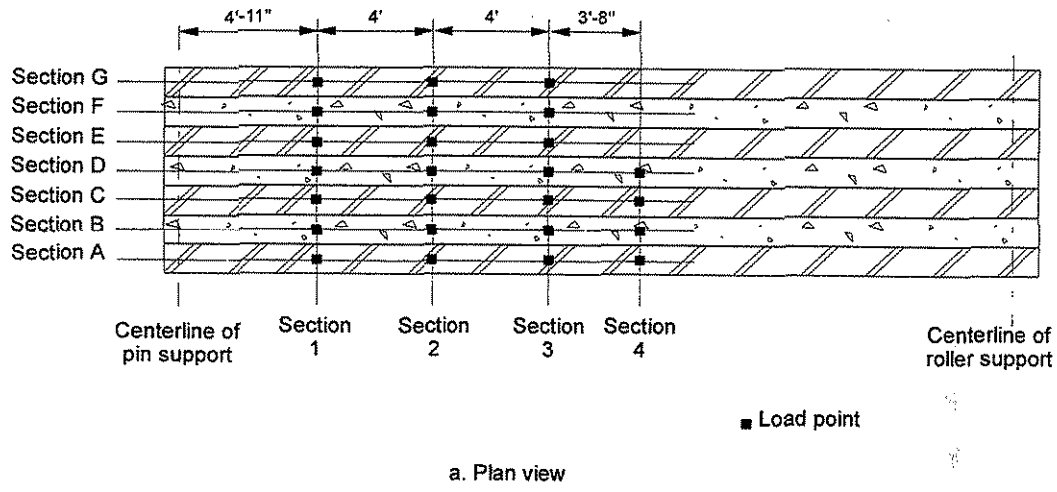


Fig. 3.6. Location of loading points for service level load testing the four-beam specimen.

the longitudinal location of the load. For example, Test A1 refers to the load being placed on the exterior steel beam at a distance of 1,500 mm (4 ft - 11 in.) from the pin support. Similarly, Test D3 refers to the load being placed on the center concrete section at a distance of 3,940 mm (12ft - 11 in.) from the pin support. The location of these load points and corresponding sections are shown in Fig. 3.6.

The loading setup shown in Fig. 3.7 consisted of a neoprene pad, 305 mm x 305 mm x 25 mm (1 ft x 1 ft x 1 in.), placed on top of the specimen. Placed directly on top of the neoprene pad were 25 mm (1 in.) thick steel plates with the same dimensions as those of the neoprene pad. The purpose of these steel plates was to provide a uniform distribution of load to the specimen and to reduce the space between the loading frame and the specimen. The applied load was measured by a load cell, which was placed on top of the steel plates. A steel spacer plate was positioned on top of the load cell to insure that the load was applied to the center of the load cell; this is required for correct measurement of loads. A hydraulic cylinder, with a maximum load capacity of 534 kN (120 kips) and a stroke limit of 152 mm (6 in.) was used to apply the load. As shown in Fig. 3.7, four point loads were used in the ultimate load test. Load were applied through holes formed in concrete in the specimen when it was cast. The holes were located 2,970 mm (9 ft - 9 in.) from the center of the supports in the center of the concrete sections. A Dywidag bar was position in the precast holes in the specimen and connected to the tie down floor. With the hydraulic cylinder positioned as shown, load could be applied to the specimen.

Deflection and strain readings were taken using the same program and DAS used in the service load tests. Because all four hydraulic cylinders were connected in parallel to the same hydraulic pump, it was necessary to monitor the applied load at only one load point. Strains, deflections, and loads were measured and recorded using the DAS after every 2.22 kN (500 lbs) increment of load.

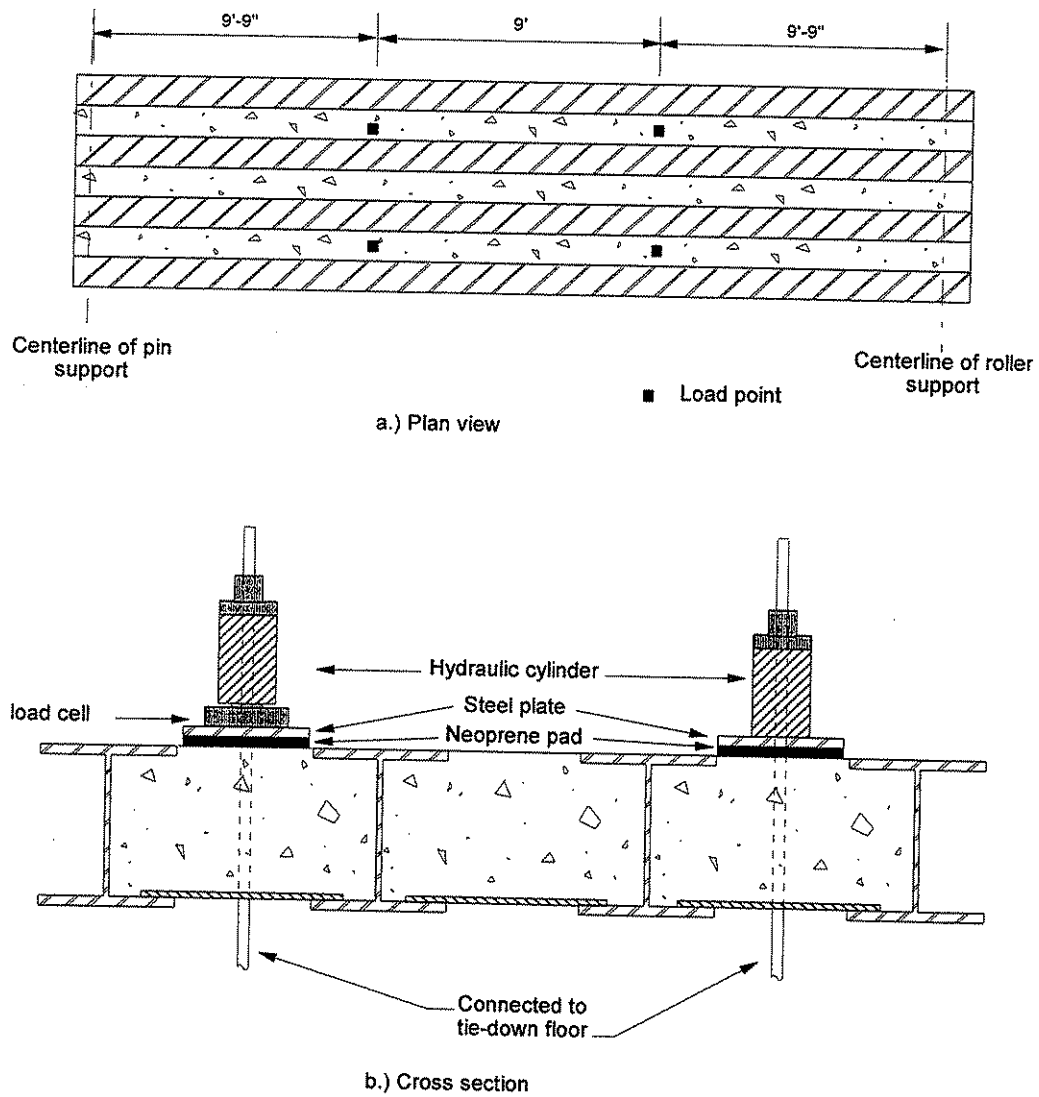


Fig. 3.7. Locations of load points for ultimate load test of the four-beam specimen.

### 3.3 Composite Beam Tests

Strain gages were placed at the quarter point, centerline, and three-quarter point of the specimens. The same sections in each specimen were instrumented; however, the location of the strain gages at each section varied from specimen to specimen, as is shown in Fig. 3.8. The instrumentation for measuring the deflections was the same for each specimen. Seven Celescopes were placed along the length of the span and were positioned as shown in Fig. 3.9. Two DCDT's were placed at each end of the beam to measure the slip between the concrete slab and steel beam.

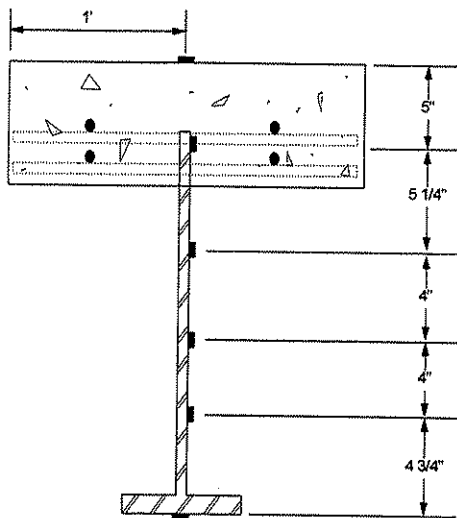
#### 3.3.1 Service Load Tests

The total length of each specimen was 10,360 mm (34 ft), and the clear span was 9,750 mm (32 ft). Each specimen was tested as a simply supported beam.

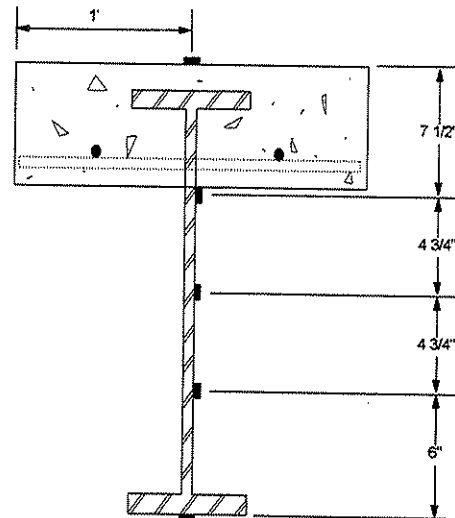
Prior to testing, an initial calculation determined that yielding of the specimen would occur when a load of 133 kN (30 kips) was applied. To insure that the specimen stayed in the elastic range, a maximum load of 89 kN (20 kips), 66% of the load required for yielding, was used during the service tests. As shown in Fig. 3.10, load was applied at two points, each 610 mm (2 ft) from the center of the specimen. The applied load was transferred through a steel plate to a 305 mm x 305 mm (1 ft x 1 ft) neoprene pad. Loading was applied using hydraulic cylinders connected to the same pump. Thus, only one load cell was required to measure the applied force. There were three service load tests for each specimen to check the reproducibility of the response. The service tests consisted of loading each specimen to a maximum total load of 89 kN (20 kips) in increments of 2.22 kN (500 lbs). As with previous tests, strains and deflections were measured and recorded using the DAS after each load increment.

#### 3.3.2 Ultimate Load Tests

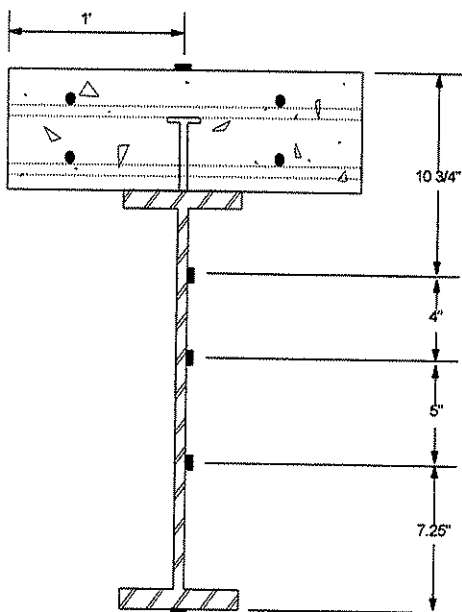
After completion of the service load tests, each specimen was loaded to failure. The failure tests were setup the same as the service test with two load points placed 1,220 mm (4 ft) apart (see Fig. 3.10). As during the service load tests, the strains and deflections were measured after each 2.22 kN (500 lbs) load increment. In each test, the stroke limit of the cylinder was reached before failure of the specimen occurred. At this



a. Specimen 1



b. Specimens 2 and 3



c. Specimen 4

■ Strain gage

Fig. 3.8. Location of strain gages on composite beam specimens.



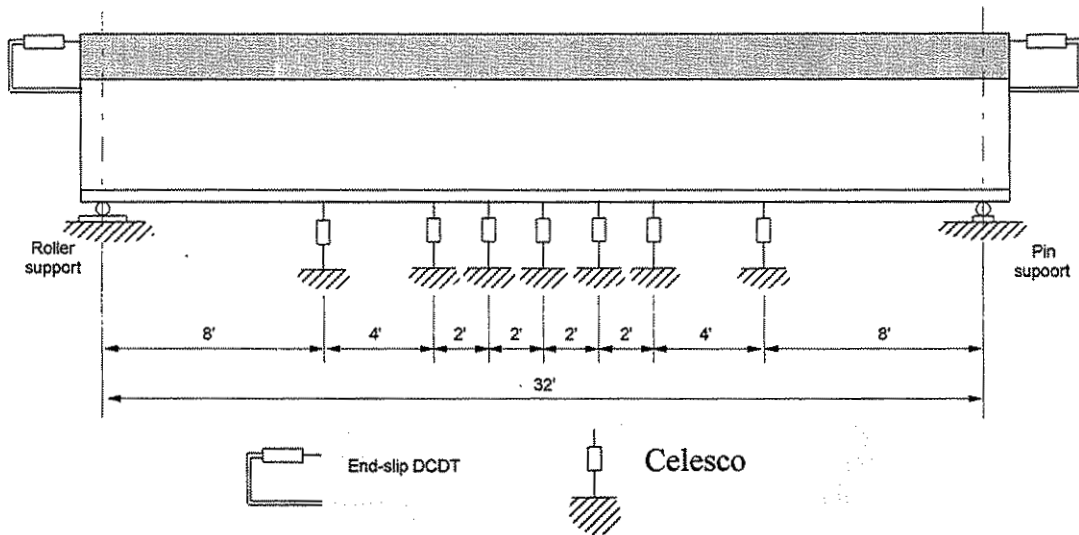


Fig. 3.9. Location of deflection instrumentation in composite beam tests.

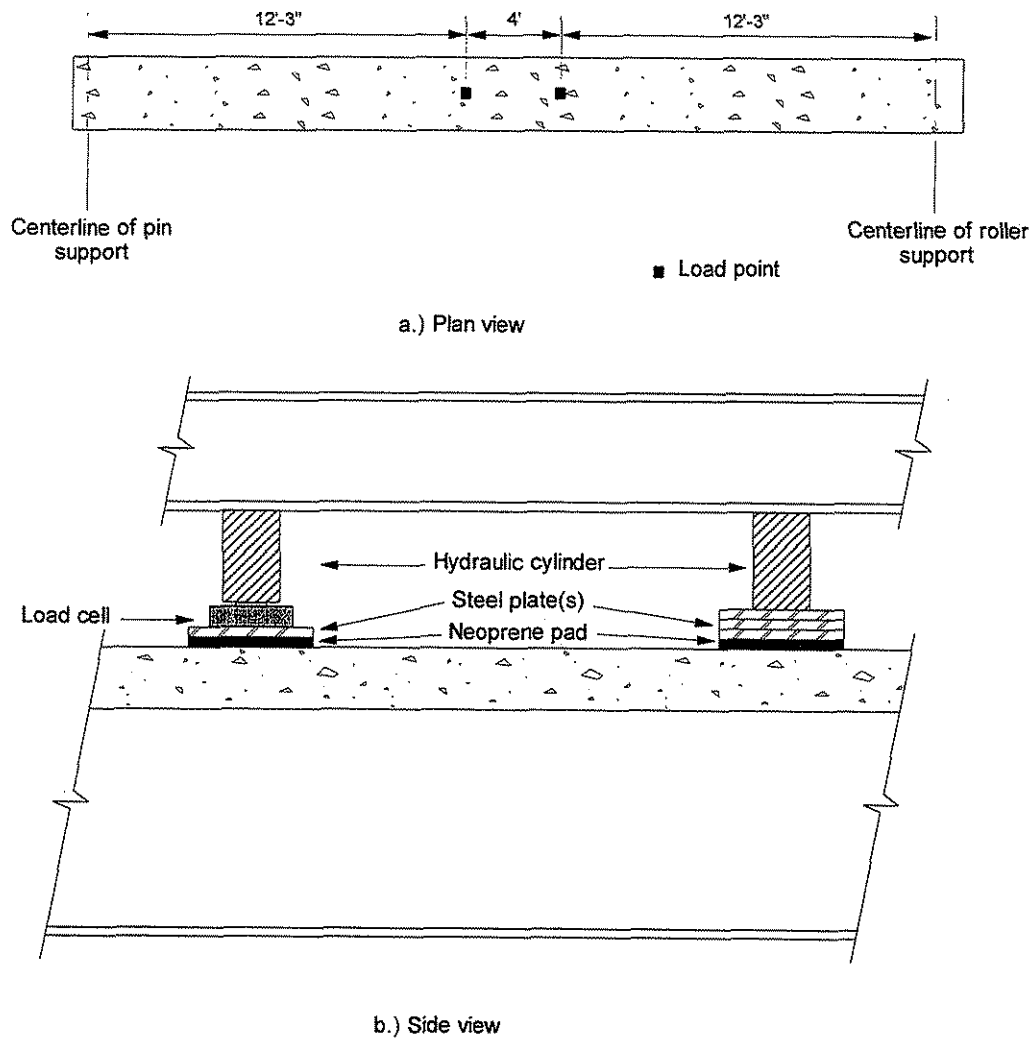


Fig. 3.10. Composite beam test setup.

time, the load was removed and additional steel plates were placed between the cylinder and the specimen. When loading resumed, strains and deflections were measured after every 22.5 kN (5 kips) increment of load until the load associated with repositioning the hydraulic cylinders was reached. The load was then increased in increments of 2.22kN (500 lbs) until failure of the concrete slab occurred.

### 3.4 BISB Field Tests

Figure 3.11 indicates the location of the strain gages and Celescopes used on the BISB field test. As the bridge was not on a heavily traveled road, the instrumentation was placed without obstruction to traffic, or danger to the crew installing the instrumentation. With this type of bridge, the webs of the steel beams are not exposed; thus, the beam flanges are the only part of the steel available for mounting strain gages. All strain gages were "centered" on the bottom beam flange or bottom channel flange. Celescopes were placed as close to the center as possible without disturbing the strain gages. At each location indicated in Fig. 3.11, a strain gage was placed with its axis parallel to the axis of the steel beam. The majority of the strain gages and Celescopes were located at midspan so that recorded strain and deflection data could accurately depict the strain profile and deflected shape across the width of the bridge. Some of the instrumentation (for example, Celesco at mid-width at Sections A and B) were installed to check symmetry in the bridge.

A total of 12 strain gages and 10 Celescopes were used to collect strain and deflection data from the BISB. Celescopes were fastened to tripods, set up, leveled, and secured in the stream. Small wooden blocks were epoxied to the steel beam, so that the Celesco wires could be connected to the bridge. Strain gages were waterproofed and connected to the DAS using the three-wire hook-up previously described.

The field testing involved two county tandem rear axle trucks, each weighing approximately 222.5 kN (50 kips), placed in a variety of positions along the bridge. After positioning a truck (or trucks) in the desired location, strain and deflection data were taken, and the trucks were moved to the next position. Deflection data were used to determine the deflected shape of the bridge. Strain data were used to calculate moment fractions at mid-span. The moment fraction was calculated by dividing the strain at each

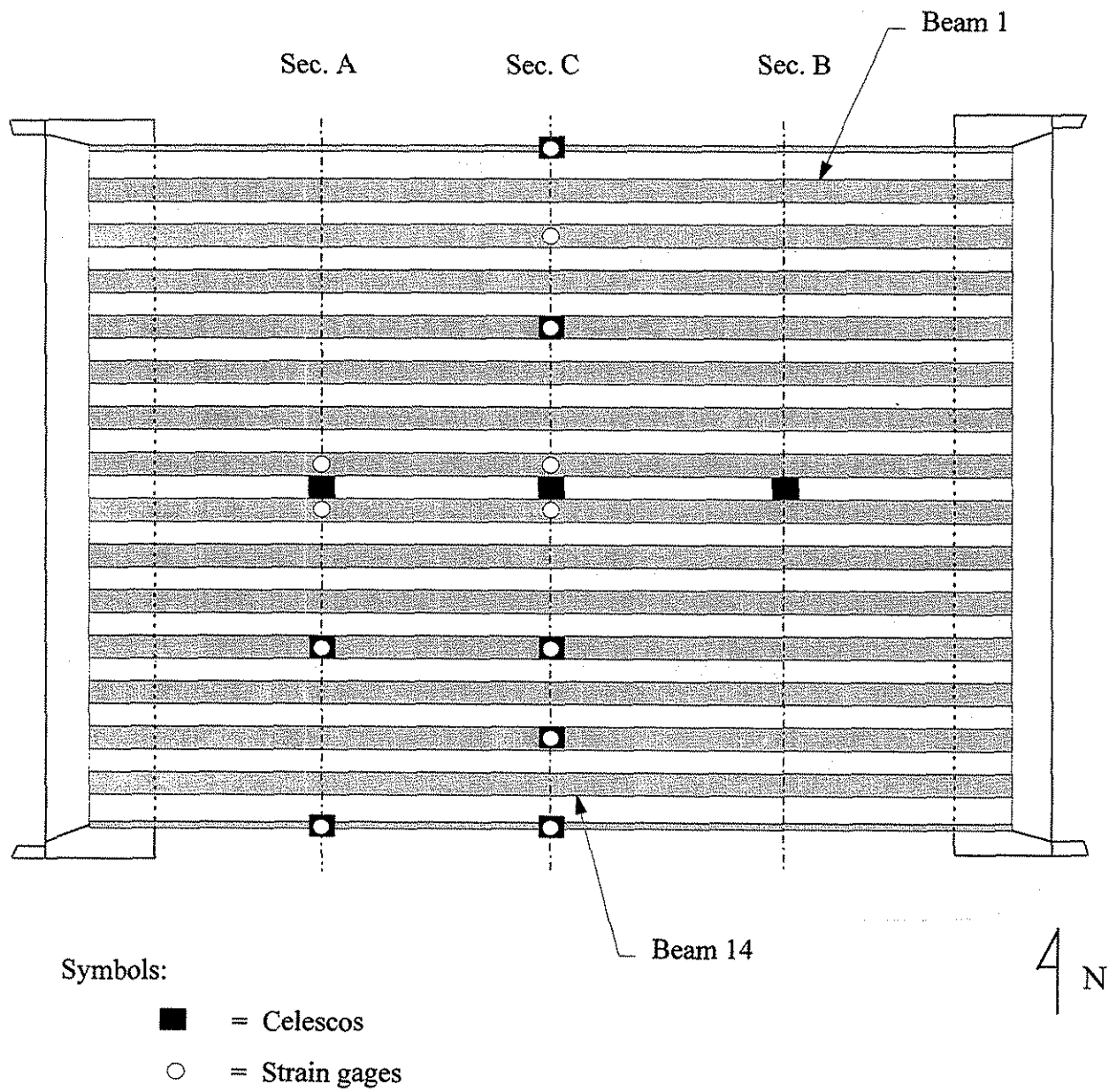


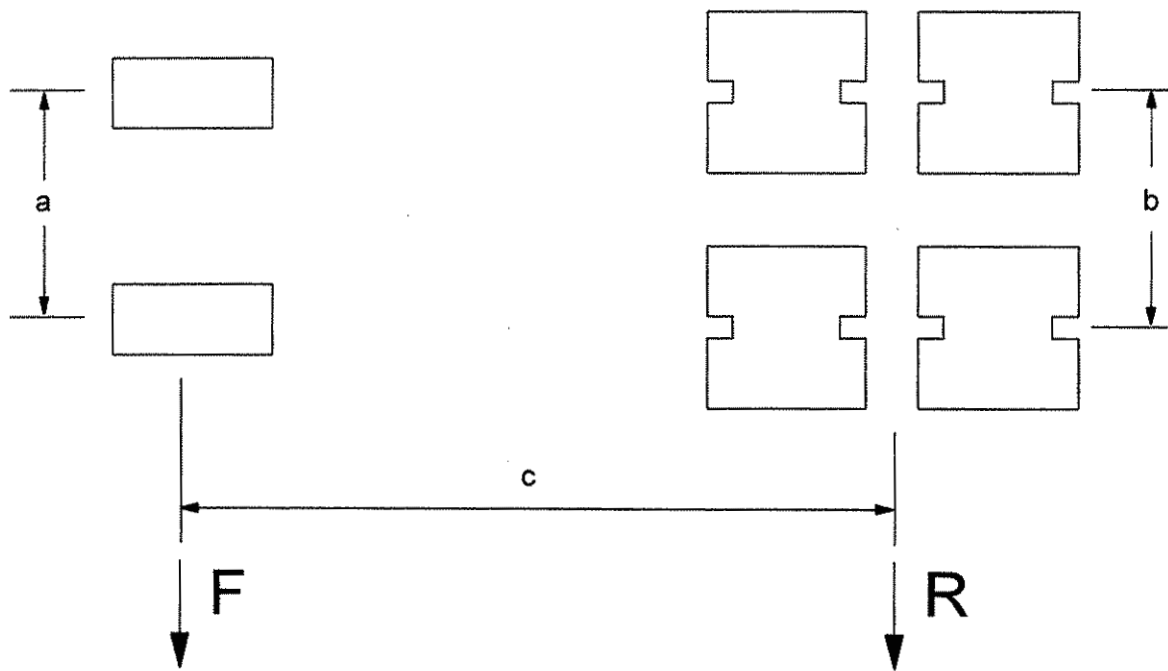
Fig. 3.11. Location of instrumentation -- field bridge.

of the 8 mid-span strain locations by the sum of the eight strain measurements across the mid-span. Thus, this moment fraction was calculated only for the eight instrumented beams. There are a total of 16 beams in the field bridge, so to calculate the actual moment fraction over the bridge width, the calculated moment fraction must be divided by two.

The two trucks used to load the bridge are illustrated in Fig. 3.12. For ease in positioning the trucks, the rear tandem axles straddled the line of interest, whether it be the quarter point, centerline, etc. The loading points are shown in Fig. 3.13. The symbols indicate the position of the center of the rear tandem axles. The trucks were positioned on the bridge heading east; therefore, for convenience in referring to positioning, the 1/4 point is labeled Section A, the 3/4 point Section B, and the centerline Section C in Fig. 3.13b.

As shown in Fig. 3.13a, five lanes, intending to maximize the loading effects of the trucks, were designated as test lanes in lanes 1 and 5, and the center of the outer tires were positioned 760 mm (2.5 ft) from the edge of the bridge. In lanes 2 and 4, the center of the inner tires were positioned 610 mm (2 ft) from the longitudinal bridge centerline, and in lane 3, the truck was centered on the longitudinal centerline. Photographs of the truck(s) on the bridges are shown in Fig. 3.14.

Each of the eight tests conducted consisted of recording strain and deflection data with the truck(s) positioned in a given lane at each of the three sections (Section A, B or C). Table 3.1 defines each test; refer to Fig. 3.12 for information on the trucks and Fig. 3.13a for the lane numbers. Each test in the table is designed to produce a maximum effect, or provide symmetry data on the bridge. For example, Test 1 is designed to determine the extent of symmetry the bridge has throughout its width. Test 2 is designed to maximize the load on interior beams, while Test 3 maximizes the load on the exterior beams. Tests 4-8 are designed to determine the effect of a single vehicle on the bridge at various locations.



Vehicle	a (in.)	b (in.)	c (in.)	F (kips)	R (kips)	Total (kips)
1	83.0	72.0	178.5	17.70	34.48	52.18
2	81.0	72.0	184.5	18.82	31.06	49.88

Fig. 3.12. Wheel configuration and weight distribution of test vehicles.

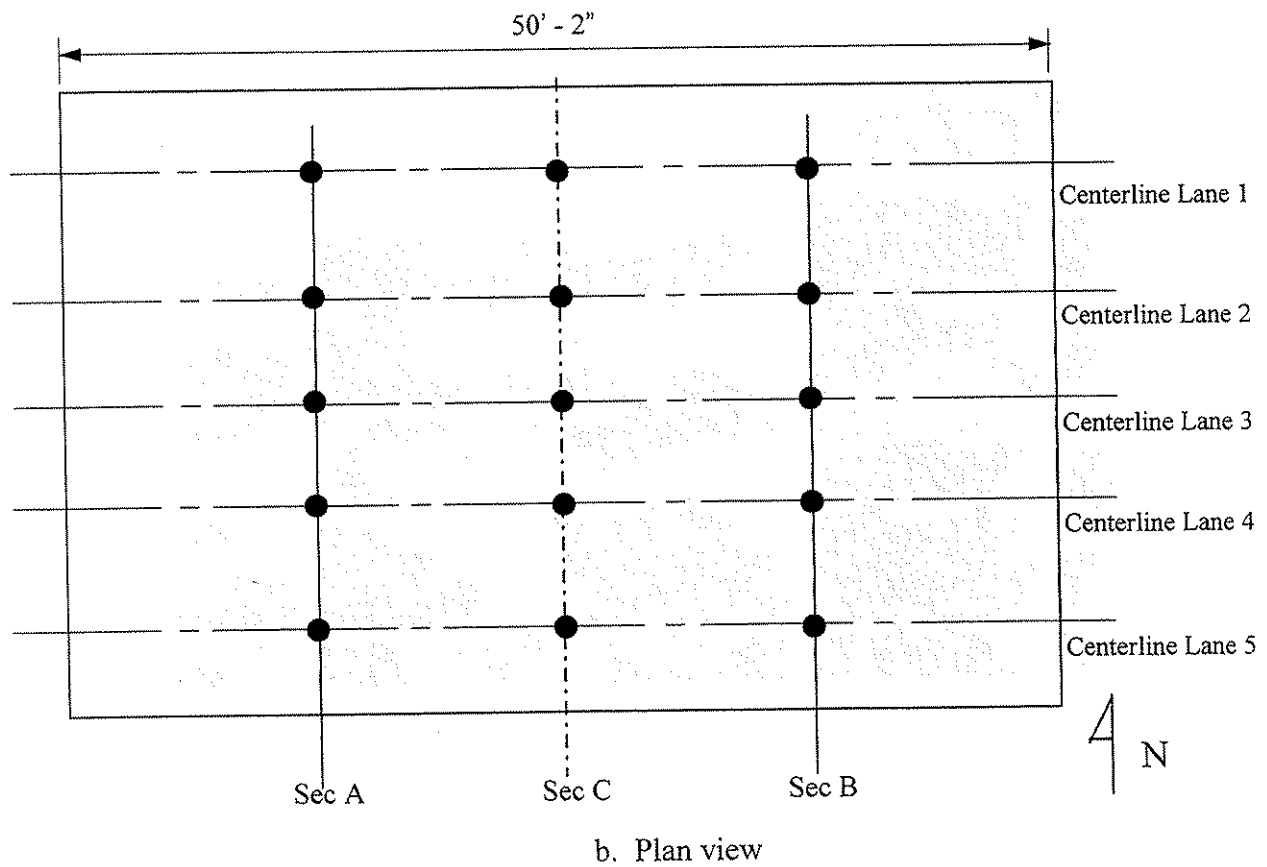
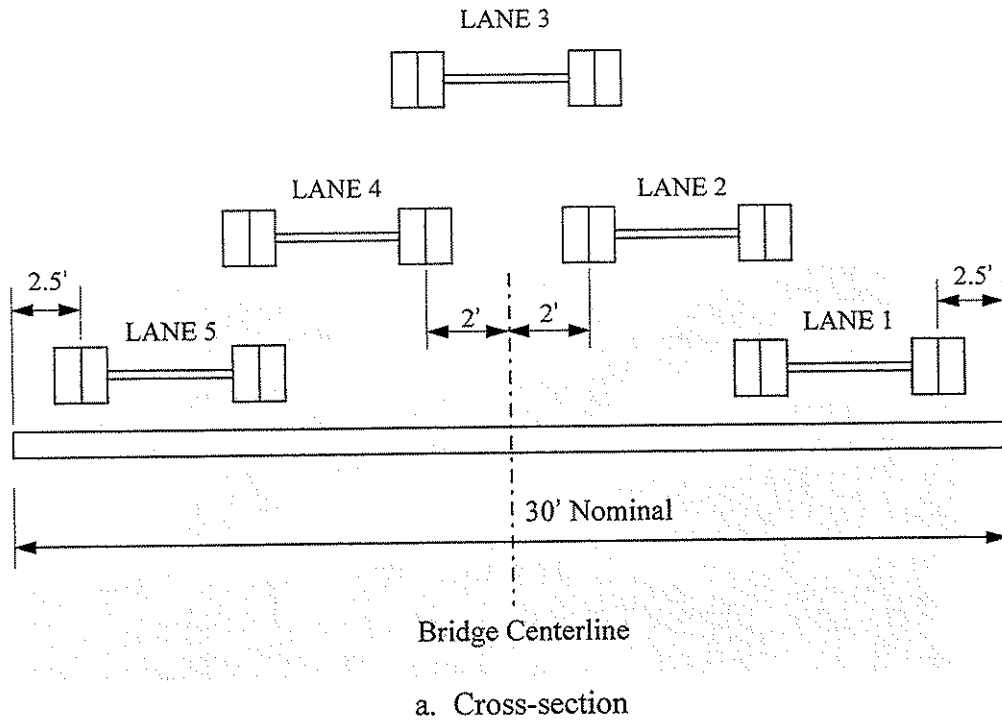
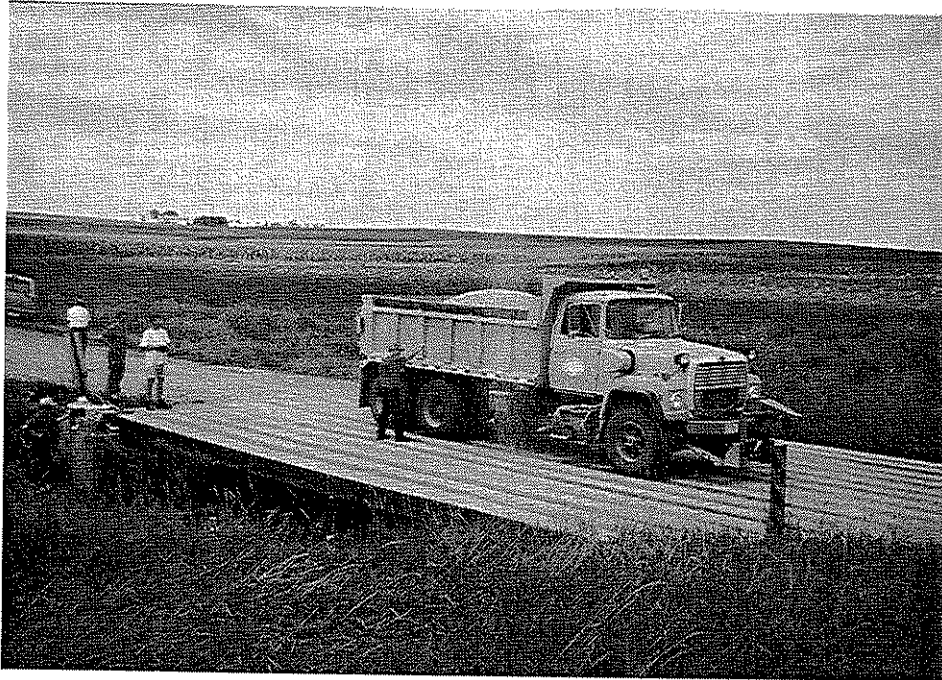
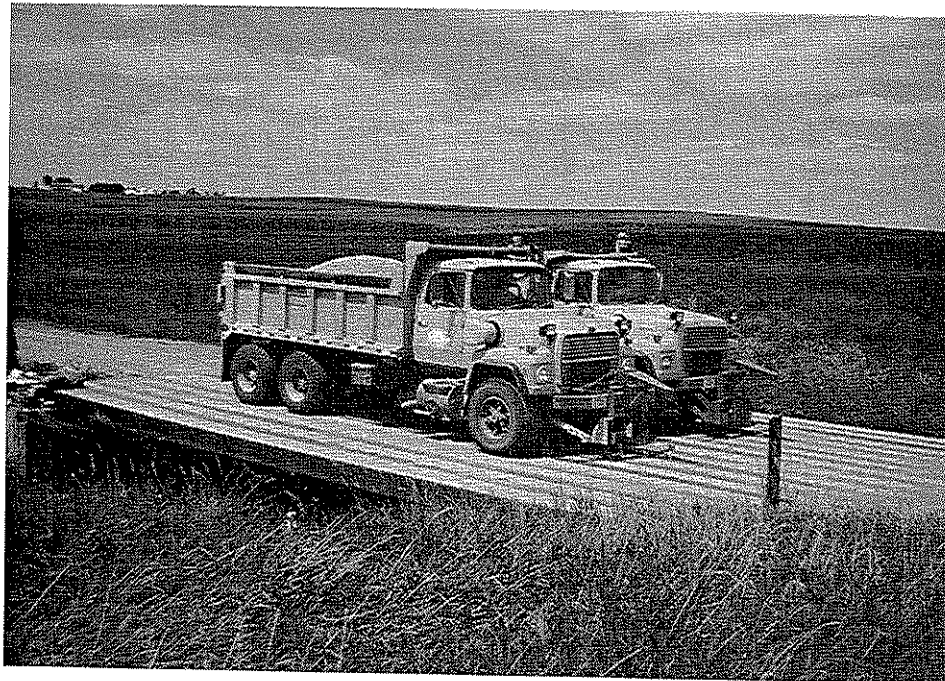


Fig. 3.13. Location of test vehicles.



a. Test vehicle in lane 3



b. Test vehicles in lanes 2 and 4

Fig. 3.14. Photographs of test vehicles on bridge.



Table 3.1. Test designations for BISB field tests.

Test Number	Truck Number (s)	Lane (s)
1	1	3
2	1	4
	2	2
3	1	5
	2	1
4	1	1
5	1	2
6	1	3
7	2	5
8	2	4

Data were recorded by the following procedure:

- Zero the DAS readings, including all the strain and deflection readings.
- Position the truck(s) in the desired lane(s) at Section A, B, or C.
- Record strain and deflection data for truck in desired position.
- Remove truck from bridge and record second zero

This procedure was repeated until data were obtained for all the predetermined locations of the trucks.

#### 4. BEAM-IN-SLAB BRIDGE GRILLAGE ANALYSIS

The grillage method of analysis was selected for modeling the BISB system. The term "grillage analogy" is used to describe an assembly of one-dimensional beams which are subjected to load acting perpendicular to the plane of the assembly (16). Grillage analysis differs from plane frame analysis in that the torsional rigidities are incorporated into the analysis. To perform the analysis, a finite element program was used; ANSYS 5.3 (17) was chosen because it has a large number of different types of elements available.

##### 4.1 Element Types

The FEM of the BISB used two different types of elements for the components in the bridge system. The element types are described in the ANSYS 5.3 Users Manual (17).

###### 4.1.1 BEAM4 Element

From the ANSYS 5.3 Users Manual:

"BEAM4 is a uniaxial element with tension, compression, torsion, and bending capabilities. The element has six degrees of freedom at each node; translation in the nodal x, y, and z directions and rotations about the nodal x, y, and z axes."

"The geometry, node locations, and coordinate system are shown (see Fig 4.1). The element is defined by two or three nodes, the cross-sectional area, two area moments of inertia (IZZ and IYY), two thicknesses (TKY and TKZ), an angle of rotation about the element x-axis, the torsional moment of inertia, and the material properties."

"The beam must not have zero length or area. The moments of inertia, however, may be zero if large deflections are not used. The beam can have any cross-sectional shape for which the moments of inertia can be computed. The stresses, however, will be determined as if the distance between the neutral axis and the extreme fiber is one-half of the corresponding thickness."

###### 4.1.2 BEAM44 3-D Tapered Unsymmetric Beam Element

From the ANSYS 5.3 Users manual:

"BEAM44 is a uni-axial element with tension, compression, torsion, and bending capabilities. The element has six degrees of freedom at each node: translations in the nodal x, y, and z directions and rotations about the nodal x, y, and z axes (see Fig. 4.2). The element allows different unsymmetrical geometry at each end and permits the end nodes to be offset from the centroidal axis of the beam."

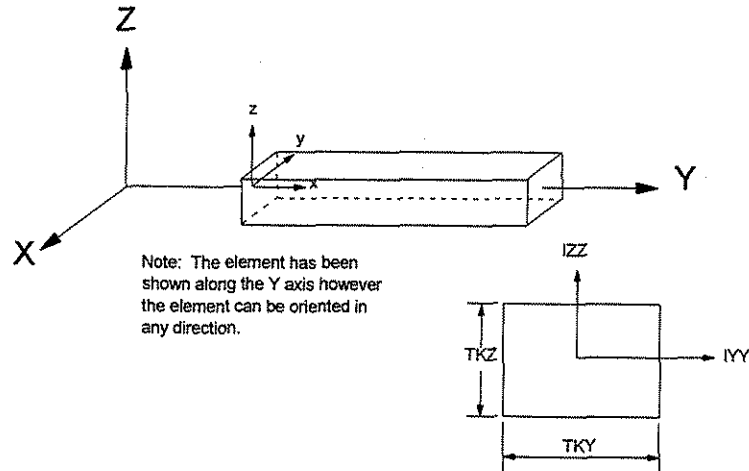


Fig. 4.1. Geometry of BEAM4 element.

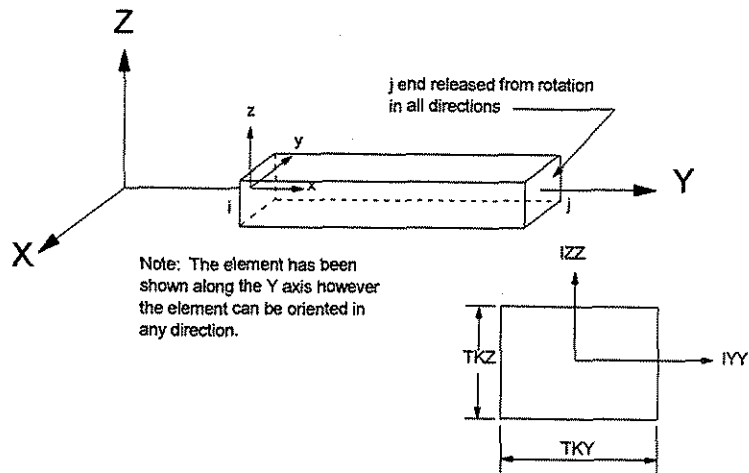


Fig. 4.2. Geometry of BEAM44 element.

There are options with ANSYS that allow element stiffness releases at the nodes in the element coordinate system. Releases should not be such that that free-body motion could occur.

## 4.2 Grillage Analogy Model

The grillage analogy model consisted of a grid of longitudinal beams and transverse beam elements. The longitudinal beams simulated the longitudinal flexural

stiffness and torsional stiffness of the steel beam and concrete deck, which is assumed to have participated in the longitudinal load resistance. The ANSYS BEAM4 element was used to characterize the longitudinal member. The transverse beams in the grillage simulated the transverse stiffness and torsional stiffness of the concrete deck. The ANSYS BEAM44 element was used to characterize the transverse member. A typical grillage for the BISB system is shown in Fig. 4.3.

The response of the grillage model is affected by some basic parameters, such as the spacing of the transverse beams, the end restraint of both the longitudinal and transverse beams, and the section properties (flexural and torsional) of both the longitudinal and transverse beams. To determine the appropriate choices for these parameters, sensitivity studies were performed. Following are the parametric values used in the study:

- Spacing of transverse beams at 5 mm, 8 mm, 15 mm, 30 mm, and 91 mm (2 in., 3 in., 6 in., 12 in., and 36 in.)
- Transverse beam end conditions (fixed and pinned).
- Transverse beam flexural stiffness (as a percentage of the contributory concrete area).
- Longitudinal beam end condition (fixed and pinned).
- Longitudinal beam flexural stiffness.
- Longitudinal beam torsional stiffness.

Regarding the appropriate longitudinal flexural stiffness, three different values were investigated. The modulus of elasticity of steel,  $E = 200 \text{ GPa}$  (29,000 ksi), was used and the moment of inertia was varied. The first value of the moment of inertia used was that of the steel beam alone, without regard to any contribution from the concrete. The second moment of inertia was based upon the calculated flexural stiffness of the two-beam BISB specimen, which is presented in the next chapter. The third value was based

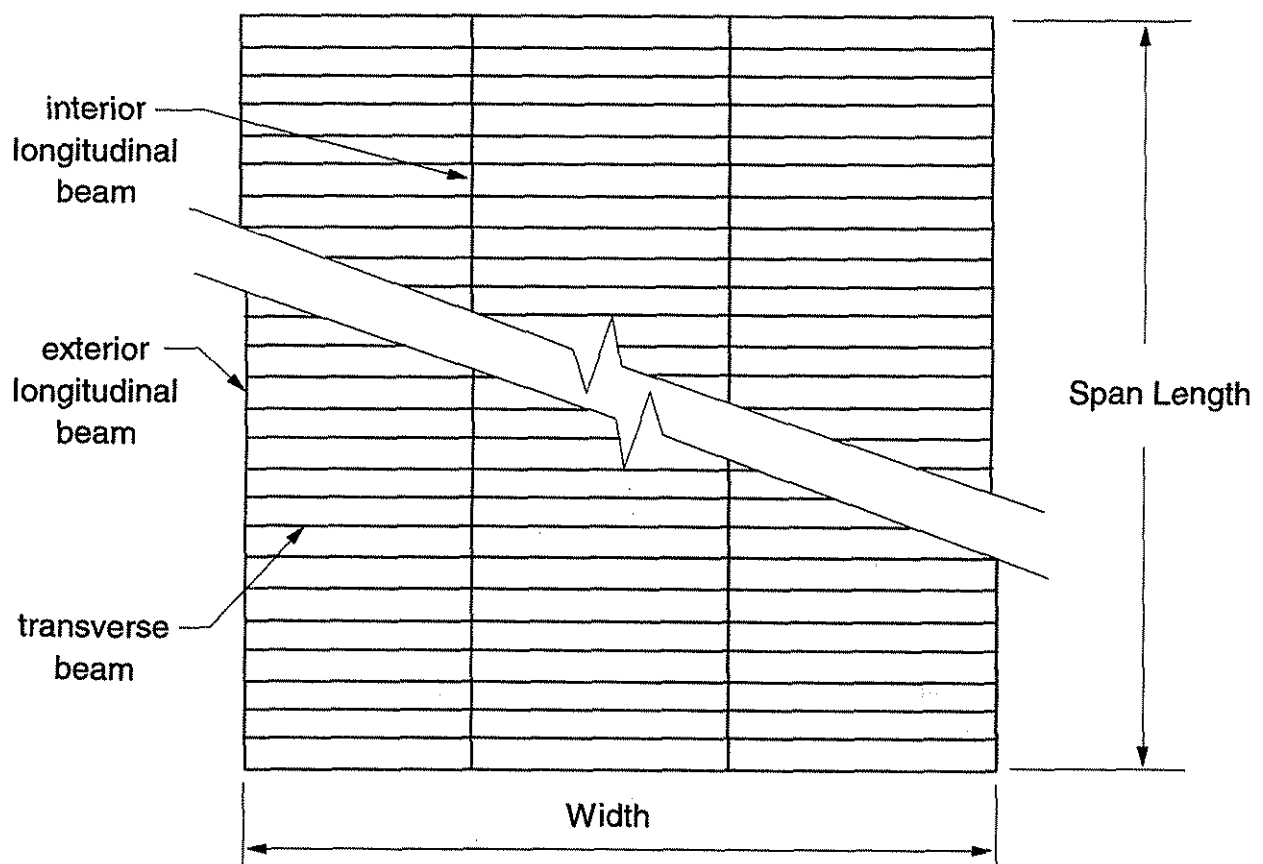


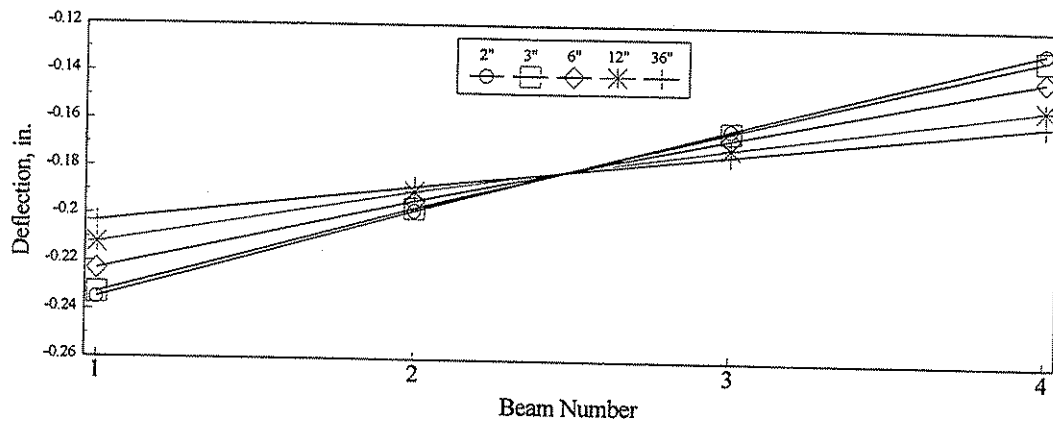
Fig. 4.3. Basic Grillage Model for BISB System.

upon recommendations by Jaeger and Bakht for slab and girder bridges (16). Their value assumes complete composite action between the concrete (based on contributory area) and the steel, and uses a transformed value for the entire concrete section. The modulus of elasticity of the concrete used for this and all subsequent transformations was  $E = 29$  GPa (4,200 ksi). Note that different values were calculated for the exterior and interior longitudinal beams because of the different amounts of contributing concrete. For the exterior beams, the moments of inertia for the three cases were  $1.76 \times 10^8 \text{ mm}^4$  (662 in<sup>4</sup>),  $3.08 \times 10^8 \text{ mm}^4$  (740 in<sup>4</sup>), and  $3.50 \times 10^8 \text{ mm}^4$  (840 in<sup>4</sup>). For the interior beams, the moments of inertia were  $1.76 \times 10^8 \text{ mm}^4$  (662 in<sup>4</sup>),  $3.41 \times 10^8 \text{ mm}^4$  (820 in<sup>4</sup>), and  $4.25 \times 10^8 \text{ mm}^4$  (1020 in<sup>4</sup>).

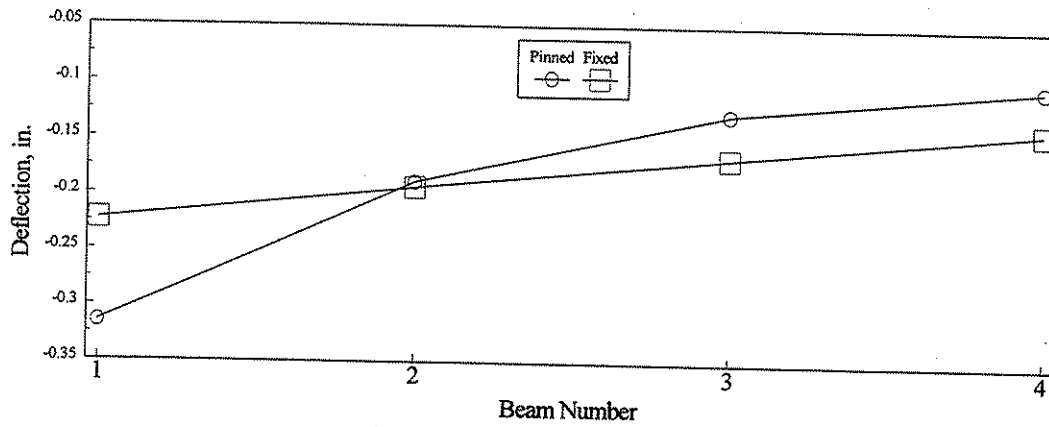
The torsional stiffness of the longitudinal beams was also studied by using the modulus of elasticity of steel and by varying the torsional moment of inertia. The first value assumed that the steel beam had a value of  $1.60 \times 10^6 \text{ mm}^4$  (3.84 in<sup>4</sup>). A second value based on recommendations by Jaeger and Bakht assumed that all of the concrete contributed to the torsional stiffness of the specimen, and a transformed section was used to calculate the torsional moment of inertia. The value of the torsional moment of inertia for the entire section was  $6.24 \times 10^7 \text{ mm}^4$  (150 in<sup>4</sup>). A third value midway between these two was also selected, resulting in a torsional stiffness of  $3.12 \times 10^7 \text{ mm}^4$  (75 in<sup>4</sup>).

The transverse beam properties were investigated assuming that only the contributory region concrete contributed strength. The study considered varying percentages (10 %, 25%, 50%, 75%, 90%, and 100%) of the transverse beam width (which varied depending on the assigned spacing of the transverse beams) as contributing to the transverse beam stiffness.

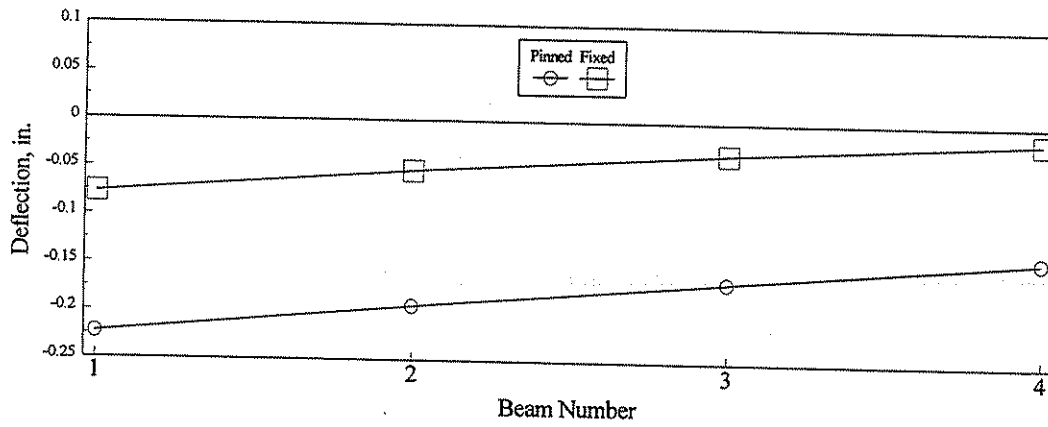
The sensitivity of the analytical response of a BISB system based on the four-beam BISB specimen described in Chp 2 of this report was also studied. In each of these analyses, an 89 kN (20 kips) load was applied at midspan of an exterior beam. The deflection data shown refer to the midspan deflections of each of the four beams. Figure 4.4a shows the effect of the transverse beams spacing. Large spacing increases the transverse stiffness. In Fig. 4.4b., the effect of the connection between the transverse and longitudinal beams is illustrated. As shown, the fixed connection has a greater transverse



a. Transverse beam spacing



b. Transverse beam end conditions



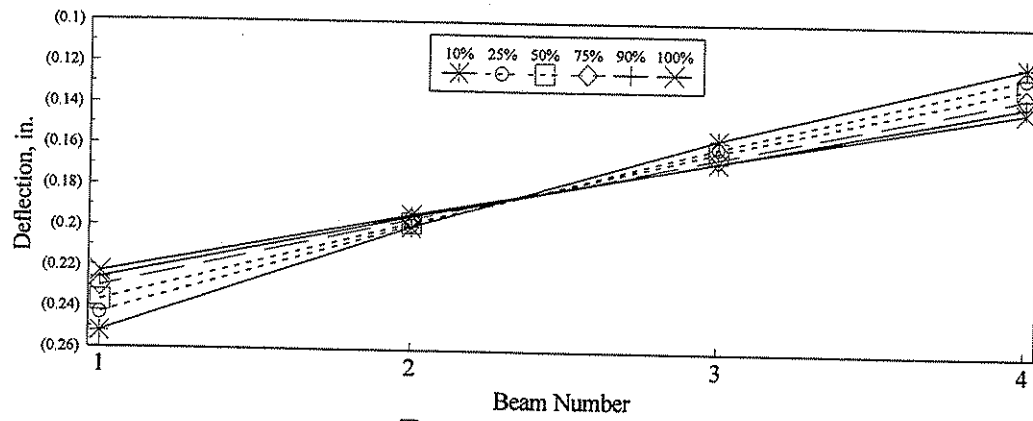
c. Longitudinal beam end conditions

Fig. 4.4. Sensitivity study results for basic parameters.

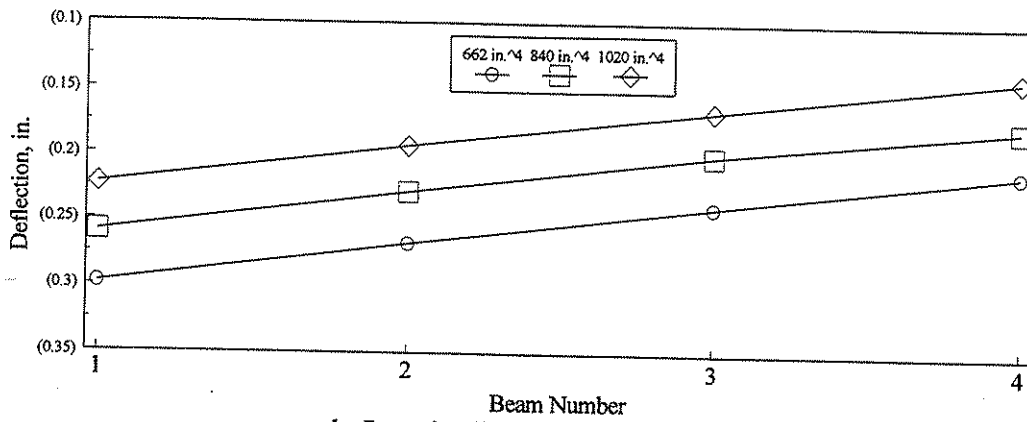
stiffness than the pin connection. The effect of the longitudinal beam support conditions is shown in Fig. 4.4c and, as expected, the deflections are significantly smaller when fixed end conditions are used.

The results of the study on the section properties for the transverse and longitudinal beams are shown in Fig. 4.5. As can be seen in Fig. 4.5a, the change in properties for the transverse members (defined as a percentage of the contributory concrete area) has a significant effect on the load distribution characteristics of the model. As expected, the larger the percentage of section used to determine the transverse beam properties, the greater the transverse load distribution. Figure 4.5b shows the variation among the three values for the flexural stiffness of the longitudinal beams. Figure 4.5c illustrates the effect of the different values of torsional moment of inertia upon the model.

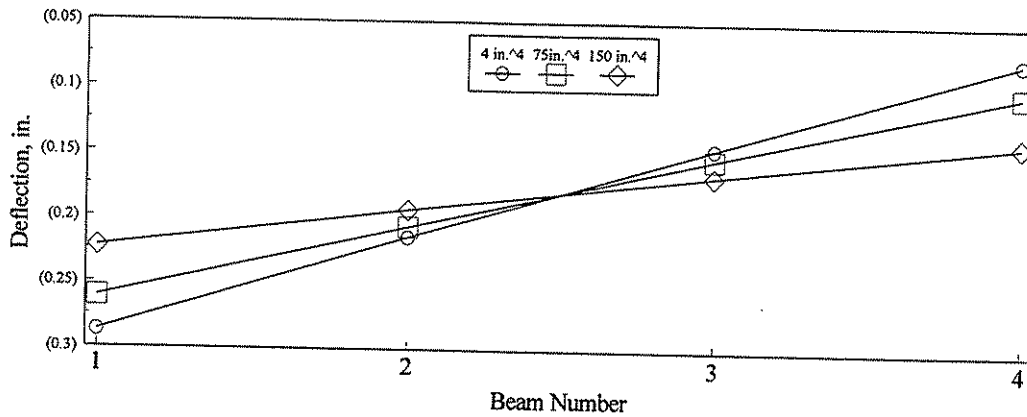




a. Transverse beam properties



b. Longitudinal beam flexural stiffness



c. Longitudinal beam torsional stiffness

Fig. 4.5. Sensitivity studies for beam properties.

## 5. EXPERIMENTAL AND ANALYTICAL RESULTS

### 5.1 Push-out Test Results and Theoretical Analysis

#### 5.1.1 Experimental Results

The data from the push-out test included slip, separation, plate movement, and ultimate load values for each specimen. Two measurements of slip were recorded; these were averaged to determine the average slip for a given shear connection. The majority of the specimens contained ten shear holes, five on each side, and thus the load per shear hole is 1/10 of the total load applied to the steel plate.

According to Yam (18), if the “uplift” of the slab from the beam, or separation, is “less than half the interface slip at the corresponding load level,” then this effect can be considered to have minimal effect on the connector behavior. All of the specimens tested exhibited separation less than 50% of the slip, with the majority falling below 25% of the slip. Based on this information, the separation was considered to be a negligible factor in the behavior of the connectors.

In two of the specimens, separation of approximately half the interface slip were recorded. This was most likely caused by the steel plate bearing on excess concrete not having been properly cleaned out of the voids created by the styrofoam. In two cases, the styrofoam insert slipped while pouring concrete, which allowed concrete to penetrate the void. An attempt was made to clean out the excess concrete; however, after testing, it was determined that the steel plate was not able to slip without resistance due to excess concrete in the void. Although data were recorded, the results from these two specimens have not been included in the final results.

Another concern with the testing procedure was the failure of the steel shear plate by bending under applied loading. The displacement of the steel plate was recorded at one point near the middle of the steel shear plate to determine if plate bending was occurring. In most cases, the displacement of the plate was less than 5% of the average slip, and thus determined to be insignificant in the behavior of the connectors.

In an attempt to eliminate some of the variables, the physical dimensions of the concrete slabs were kept constant and the same strength of concrete used. Although the same type and strength of concrete was ordered each time, the concrete strength ranged

from 34.70 MPa (5,040 psi) to 56.85 MPa (8,250 psi). Therefore, the experimental results are presented, along with results normalized for a concrete strength of 41.35 MPa (6,000 psi). Since shear is the main mechanism of failure, the  $\sqrt{f'_c}$  is used to convert the measured data to normalized data. This is done by using the following expression:

$$\text{Normalized value} = \text{Measured value} \times [6,000 \text{ psi}/(f'_c)]^{1/2} \quad (5.1)$$

where  $f'_c$  is the actual concrete compressive strength, and 6,000 psi is the desired concrete compressive strength. Normalizing the concrete strengths allowed for a direct comparison of the variables in the various series. Complete results are shown in Table 5.1. Results from Series 6 have been neglected due to inconsistent fabrication of the specimens. The reinforcing bar placed in the middle shear hole was welded instead of simply placed in the hole, thus preventing movement of the reinforcing bar. The average for the normalized maximum load for Series 6 was 465.5 kN (104.6 kips), a value that is too large based on the maximum loads of Series 4, 8, 9, and 10.

Results in Table 5.1 indicate that Series 4, 8, 9, and 10 far exceeded the load carrying capacity of the other series. All of the specimens in Series 4, 8, 9, and 10 were at or near 445 kN (100 kips) for the normalized maximum load. Initial slip data, however, showed that the connections without reinforcement through the shear holes provided a stiffer connection. Series 1, without reinforcement through the shear holes, had an initial slip of 1,275 kN/mm (7,290 kip/in.), whereas values for Series 4, 8, 9, and 10, with reinforcement through the shear holes, varied from 795 kN/mm (4,550 kip/in.) to 990 kN/mm (5,650 kip/in.). Therefore, although the reinforcing bar added strength to the shear connection, the reduction in shear hole area by inserting the reinforcement in the hole reduced the stiffness of the shear connection.

Table 5.1. Push-out test results.

Series	$f'_c$ (psi)	Maximum Load (kips)	Initial Slip (kip/in. x $10^3$ )	Maintenance at 0.3 in. Slip Percent of Maximum Load	Normalized Maximum Load (kips)
1	6790	77.8	7.29	90.1	73.1
2	8250	91.0	8.75	81.9	77.6
3	8250	60.2	4.40	79.2	51.3
4	6480	98.8	5.43	89.4	95.1
5	6480	84.2	5.68	85.9	81.0
7	5380	7.7	--	73.3	8.1
8	5040	86.5	5.10	75.4	94.4
9	5040	92.1	5.65	81.7	100.5
10	5500	89.7	4.55	91.5	93.7
11	5500	40.0	--	88.3	41.8

Note: 1 psi = 6.89 kPa  
1 kip = 4.45 kN

1 kip/in. = 0.175 kN/mm  
1 in. = 25.4 mm

It can also be seen in Table 5.1 that all of the specimens maintained a large percentage of the maximum load up to an average slip of 7.6 mm (0.3 in.). It was at this point in the tests that the load carrying capacity of the shear connection began to decrease rapidly in the weaker connections, and thus an average slip of 7.6 mm (0.3 in.) was selected as the magnitude of slip for load maintenance after failure of the shear connection.

Figure 5.1 presents a comparison of the variables investigated as follows: size of holes, spacing of holes, alignment of holes, inclusion of reinforcing steel in holes, and effects of "sloppy" craftsmanship. These graphs are based on a normalized concrete strength of 41.35 MPa (6,000 psi). Three items of interest may be observed in these graphs. First, all of the specimens with shear holes demonstrated a nearly linear phase up to the point of maximum load. This linear phase is noted as the initial slip in Table 5.1,

and represents the stiffness of the connection up to the point of maximum load.

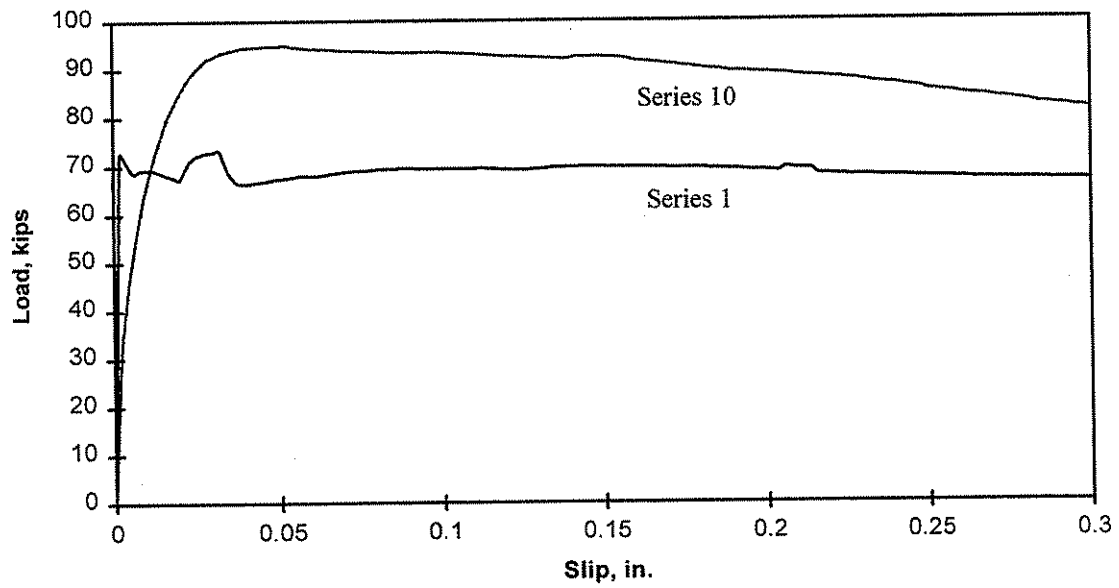
Generally, the maximum load is reached at an average slip of between 0.25 mm (0.01 in.) and 1.0 mm (0.04 in.). After the maximum load is reached, the connection weakens and slips at an increasing rate as the load gradually decreases. In most of the tests, over 80% of the maximum load was maintained at an average slip of 7.6 mm (0.3 in.). This is what sets the shear hole connector apart from other types of shear connectors. Not only can the connector resist a large amount of shear, but upon reaching its maximum capacity, the connector continues to resist large amounts of shear, thereby preventing a sudden failure.

Figure 5.1a. presents a comparison of Series 1 with Series 10. In Series 10, a #4 reinforcing bar was added to the middle shear hole. In each of the two series, the shear holes were 32 mm (1 1/4 in.) in diameter, and were spaced on 76 mm (3 in.) centers (refer to Fig. 2.2).

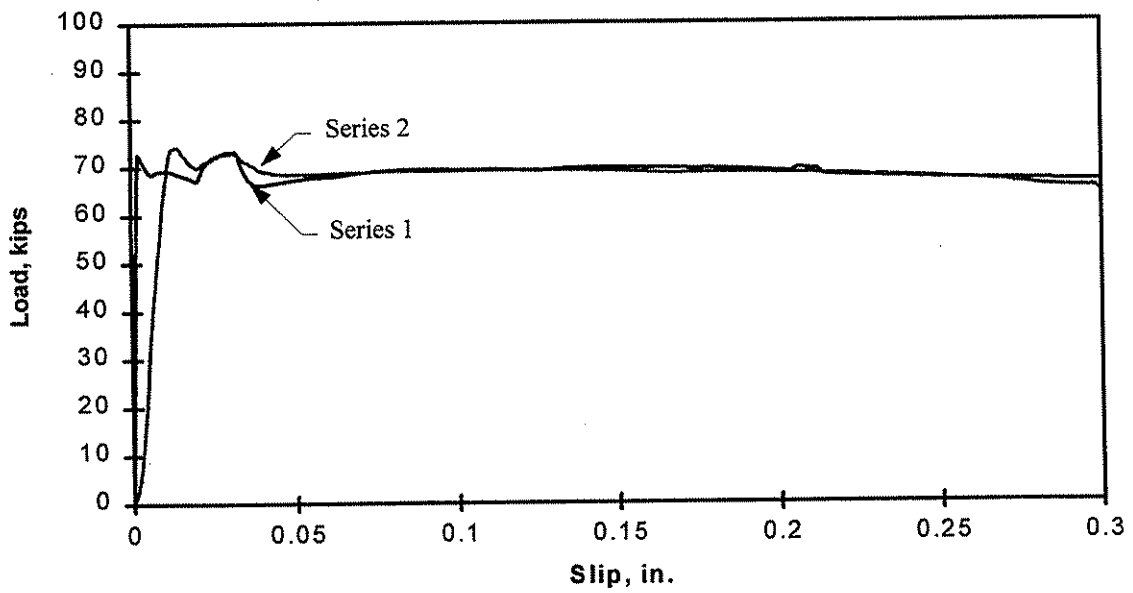
The strength of the connection is greatly increased by the addition of a reinforcing bar through one of the holes. Not only did the strength increase nearly 89 kN (20 kips), but the strength was slightly better maintained at a slip of 7.6 mm (0.3 in.). However, as previously noted, the series without the reinforcing bar through the shear hole provided a stiffer connection up to the point of maximum load. Series 1 reached its maximum load at an average slip of less than 0.25 mm (0.01 in.), whereas Series 10 reached its maximum load at an average slip of approximately 1.0 mm (0.04 in.).

Figure 5.1b involved Series 1 and Series 2 where the hole diameter (32 mm (1 1/4 in.)) was kept constant, but the spacing of the shear holes was reduced from 76 mm (3 in.) to 51 mm (2 in.). Previous research by Oguejiofor and Hosain (8) had indicated that the strength would increase with increased spacing up to two times the diameter of the shear hole. However, after normalizing the strength data for a concrete strength of 41.35 MPa (6,000 psi), there was no significant difference between the maximum loads obtained for Series 1 and Series 2.

Data in Fig. 5.1c indicates that strength increased approximately 50% when the shear hole diameter was increased from 19 mm (3/4 in.) to 32 mm (1 1/4 in.), an area increase of 67%, while all other variables were held constant (comparison of Series 3 to

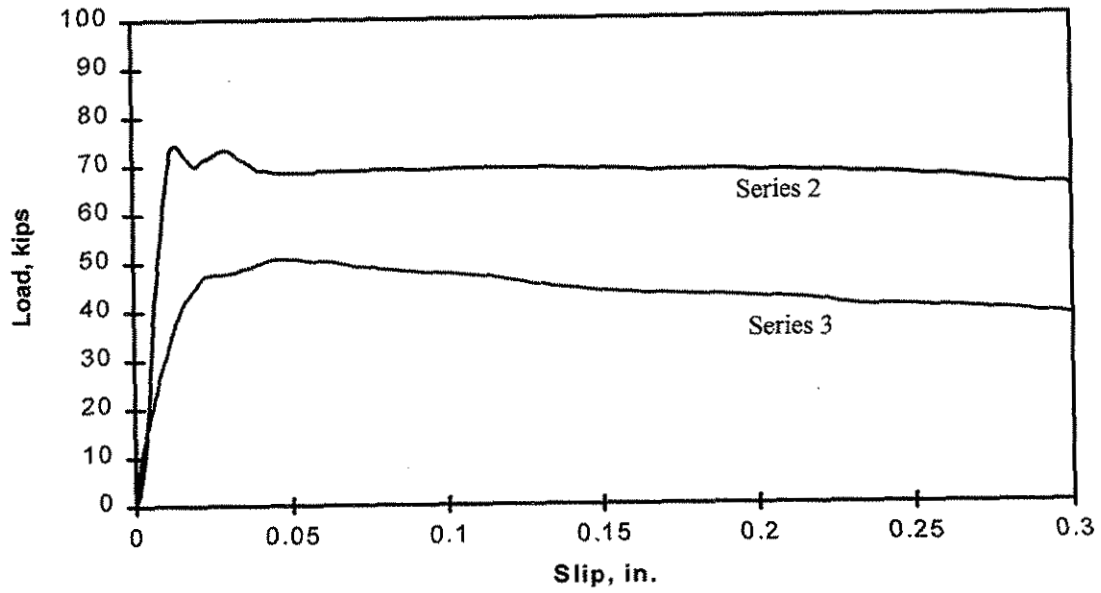


a. Load slip curves for Series 1 and 10

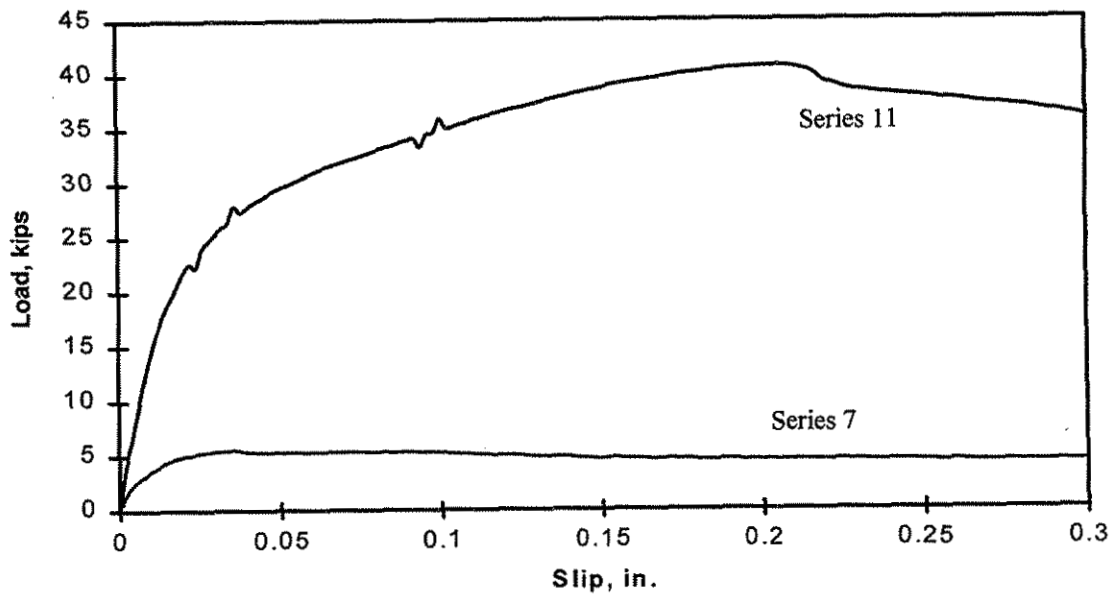


b. Load slip curves for Series 1 and 2

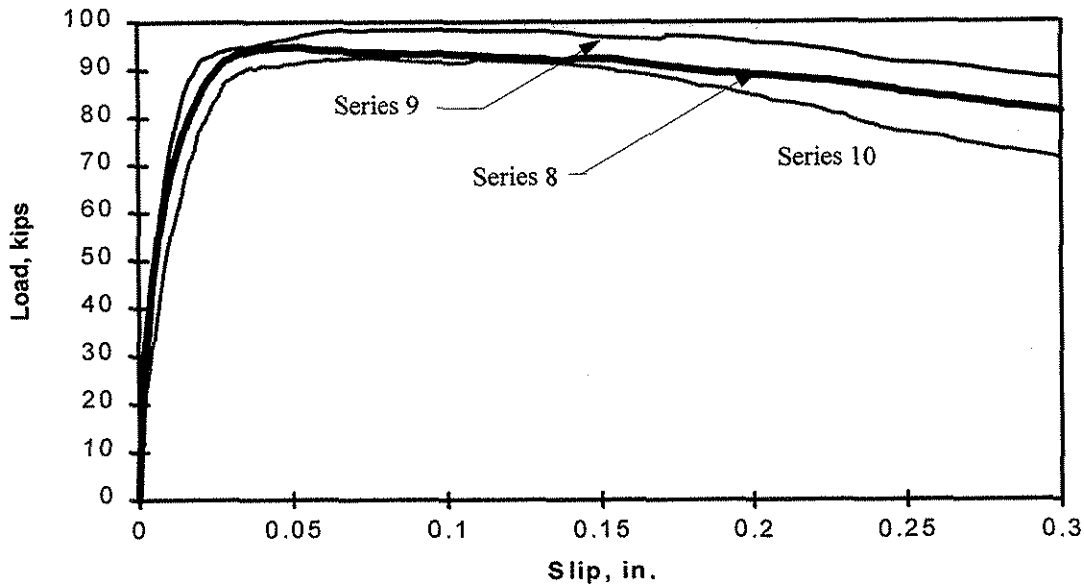
Fig. 5.1. Load slip curves for various test sequences.



c. Load slip curves for Series 2 and 3



d. Load slip curves for Series 7 and 11



e. Load slip curves for Series 8, 9, and 10

Fig. 5.1. Continued.

Series 2). Likewise, the stiffness of the connection almost doubled with the area increase of 67% (770 kN/mm (4,400 kip/in.) to a stiffness of 1,530 kN/mm (8,750 kip/in.)). Both of the connections maintained approximately 80% of the maximum load at a slip of 7.6 mm (0.3 in.). However, increasing the shear hole area is not always the answer when additional strength is necessary. The shearing of the concrete dowel is the desired failure mechanism; thus, increasing the dowel area beyond the bearing strength of the concrete dowel or shearing strength of the steel between the holes could cause a sudden failure instead of the desired gradual failure.

Illustrated in Fig. 5.1d is the shear resistance of the steel alone in contact with the concrete (Series 7), and the shear resistance of a portion of one hole with a reinforcing bar placed through the hole (Series 11). These two graphs indicate a significant increase in shear strength by the addition of a portion of a hole and a reinforcing bar. This demonstrates that, although the shear holes carry much of the shear load, the addition of a reinforcing bar can significantly increase the load carrying capacity of a shear connector.



Neither of these two graphs demonstrate the linear relationship between load and slip up to maximum load, and therefore the stiffness of the corresponding series cannot be compared.

Lastly, a series of tests were completed, varying only the manner in which the holes were manufactured. Data from specimens with drilled holes (Series 10), torched holes (Series 8), and poorly torched holes (Series 9) are compared in Fig. 5.1e. After adjusting the results for a concrete strength of 41.35 Mpa (6,000 psi), the maximum loads for all the specimens in this sequence were within 8% of each other. The slightly higher strength associated with the torched holes could be due to a small increase in the hole area caused by the inaccuracies associated with torching rather than drilling. In addition, the stiffness of all three series were within 20% of each other. The lower values associated with maintenance of the maximum load for Series 8 and 9 (75.4% and 81.7%, respectively) in comparison with Series 10 (91.5%) could be explained by the lower concrete strength in Series 8 and 9 (34.7 Mpa (5,040 psi) compared to 37.9 Mpa (5,500 psi)) for Series 10.

#### 5.1.2 Analysis of Experimental Results and Development of Strength Equation

From the results of the tests, it was determined that the strength of the ASC was influenced by five items: concrete compressive strength, the friction between the steel plate and the concrete, the concrete dowel formed by concrete, the reinforcing bar placed through the shear hole, and the transverse slab reinforcing. From the results of the pushout tests, it was determined that hole spacing was not an important influence on the strength of the connection if the spacing was at least 1.6 times the hole diameter. Therefore, spacing of the shear holes was not included in the design equation; the design equation is only valid for hole spacings greater than 1.6 times the shear hole diameter. Using data from the push-out tests, an equation was developed that can predict the shear strength of the ASC.

To determine the shear capacity of a stud connector based on the resistance of the concrete slab to longitudinal splitting, Davies (10) developed the following equation:

$$q = 8.5A_{cc}\sqrt{u_w} + 2.4A_{tr}f_{yr} \quad (5.2)$$

where:

$q$  = shear capacity per perfobond rib connector, lbf.

$A_{cc}$  = shear area of concrete per connector, in<sup>2</sup>.

$u_w$  = concrete cube strength, psi.

$A_{tr}$  = area of transverse reinforcement, in<sup>2</sup>.

$f_{yr}$  = yield strength of reinforcement, psi.

The longitudinal splitting of the specimens in tests performed by Davies is similar to that observed in the push-out tests in this investigation. Therefore, his equation was used as a basis for deriving a similar equation for the ASC.

The two terms of Davies' equation account for the contribution of the concrete slab and the transverse reinforcement, respectively. Since the push-out specimen are subjected only to direct stress, the potential of the slab to resist longitudinal splitting would be dependent on the concrete strength, and the amount and strength of transverse reinforcement. In addition, this investigation plus those of other researchers have shown that the concrete dowel formed through the shear hole, as well as a reinforcing bar placed through the hole, will contribute to the capacity of the shear connection. Therefore, a modification of the equation developed by Davies to incorporate these additional strength parameters was developed. This modified equation follows:

$$q = \beta_1 A_s \sqrt{f'_c} + \beta_2 A_r f_{yr} + n(\beta_3 A_{tr} f_{yr} + \beta_4 A_{cd} \sqrt{f'_c}) \quad (5.3)$$

where:

$A_s$  = Total area of steel in contact with the concrete, in<sup>2</sup>.

$f'_c$  = Concrete compressive cylinder strength, psi.

$A_r$  = Area of reinforcing bar through shear holes, in<sup>2</sup> per five holes.

$f_{yr}$  = Yield strength of reinforcing bar, psi.

$A_{tr}$  = Area of transverse reinforcement per hole divided by two, in<sup>2</sup>.

$f_{ytr}$  = Yield strength of the transverse reinforcement, psi.

$A_{cd}$  = Shear area of each concrete dowel, in<sup>2</sup>.

$n$  = Number of concrete dowels.

$q$  = strength of ASC, lbs.

$\beta_1, \beta_2, \beta_3, \beta_4$  = constants.

The equation has been modified to include the more traditional concrete compressive strength,  $f'_c$ , instead of the cube strength,  $u_w$ . The term  $A_{tr}$  has been divided by two because two layers of transverse reinforcement were used in the design of the push-out specimens. A diagram illustrating the variables  $A_s$ ,  $A_{tr}$ , and  $A_{cd}$  is shown in Fig. 5.2.

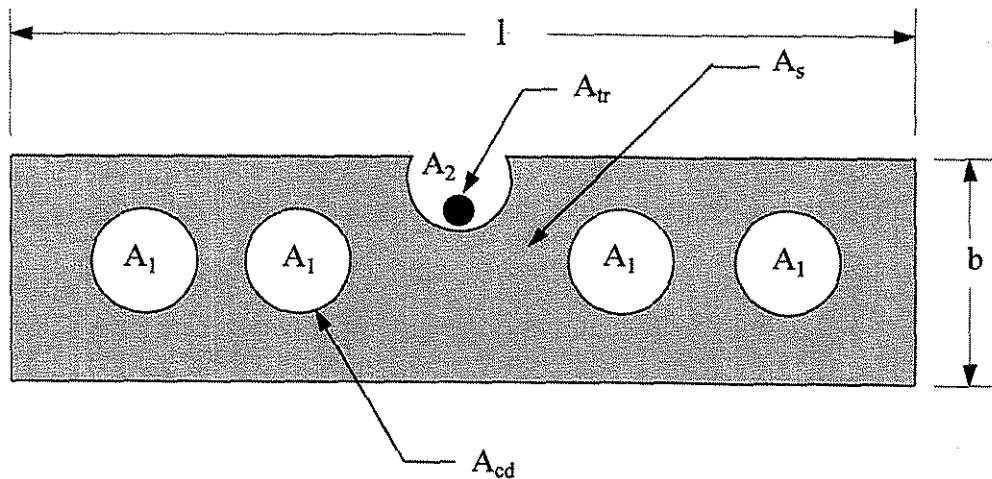


Fig. 5.2. Illustration of equation variables.

The equations for  $A_s$ , and  $A_{cd}$  are as follows:

$$A_s = 2(bl - 4A_1 - A_2) \quad (5.4)$$

$$A_{cd} = 2(\pi d^2/4) \quad (5.5)$$

By reviewing beam sizes that might be used for bridge stringers, it was determined that the smallest web thickness that might be encountered in the field would be approximately 9.5 mm (3/8 in.). Therefore, steel plate thickness was not included as a variable; the expression developed will thus result in conservative strength values for web

variable; the expression developed will thus result in conservative strength values for web thicknesses greater than 9.5 mm (3/8 in.). Additionally, as previously noted, the holes must be spaced at least 1.6 times the diameter of the shear hole so that the stress fields do not overlap, causing a decrease in strength.

The  $\beta_1$ ,  $\beta_2$ ,  $\beta_3$ , and  $\beta_4$  in Eqn. 5.3 are constants that were determined statistically from the experimental results. The personal computer version of Mathcad was used to solve for the most fitting equation from the experimental data. For each series, the experimental strength was used as strength  $q$  in Eqn. 5.3, and the constants,  $\beta_1$ ,  $\beta_2$ ,  $\beta_3$ , and  $\beta_4$ , were determined for the geometry of each shear hole connection. The values of these constants were determined as follows:  $\beta_1 = 0.618$ ,  $\beta_2 = 0.354$ ,  $\beta_3 = 0.353$ ,  $\beta_4 = 19.050$  to three decimal places. Practical values of these constants which lower the theoretical strength,  $q$ , by approximately 0.5% are used in Eqn. 5.6, which may be used to predict the shear strength of this type of connector.

$$q = 0.62 A_s \sqrt{f'_c} + 0.35 A_t f_{yt} + n (0.35 A_{tr} f_{yt} + 19 A_{cd} \sqrt{f'_c}) \quad (5.6)$$

Since the concrete dowels are subjected to double shear, the term  $A_{cd}$ , the total shear area, would be calculated as  $2(\pi d^2/4)$  where  $d$  is the diameter of the shear hole in inches. Likewise, the steel is in contact with the concrete on both sides; thus,  $A_s$  is two times the cross-sectional area of the steel in contact with the concrete. If different areas are used in the same shear connector, Eqn. 5.6 can be modified using  $n_1$  (number of holes of area 1),  $n_2$  (number of holes of area 2), etc., so that only the portion of Eqn. 5.6 in parentheses needs to be modified.

Comparisons of the results obtained from the preceding analysis to actual strength data are presented in Table 5.2. Series 6 is excluded from the table for previously stated reasons. Series 7 and 11 are also excluded from the table, as these two series were only performed to obtain information on the steel-concrete friction (Series 7) and to determine the effect of passing the reinforcement through the shear holes (Series 11).

As can be seen, Eqn. 5.6 accurately predicts the strength of the ASC to within 10% of the measured strength in most cases. Note that Eqn. 5.6 provides failure

strengths. Thus, an appropriate factor of safety will be needed before the equation values can be used in design.

Table 5.2. Theoretical Strengths vs. Experimental Strengths.

Series Number	Experimental Strength (kips)	Theoretical Strength (kips)	Percent Difference
1	77.8	88.3	-13.60
2	91.0	93.0	- 2.28
3	60.2	66.7	-10.66
4	98.8	87.1	11.80
5	84.2	87.1	-3.33
8	86.5	84.0	3.00
9	92.1	84.0	9.50
10	89.7	85.6	4.67

### 5.1.3 Sensitivity Study of Theoretical Strength Equation

An analysis was conducted to determine the contribution of each of the four terms in Eqn. 5.6. The results of this part of the sensitivity study are presented in Table 5.3.

Overall, Terms 1-4 contribute an average of 8.9%, 2.6%, 50.8%, and 38.2%, respectively, to the theoretical strength of the ASC. As can be seen, Term 2 could conservatively be eliminated from Eqn. 5.6 without significantly reducing the theoretical strength.

Equation 5.6 involves five variables, which influence the shear strength of the ASC: hole size, amount of reinforcing steel through the shear holes, amount of transverse slab reinforcement, concrete strength, and number of shear holes. To determine the influence of these variables, several sensitivity analyses were completed and presented in Figs. 5.3-5.6.

Table 5.3. Results of sensitivity investigation.

Series Number	Term 1 (kips)	Term 2 (kips)	Term 3 (kips)	Term 4 (kips)	Total Strength (kips)
1	7.4	0	42.4	38.6	88.3
2	8.2	0	42.4	42.5	93.0
3	9.0	0	42.4	15.3	66.7
4	7.3	2.3	42.4	35.1	87.1
5	7.3	2.3	42.4	35.1	87.1
8	6.5	4.2	42.4	30.9	84.0
9	6.5	4.2	42.4	30.9	84.0
10	6.7	4.2	42.4	32.3	85.7

Note: Term 1 =  $0.62 A_s \sqrt{f'_c}$

Term 3 =  $0.35 n A_{tr} f_{tr}$

Term 2 =  $0.35 A_{tr} f_{tr}$

Term 4 =  $19 n A_{cd} \sqrt{f'_c}$

Figure 5.3 shows the sensitivity of the shear strength to an increase in the shear hole area. In this figure, the reinforcement included in the shear holes was constant at  $130 \text{ mm}^2$  ( $0.2 \text{ in}^2$ ) (#4 reinforcing bar), and the area of transverse reinforcement ( $A_{tr}$ ) was held constant at  $130 \text{ mm}^2$  ( $0.2 \text{ in}^2$ ). A total of ten shear holes were included in the analysis (simulating Series 10 push-out tests). Five different concrete compressive strengths were examined to determine the effect of concrete strengths on the strength of the ASC. As can be seen in Fig. 5.3, as the hole area increases, the shear strength also increases in a nearly linear fashion. It also can be observed that the concrete strength has a direct influence on the shear strength.

In Fig. 5.4, the hole area was kept constant at  $3,690 \text{ mm}^2$  ( $5.72 \text{ in}^2$ ) per five holes (Series 10), and the area of transverse reinforcement ( $A_{tr}$ ) was held constant at  $130 \text{ mm}^2$

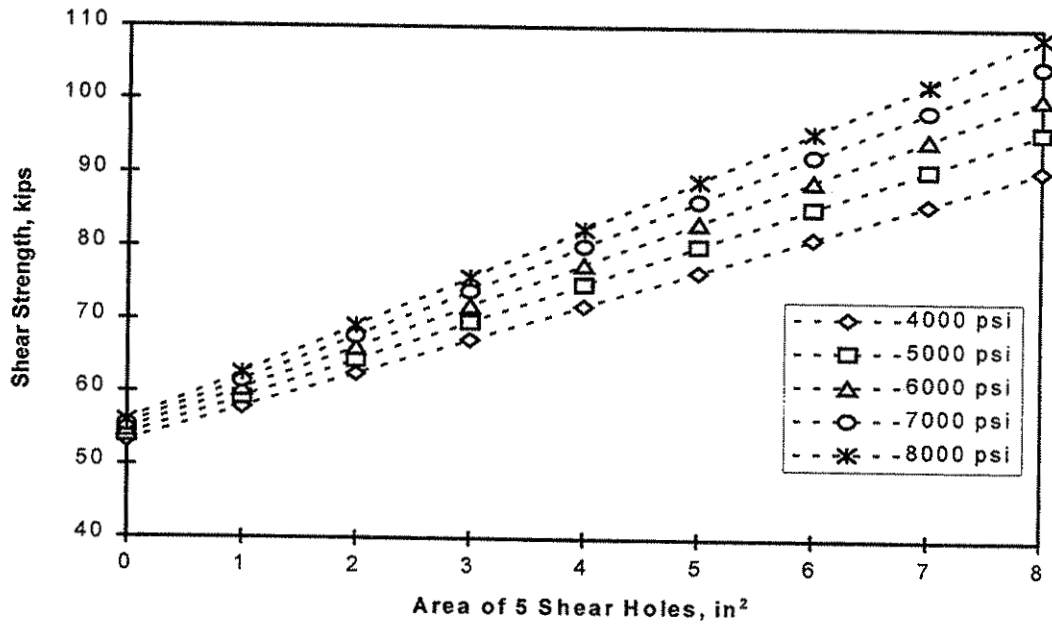


Fig. 5.3. Shear strength vs. hole area.

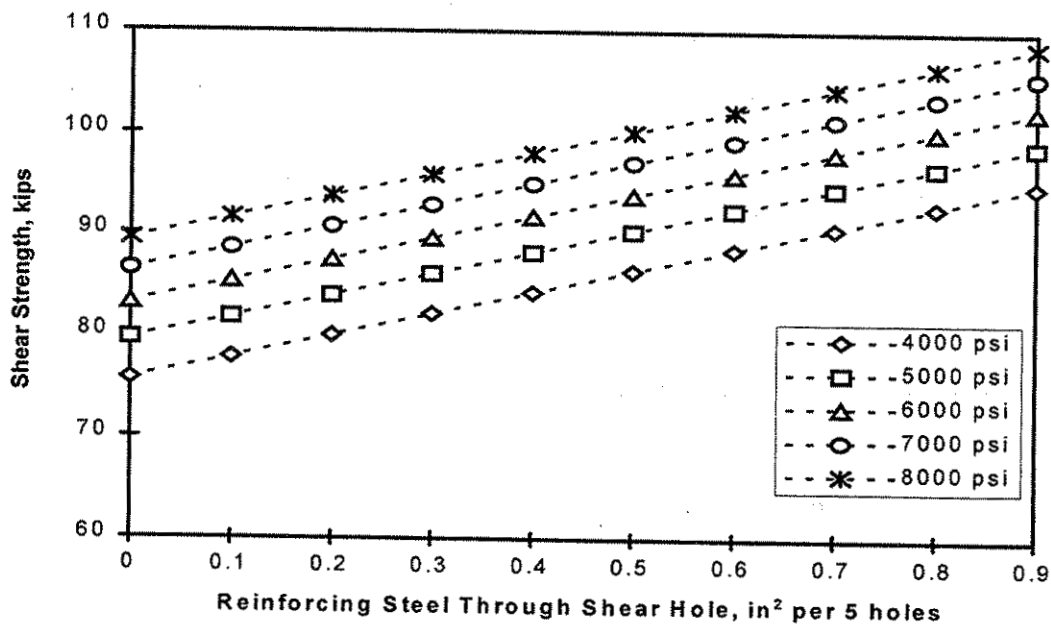


Fig. 5.4. Shear strength vs. area of reinforcing steel through shear hole.

(0.2 in<sup>2</sup>). As the amount of reinforcing steel in the shear hole increases, so does the shear strength. However, the equation is not very sensitive to an increase in reinforcing steel in the shear hole, as the strength only increases 8.9 kN (2 kips) for every additional 65 mm<sup>2</sup> (0.1 in<sup>2</sup>) of reinforcing steel.

In Fig. 5.5, the hole area and the reinforcing steel through the shear hole were kept constant at 3,690 mm<sup>2</sup> (5.72 in<sup>2</sup>) and 130 mm<sup>2</sup> (0.2 in<sup>2</sup>), respectively. The area of transverse slab reinforcement was varied from no reinforcement to 645 mm<sup>2</sup> (1.0 in<sup>2</sup>) of reinforcing steel per shear hole. The graphs indicate that the shear strength of the connection is significantly influenced by the amount of transverse slab reinforcing used. Normally, however, this would not be a consideration, as the amount of transverse reinforcing required would be determined using Eqn 1.4.

In Fig. 5.6, the reinforcing steel through the hole and the transverse reinforcing steel were kept constant at 130 mm<sup>2</sup> (0.2 in<sup>2</sup>) and 130 mm<sup>2</sup> (0.2 in<sup>2</sup>), respectively. The number of shear holes was varied, assuming an area of 795 mm<sup>2</sup> (1.23 in<sup>2</sup>) per shear hole (diameter of 32 mm (1 1/4 in.)). The shear strength of the connection depends significantly on the shear hole area, as can be seen by the increase in shear strength of approximately 44.5 kN (10 kips) for every two additional shear holes.

Based on this sensitivity analysis, the shear hole area, the amount of transverse reinforcement, the number of shear holes, and the concrete compressive strength are the four primary factors that influence the shear strength of the ASC.

## **5.2 BISB Laboratory Test Results and Analysis**

### **5.2.1 Two-Beam Specimen**

The purpose of the BISB tests was to obtain strength and behavior data. Deflection data as well as strain data collected during the testing of the specimen will be presented and analyzed in this section. The loads presented in the following discussion and graphs represent the load applied at each of the two loading points. The total load applied to the structure is the sum of the two applied loads. The specimen supported a load of approximately 445 kN (100 kips) applied to each loading point which was the capacity of the loading frame. Non-linear strain behavior occurred at 267 kN (60 kips);



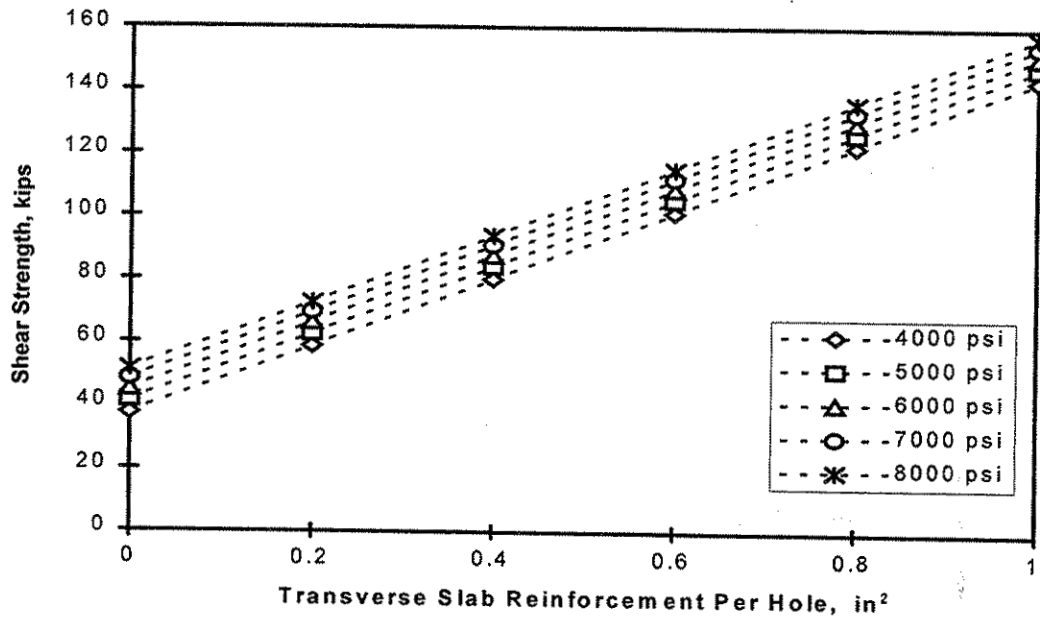


Fig. 5.5. Shear Strength vs. area of transverse reinforcement.

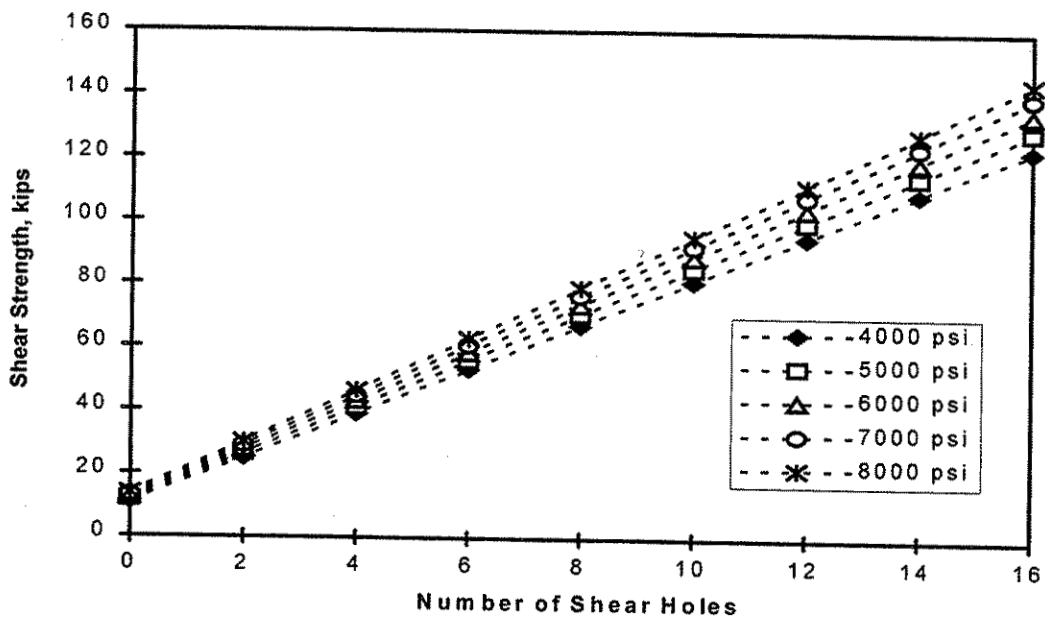


Fig. 5.6. Shear strength vs. number of shear holes.

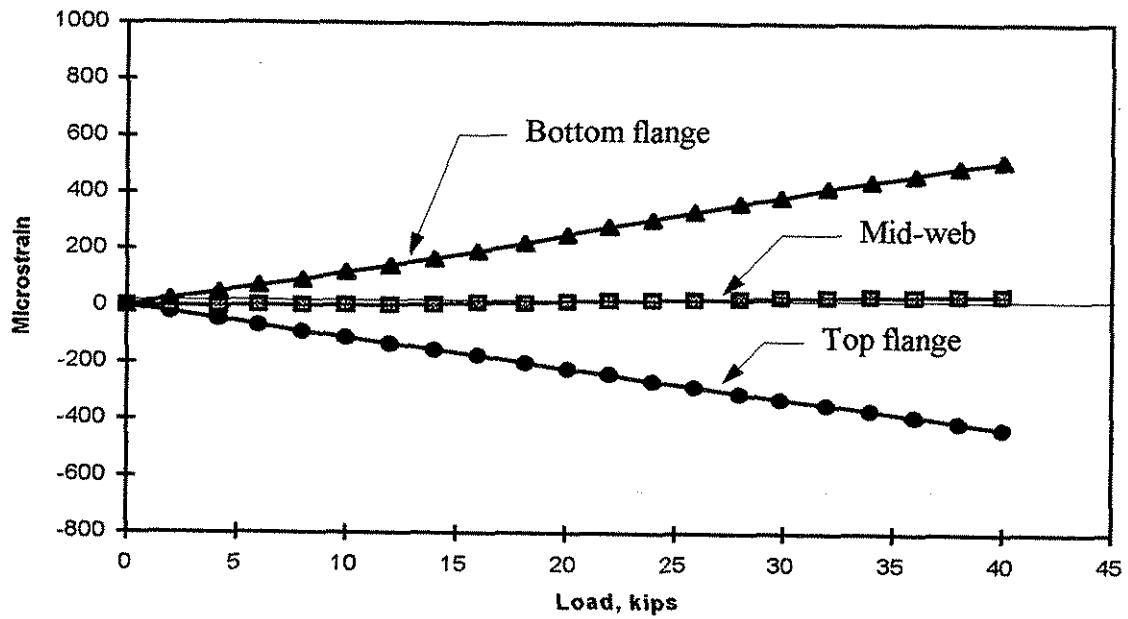
measurable end slip occurred at approximately 178 kN (40 kips). These loads are both well above service loading conditions.

Experimental strains due to vertical loads are presented in Fig. 5.7. As previously noted, strain gages were placed on the top and bottom flanges, as well as at the approximate neutral axis of the composite section. In theory, the strain at the neutral axis will be zero as long as the section remains composite. As the concrete in tension starts to crack, the neutral axis will rise, which will be indicated by an increase in the strain at the location of the composite neutral axis. As the concrete cracks, there will be a decrease in composite action, rendering the concrete useless in terms of strength. This phenomenon is indicated in the experimental results presented in Fig. 5.7.

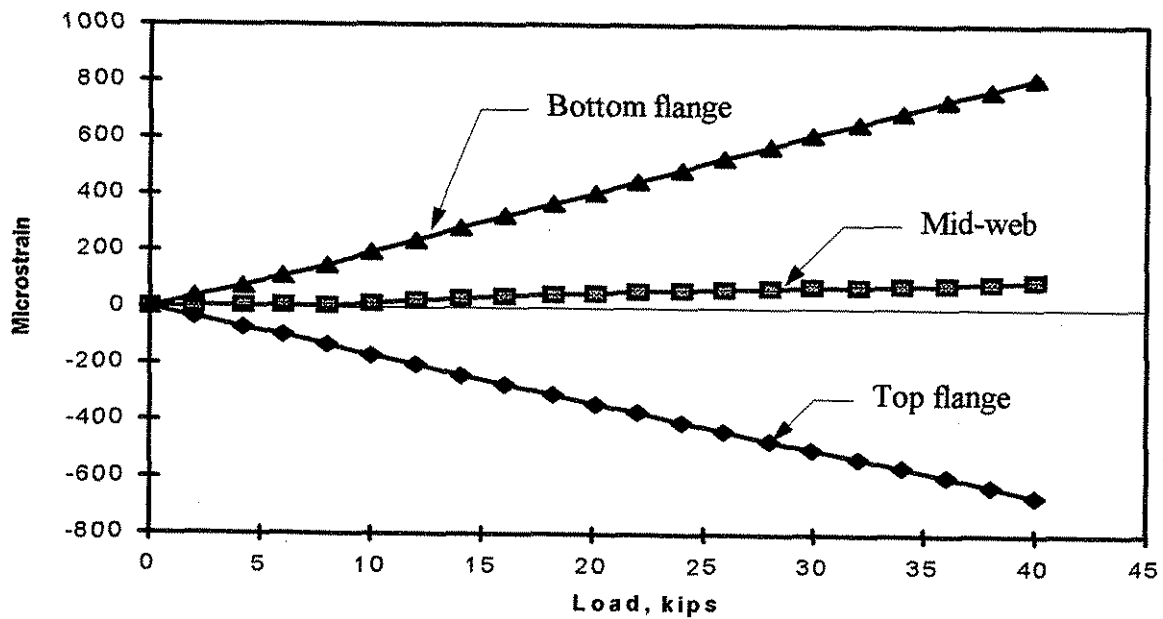
The top and bottom beam flange strains in a non-composite structure should be of approximately the same magnitude, but opposite sign, indicating the neutral axis is near the center of the girder. By this logic, Fig. 5.7 indicates that the specimen tested exhibits the behavior of a non-composite beam. A closer inspection of the results is necessary, however, as this behavior could be misleading. The concrete in the specimen tested filled the void between the girders; thus, the neutral axis for the composite section was approximately the same as the neutral axis of the non-composite section. Inspection of the deflection data, presented later, will provide more information on composite action in the tested specimen.

A "snapshot" of the strains across the depth of the cross section is shown in Fig. 5.8 for both the quarter point and the centerline. The concrete did not visually show any substantial cracking up to a load of 178 kN (40 kips) at each loading point; thus, the strain at the composite neutral axis should be zero. Data in Fig. 5.8 verify this. Likewise, in the elastic range, the steel strain also increased in a linear fashion.

As previously mentioned, measurable end slip did not occur until the load reached approximately 178 kN (40 kips) on each load point (see Fig. 5.9). This is apparently the load at which the bond between the steel and concrete was broken. Note the rate at which the concrete slipped once the steel-concrete bond was broken. This is a potential problem

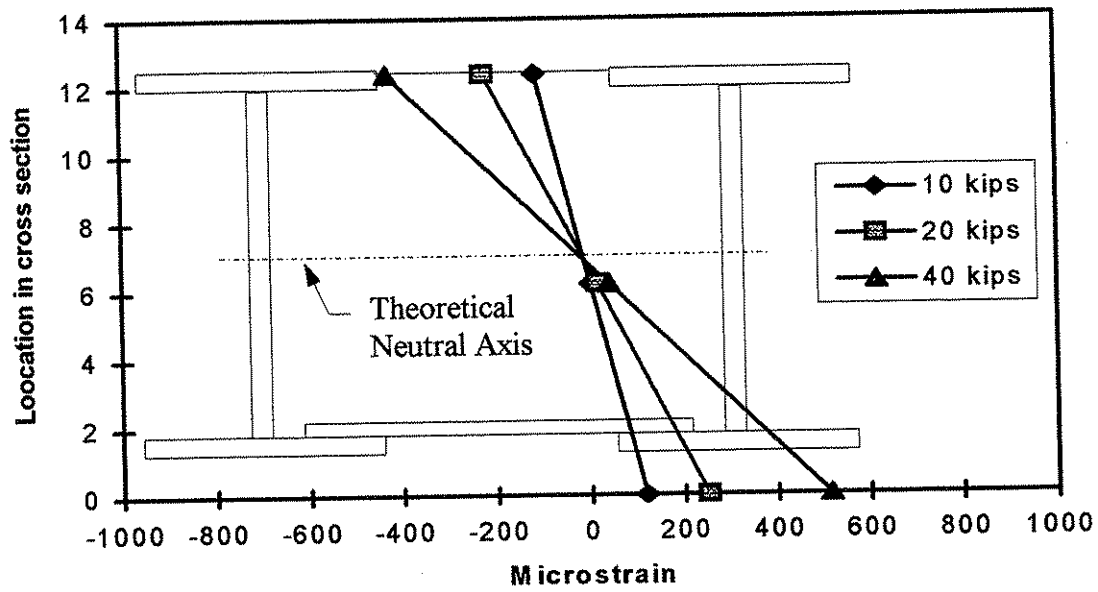


a. Quarter point

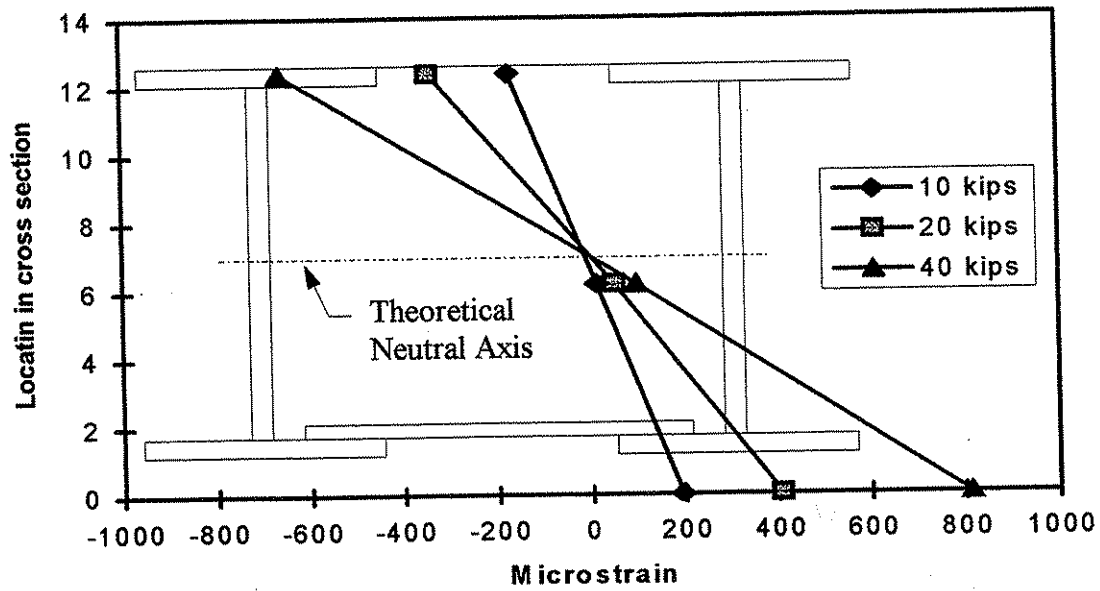


b. Centerline

Fig. 5.7. Strain response for two-beam BISB during load testing.



a. Quarter point



b. Centerline

Fig. 5.8. Strain profile for two-beam BISB during load testing.

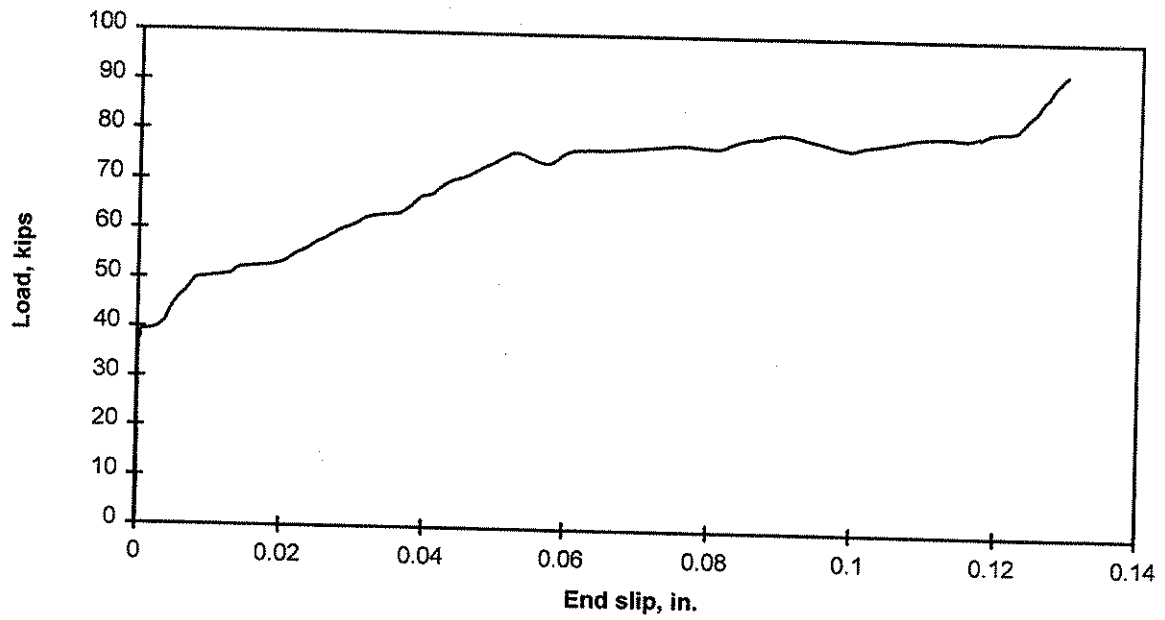


Fig. 5.9. Average end slip during load testing.

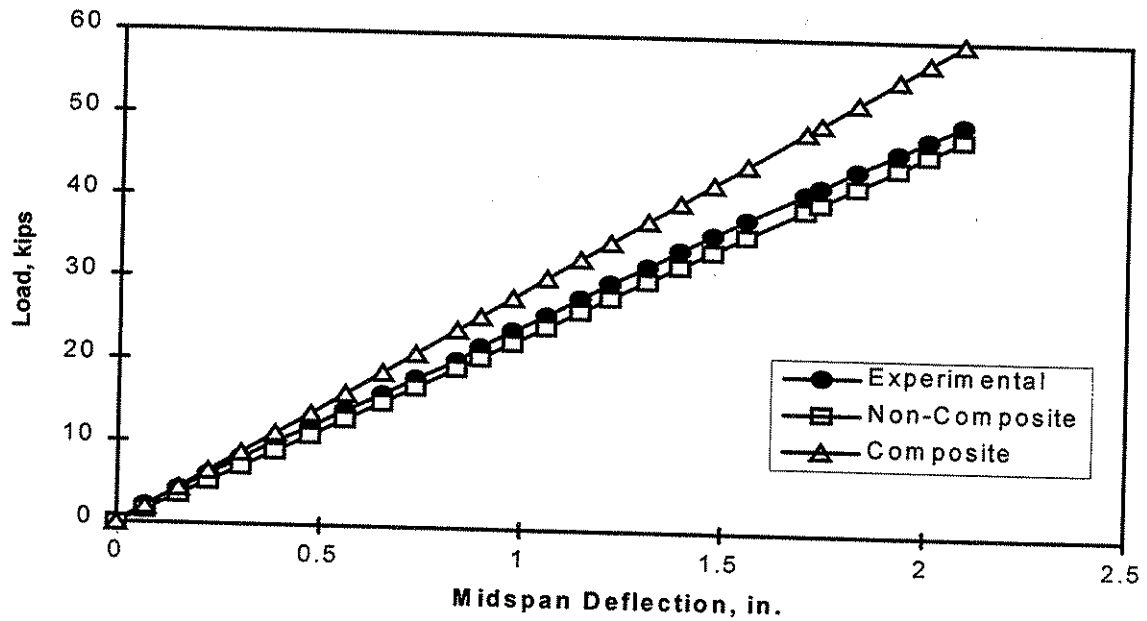


Fig. 5.10. Theoretical and experimental midspan deflection.

that the ASC will alleviate. Although minimal slip should occur throughout with increased load, once the steel-concrete bond is broken, the load would be carried by the ASC.

An attempt to quantify the amount of composite action is illustrated in Fig. 5.10. In this figure, an experimental load versus deflection curve is compared to theoretical composite action and non-composite action deflection curves. The non-composite graph was determined by using the moment of inertia for the two steel beams only, and assuming the concrete acted only as dead weight.

Similarly, the composite deflection curve was determined using the moment of inertia of the entire section. The concrete area was modified into an equivalent steel area. The theoretical load deflection curves were determined using the moment of inertia values, the geometry of the test set-up, and basic load-deflection relationships.

In theory, the load versus deflection data for the composite beam should fall between the theoretical values for complete composite action and non-composite action. If the specimen behaved as expected, the structure should initially respond more like a composite structure, as the concrete and the steel should have adequate bond. However, as the load increases, the steel-concrete bond would weaken and the concrete in tension would crack, causing the structure to behave increasingly as a non-composite structure.

As can be seen in Fig. 5.10, the structure initially responded as a composite beam. At a load of approximately 22 kN (5 kips) per load point, the structure began to make the transition to non-composite behavior, indicating that the bond between the steel and concrete had been weakened. At a load of approximately 67 kN (15 kips), the beam acted basically as a non-composite structure, with the concrete providing minimal composite action.

## 5.2.2 Four-Beam Specimen

### 5.2.2.1 *Experimental Results*

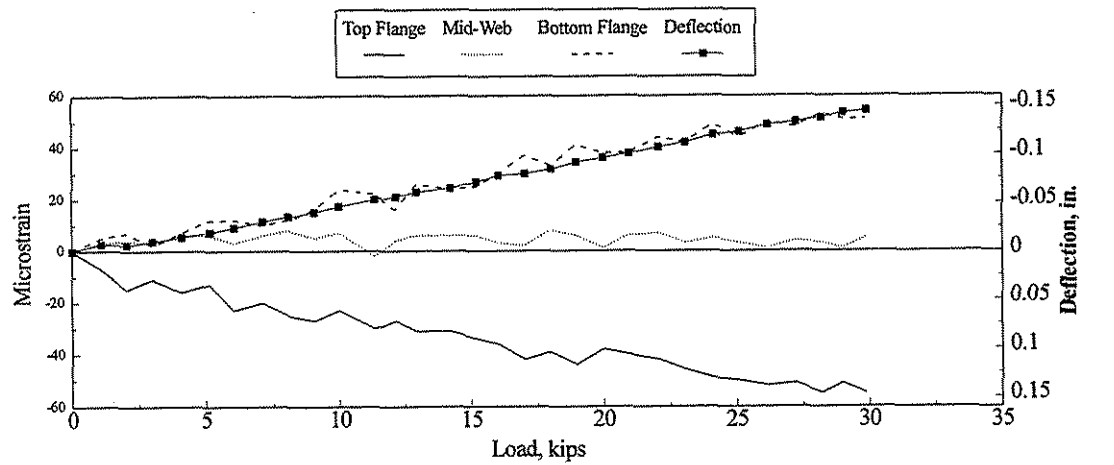
Service and ultimate load tests described in Chp 3 were performed on the four-beam specimen described earlier. The goals of these tests were to: (1) determine the

service load distribution characteristics of the system, (2) determine the ultimate load capacity of the specimen and its mode of failure, and (3) to collect sufficient behavioral data to validate an analytical model which could accurately predict the behavior of the BISB.

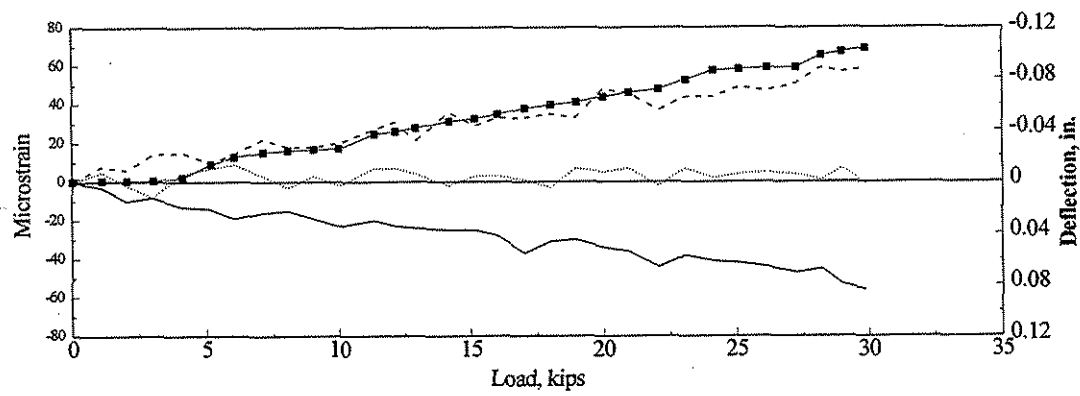
Although a large number of tests were performed and a large amount of data recorded per test, only limited results are included in this report. The results included, however, are representative samples of all of the data collected. Illustrated in Fig. 5.11 are the centerline deflections and strains from Test A1 for Beams 1, 2, and 3. As was discussed in Chp 3 and shown in Fig. 3.6, Test A1 consisted of a single point load applied on an exterior steel beam and positioned 1,500 mm (4 ft - 11 in.) from the pin support. Some electrical noise in the strain gage data (variation in the data at regular intervals) is apparent; this degree of noise appeared in all strain gage data in all of the tests. For this reason, most of the subsequent data presented are deflection data. Although there is noise in the strain data, trends in behavior are clearly visible. A linear regression was performed on all strain data to eliminate the noise variation. In subsequent plots when strain data are presented, regression values rather than actual values are presented.

To investigate the load distribution characteristics of the BISB, the deflections at the quarter point, three eighths point, and centerline were plotted for each test at a magnitude of load of 89 kN (20 kips). In each figure, there are seven curves which are the results of seven different tests with the load located at the same section of the span, but at seven different transverse locations. Figures 5.12, 5.13, and 5.14 show the results with the load at Sections 1, 2, and 3, respectively. In each of these figures, the deflections at the quarter point, three eighths point, and centerline are presented. These data indicate that the BISB is behaving symmetrically about the centerline of the cross section, and the deflection of a given beam changes in a nearly linear fashion as the load moves from one side of the cross section to the other (i.e., from section A to section G).

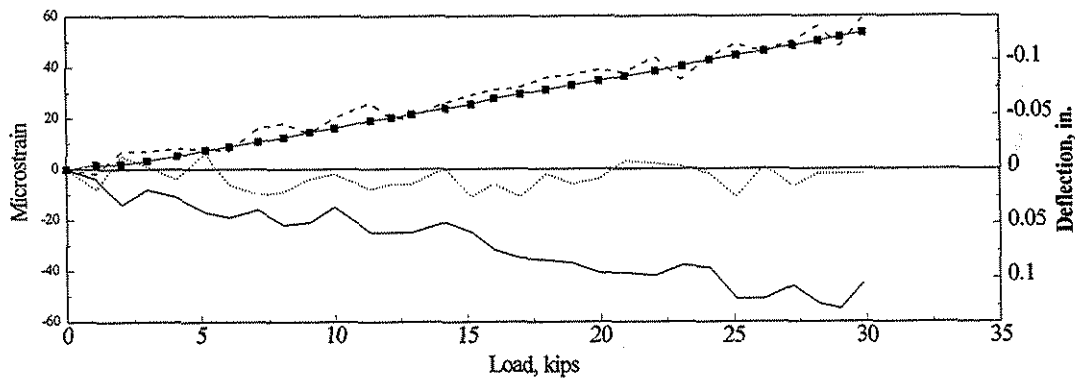
The results of the ultimate load test are shown in Figs. 5.15 and 5.16. Figure 5.15 shows the deflection at the quarter point, three eighths point, and centerline. The load deflection curve is nearly linear until 1.33 MN (300 kips) of total load are applied. Similarly, Fig. 5.16 illustrates that strains are nearly linear until the load exceeds 1.33



a. Strain and deflection in Beam 1



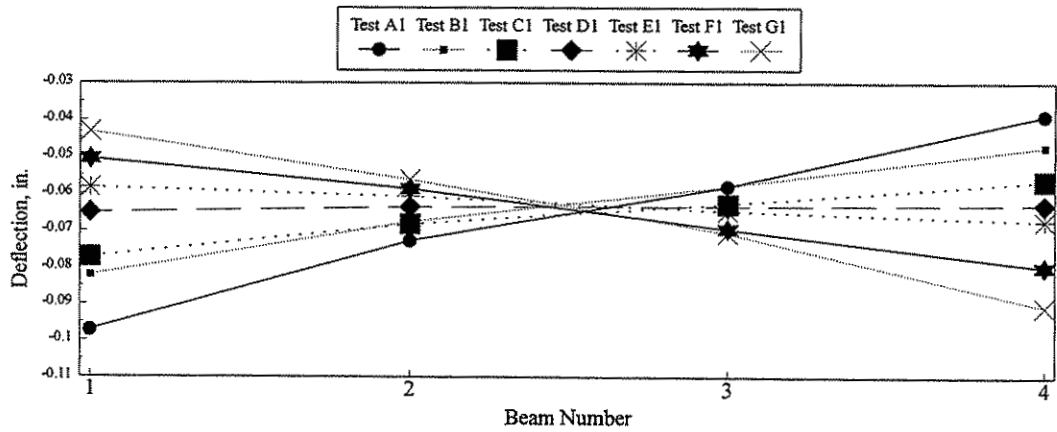
b. Strain and deflection in Beam 2



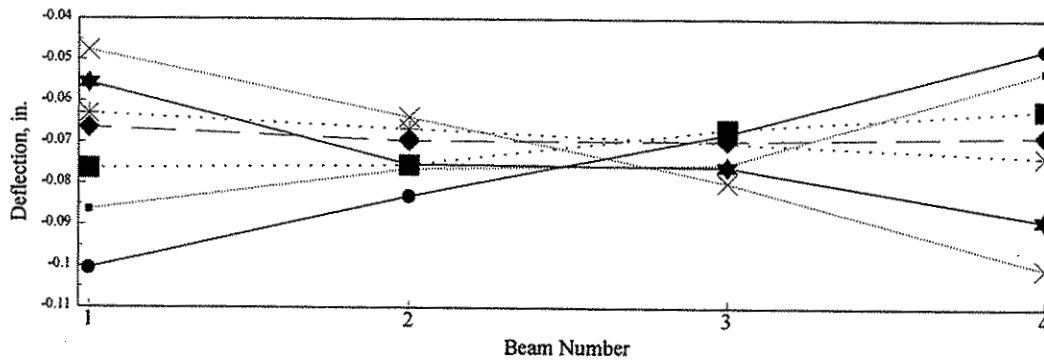
c. Strain and deflection in Beam 3

Fig. 5.11. Test A1 Results: deflections and strains at centerline.

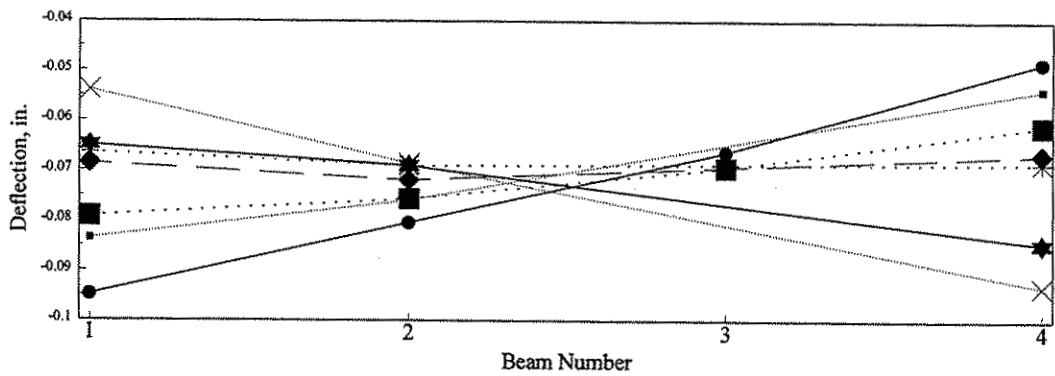




a. Deflection at the quarter point



b. Deflection at the 3/8 point



c. Deflection at the centerline

Fig. 5.12. Deflection of beams due to 20 kips load applied at Section 1.

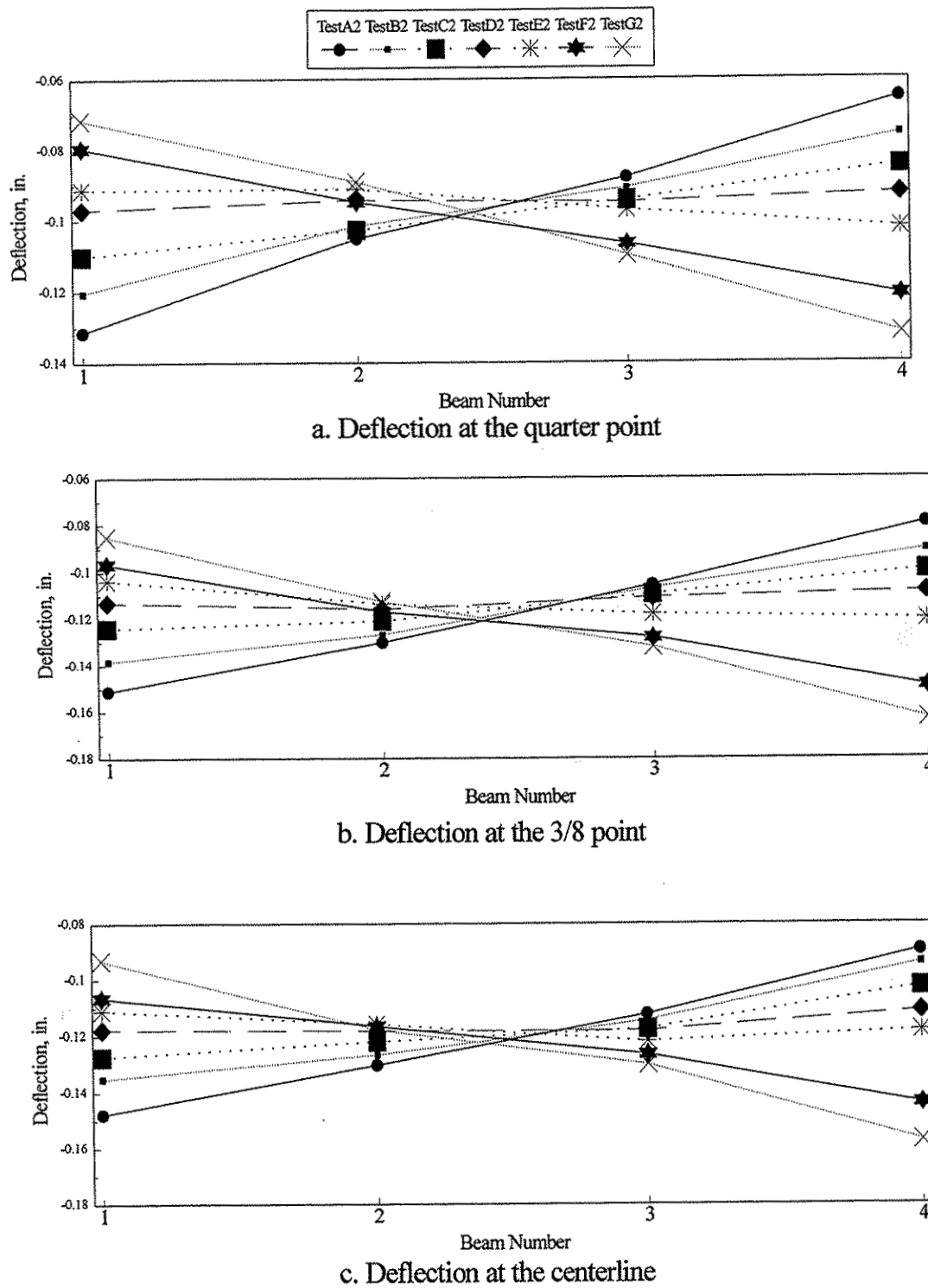
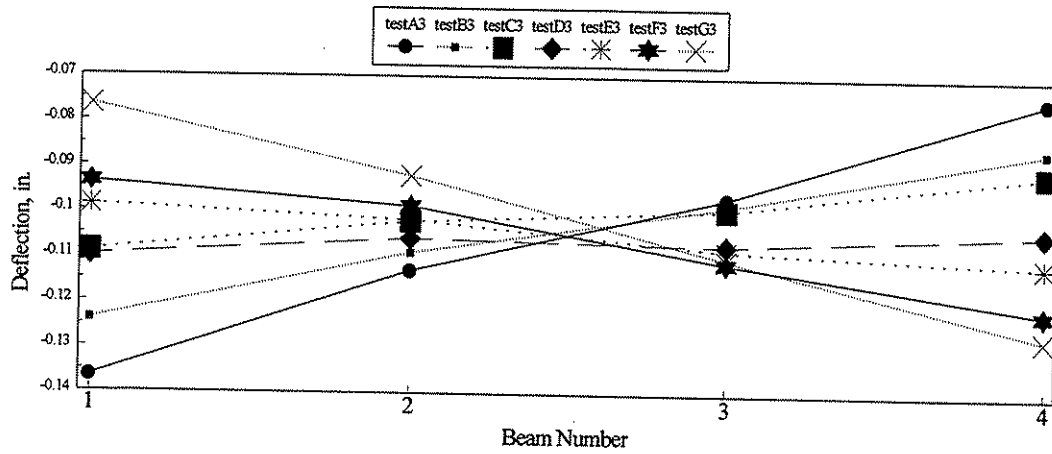
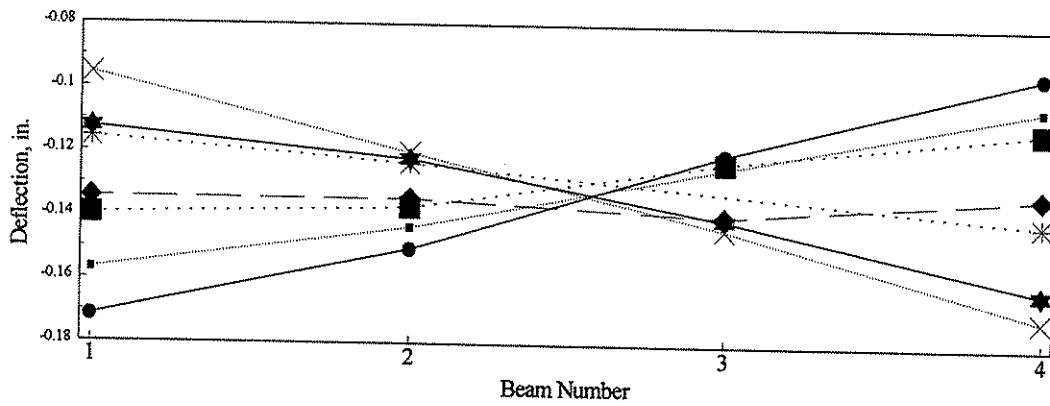


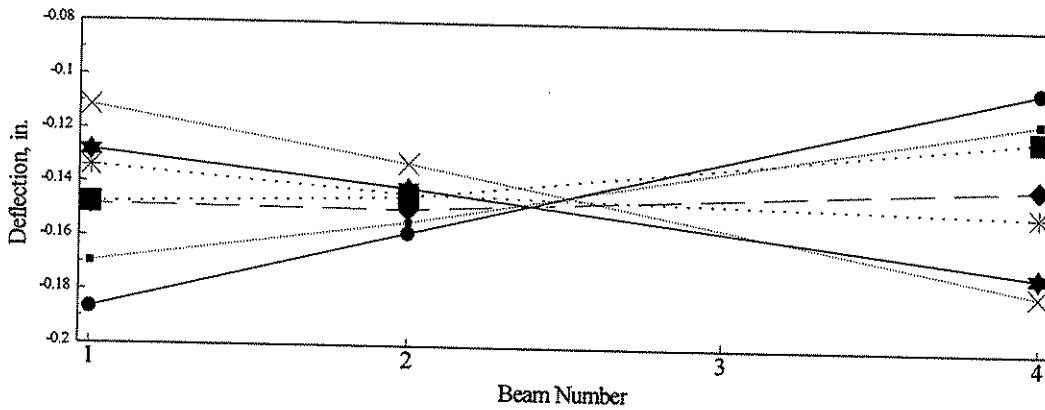
Fig. 5.13. Deflection of beams due to 20 kips load applied at Section 2.



a. Deflection at the quarter point



b. Deflection at the 3/8 point



c. Deflection at the centerline

Fig. 5.14. Deflection of beams due to 20 kips load applied at Section 3.

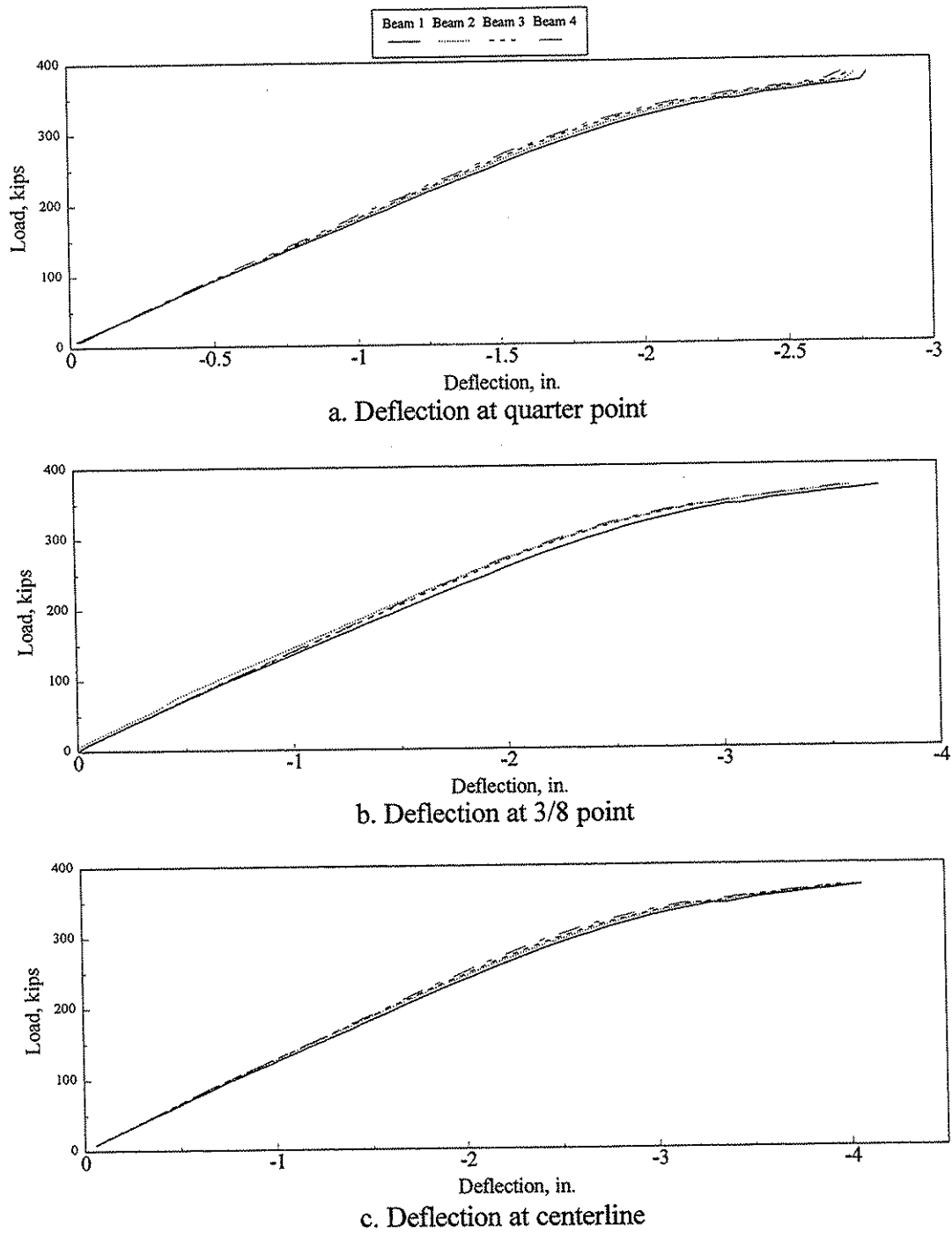
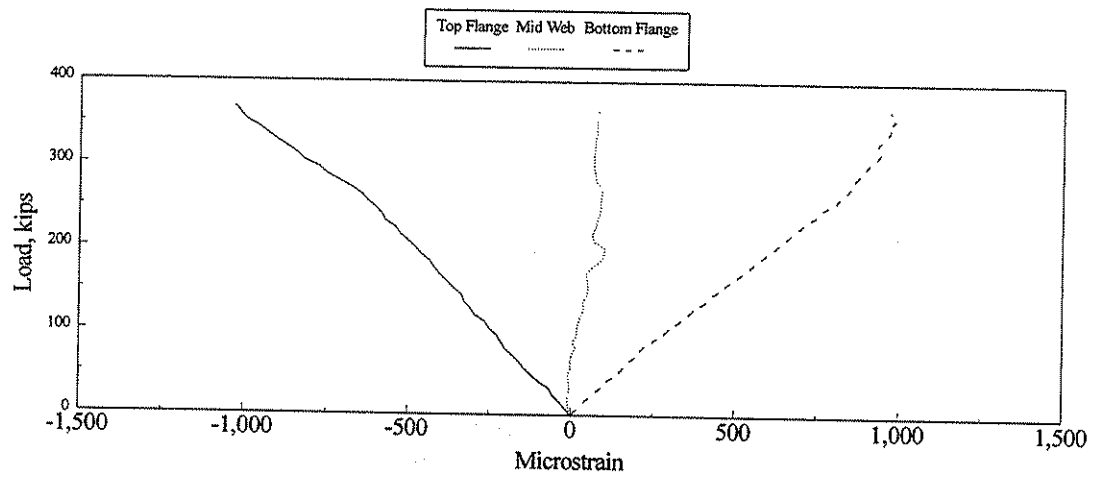
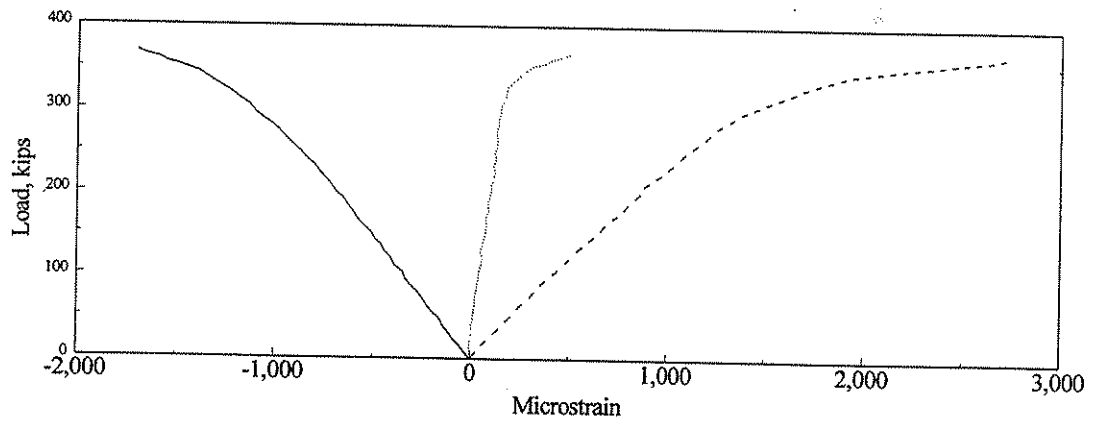


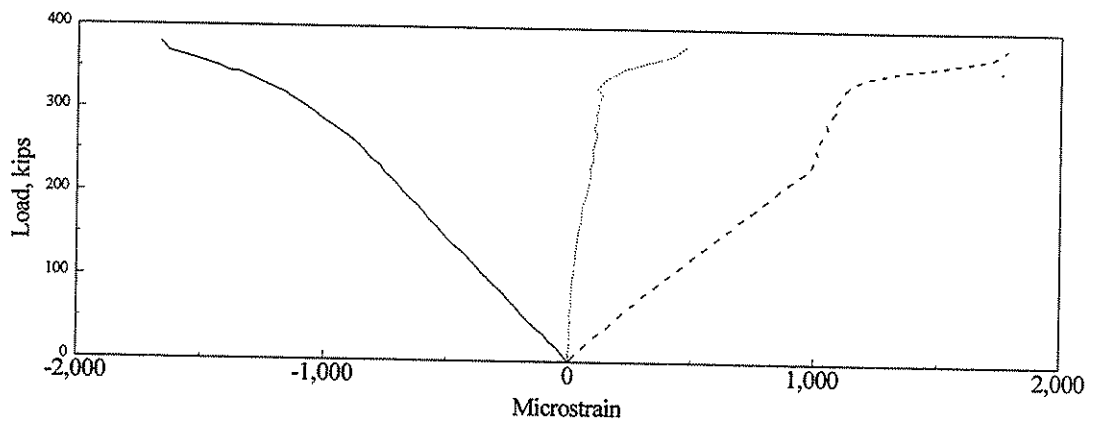
Fig. 5.15. Deflections during BISB ultimate load test.



a. Beam 1 strain at quarter point



b. Beam 1 strain at centerline



c. Beam 4 strain at centerline

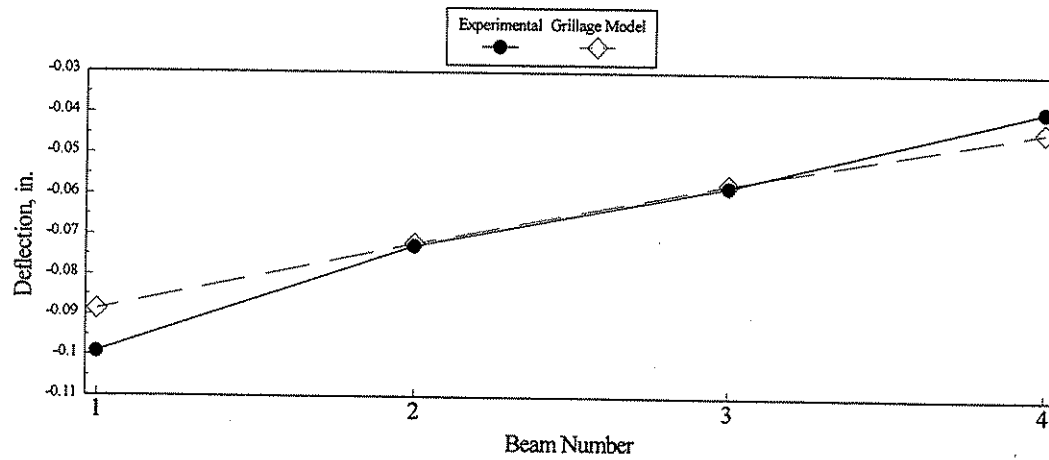
Fig. 5.16. Strains during ultimate load test.

MN (300 kips). Both the deflection and strain curves become nonlinear at loads greater than 1.33 MN (300 kips). The non-linear behavior is most likely the result of two processes: yielding of the steel and the cracking of the tension concrete. Cracks became visible between the concrete and the steel at 1.33 MN (300 kips). When the loading apparatus was removed, additional cracks were visible around the holes through which the loads were applied. The maximum load applied to the specimen was 1.65 MN (370 kips), which resulted in a maximum deflection of 103 mm (4.06 in.) at the centerline. At this point, the bottom of the BISB specimen was in contact with the Dywidag bars used to anchor the test apparatus to the tie-down floor. Continuation of the testing required the disassembly of the entire loading apparatus and the repositioning of the BISB specimen. For all practical purposes, the specimen failed; thus, the test was terminated.

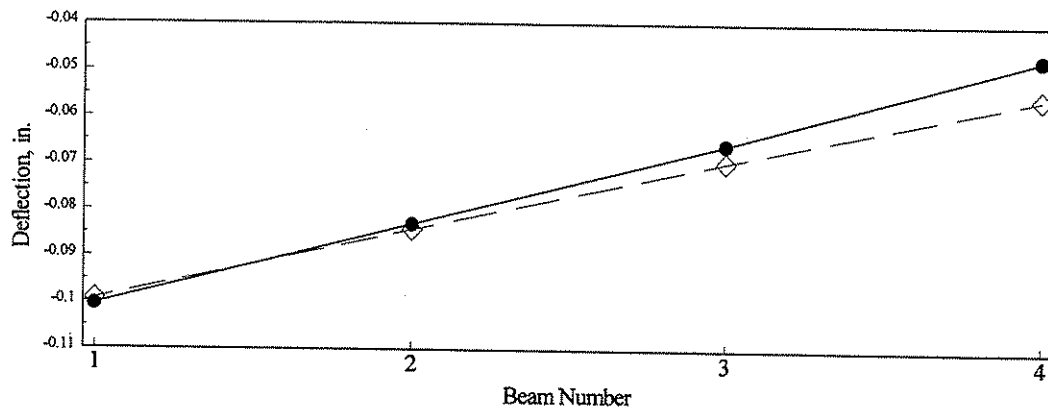
#### 5.2.2.2 *Comparison of Experimental and Analytical Results*

Based on the results of the sensitivity studies discussed in Chp 4, a grillage model of the four-beam BISB laboratory specimen was developed for comparison with experimental data. The model used a transverse beam spacing of 51 mm (2 in.). The connection between the transverse beams and longitudinal beams was modeled as fixed and the longitudinal beams were modeled as simply supported at the ends. The transverse beams were modeled using the full contributory area of the concrete section 51 mm (2 in.) wide with a height of 267 mm (10.5 in.) and the modulus of elasticity of concrete. The longitudinal members were modeled using the transformed value of the full contributory concrete width,  $4.25 \times 10^8 \text{ mm}^4$  ( $1,020 \text{ in}^4$ ) for the flexural moment. The torsional moment of inertia used was  $6.24 \times 10^7 \text{ mm}^4$  ( $150 \text{ in}^4$ ). The longitudinal beams used a modulus of elasticity of steel.

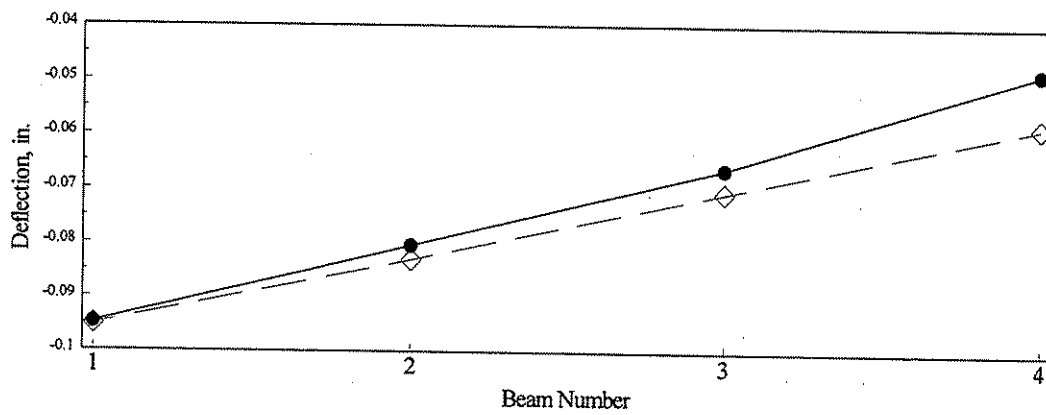
Figures 5.17 and 5.18 show a comparison of experimental and theoretical deflections (i.e., those obtained from the analytical model) for Tests A1 and C3. These tests were chosen to show the differences between the analytical and the experimental results when the load is at an edge beam (Test A1) and on an interior beam (Test C3).



a. Deflection at the quarter point

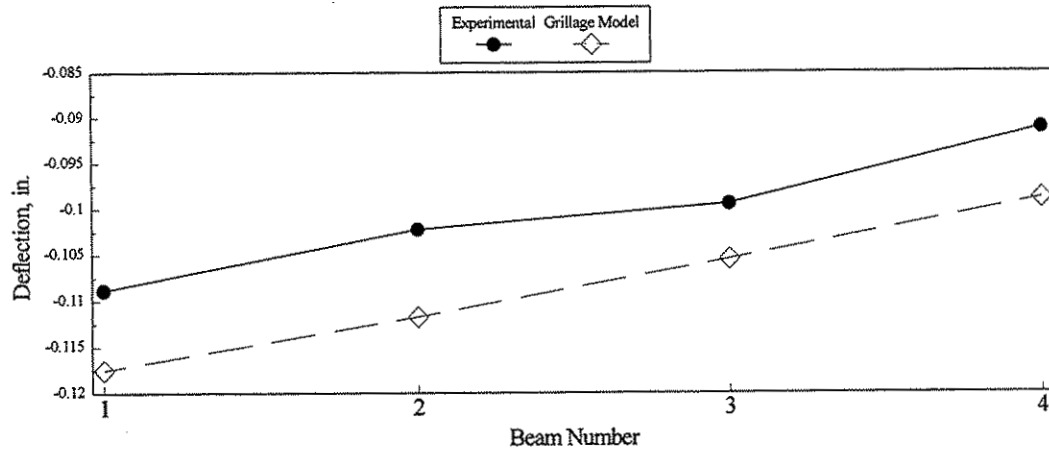


b. Deflection at the 3/8 point

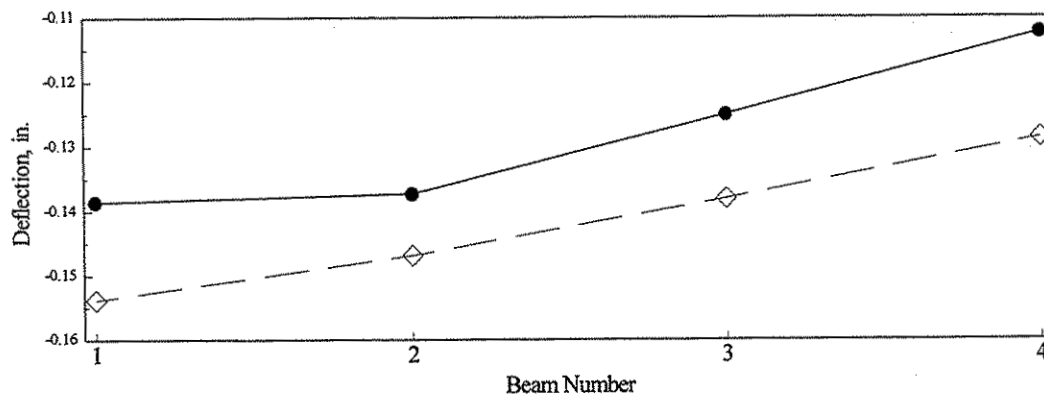


c. Deflection at the centerline

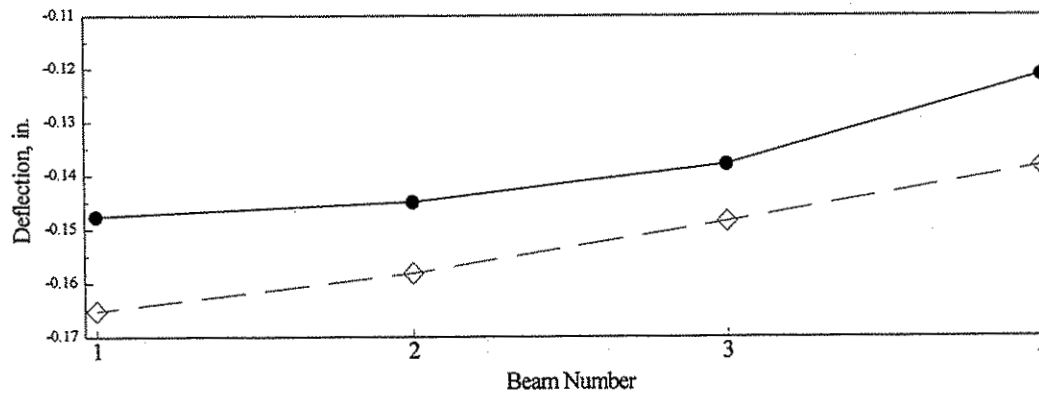
Fig. 5.17. Comparison of experimental and analytical results for BISB Test A1.



a. Deflection at the quarter point



b. Deflection at the 3/8 point



c. Deflection at the centerline

Fig. 5.18. Comparison of experimental and analytical results for BISB Test C3.



These figures show that the model gives results closer to experimental when the load is placed on exterior beams. For all cases, the analytically predicted deflection is within 15% of the experimental result.

### 5.3 Composite Beam Test Results

The composite specimen tests consisted of service and ultimate load tests of four specimens. Both the details of the specimens and their instrumentation were presented in Chp 2. These tests were performed to determine: (1) the service level strength of the cross sections, (2) the degree of composite action between the concrete and steel for each section under service level conditions, and (3) the ultimate strength and type of failure.

The results of the service level tests for Specimen 1 are illustrated in Fig. 5.19. The strain at the centerline and the deflections at the quarter point, three eighths point, and centerline are shown in Figs. 5.19a and 5.19b, respectively. It can be seen that both the strain and the deflection increased linearly with load. The strain across the section depth is shown in Fig. 5.19c. The theoretical location for the neutral axis, assuming "complete" composite behavior, was calculated and is also shown. Because the strain across the section depth is nearly linear for each load level, and also because the experimental and theoretical neutral axes are nearly the same, it is assumed that complete composite action existed during the service level tests. Based on these sets of data, it is concluded that the ASC used in the specimen was effective in creating composite action between the concrete and the steel.

As noted in Chp 2, Specimens 2 and 3 were the same. Some unexplainable test results were observed in the testing of Specimen 2; thus, Specimen 3 was fabricated to be identical to Specimen 2 and tested to provide additional data. Figure 5.20 shows a plot of both deflections and strains for Specimens 2. From these graphs, it appears that the longitudinal flexural stiffness of Specimen 2 decreased after 44.5 kN (10 kips) of load were applied.

However, this change in stiffness is suspicious to the researchers for a couple of reasons. In general, a change in longitudinal flexural stiffness could be caused by one of

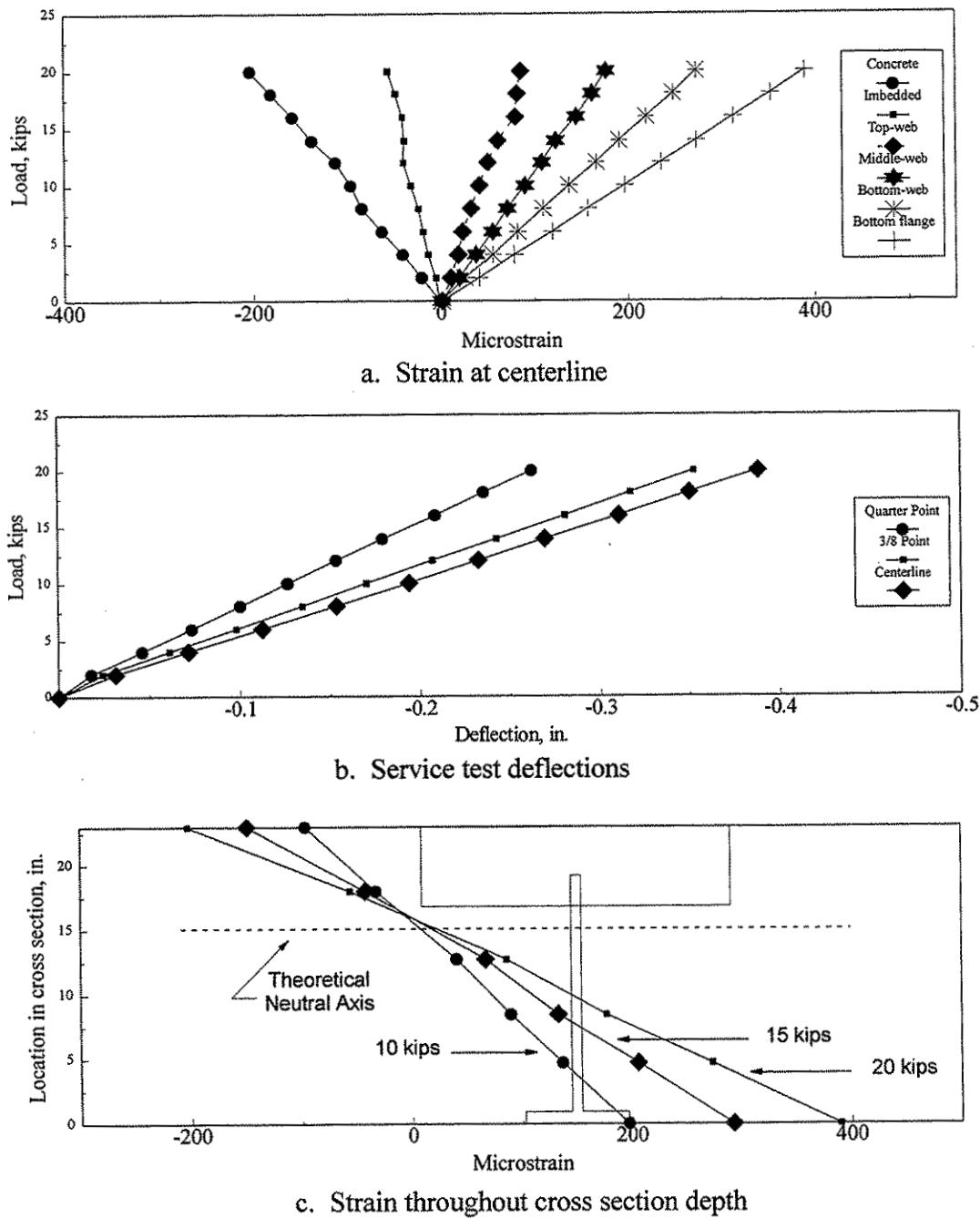
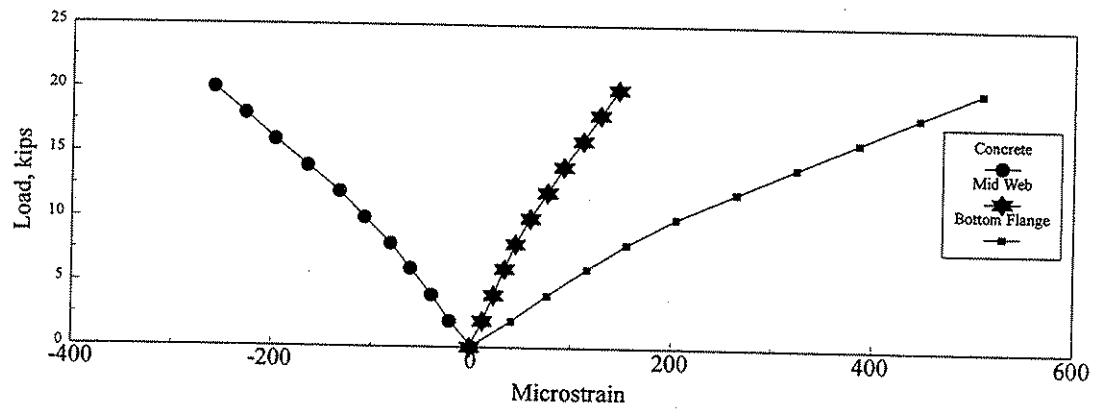
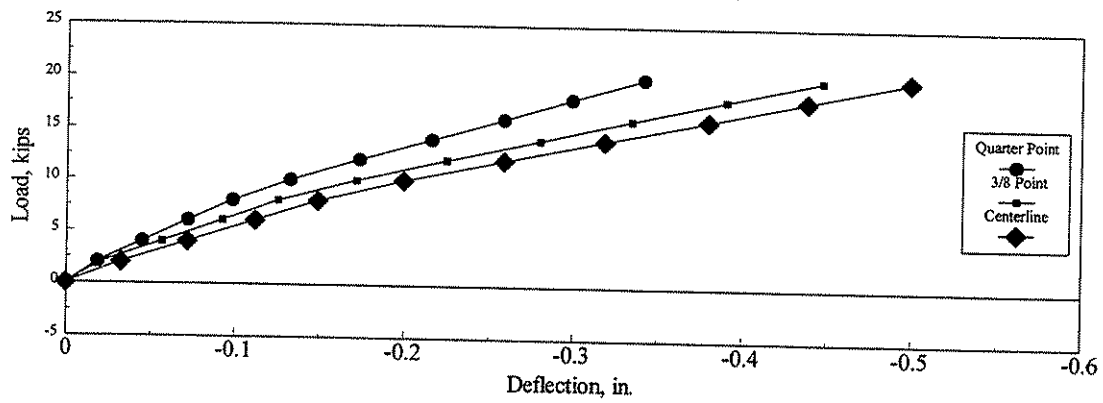


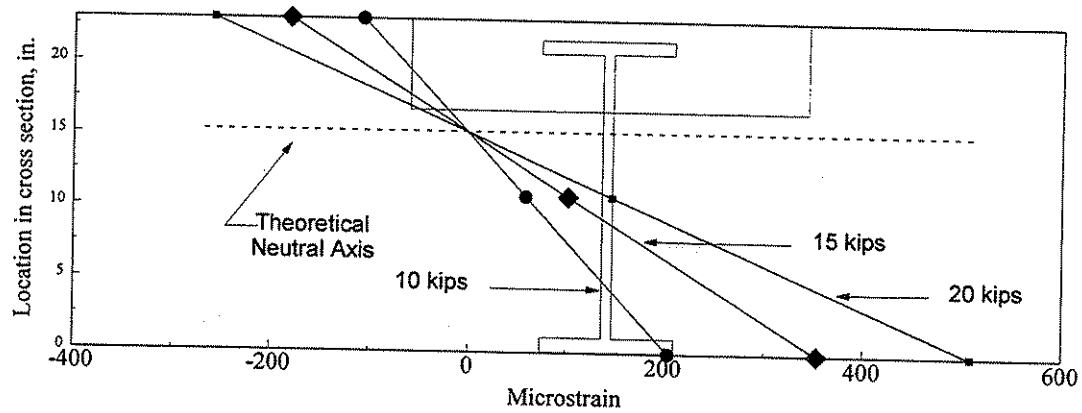
Fig. 5.19. Specimen 1 service test results.



a. Strain at the centerline



b. Service test deflection



a. Strain throughout cross section depth

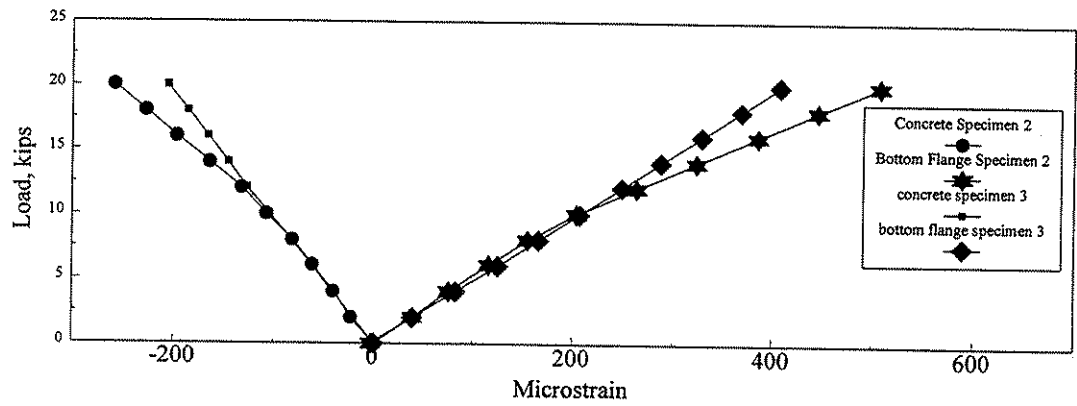
Fig. 5.20. Specimen 2 service test results.

two things: inelastic behavior or loss of composite action. Inelastic behavior is unlikely in this specimen because the strains in both the concrete and steel were within their respective elastic ranges when the behavior changed. Additionally, inelastic behavior causes permanent deformation of the material. No permanent deformation occurred in the specimen, and the change was abrupt and occurred in several service load tests of the specimen and the ultimate load test. The second explanation, loss of composite action, would correspond to a change in the location of the neutral axis; no change in the neutral axis was observed.

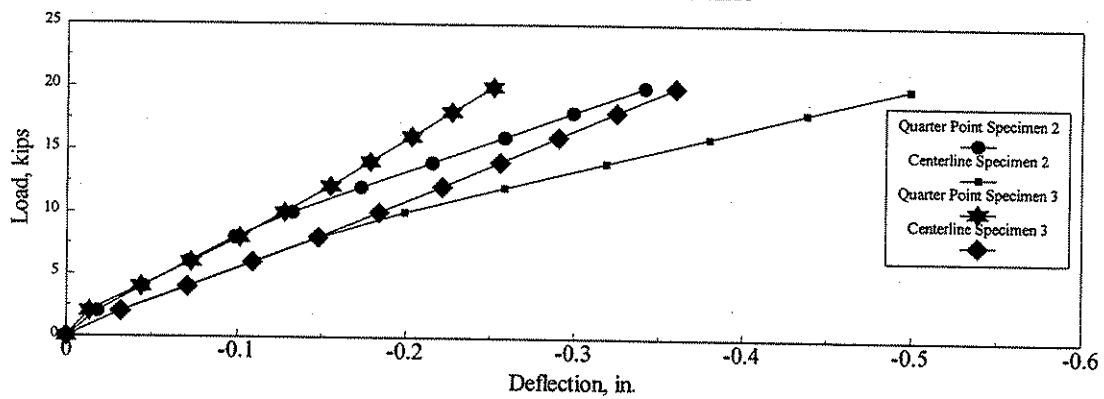
The only logical explanation for the behavior observed is an error in the measurement of the applied load. Such an error would explain strain and deflection curves; it is also likely that an electrical or mechanical error would repeat in each test, as was observed. Since the results of Specimen 2 are unexplainable, they are not used for comparison in the following sections. However, a comparison of strains and deflections for Specimens 2 and 3 were made and are illustrated in Fig. 5.21. Both the strain and deflection curves are similar up to the load of 44.5 kN (10 kips). The location of the neutral axis is the same for both specimens for a 89 kN (20 kips) load. This provides further verification that the error in Specimen 2 data was the result of an error in the measurement of the applied load.

The service test results for Specimens 3 and 4 are shown in Figs. 5.22. and 5.23, respectively. Both of these specimens exhibit linear behavior based on both deflection and strain data. Because similar behavior is inferred by both the strain and the deflection data, only deflection data are present in the rest of this section. As with Specimen 1, the strain across the section depth was nearly linear and the experimental location of the neutral axis agreed closely with the theoretical location. This indicated that both the ASC and the shear stud connector created composite action between the concrete slab and the steel beam.

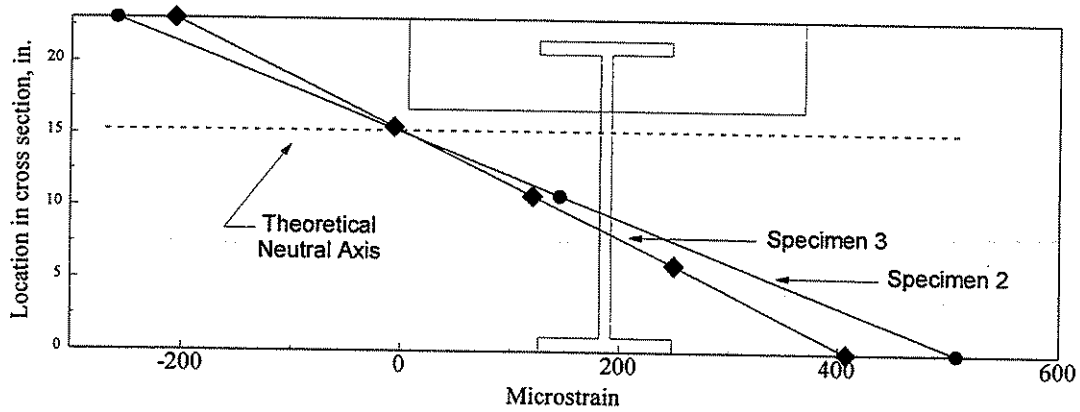
Centerline deflections for Specimens 1, 3, and 4 are compared in Fig. 5.24. As shown in Fig 5.24a., the specimens have different longitudinal flexural stiffnesses, Specimen 4 having the greatest and Specimen 1 having the least. When the deflection data are modified for the variation in longitudinal flexural stiffnesses (see Fig 5.24b.), the



a. Strain at the centerline



b. Service test deflection



a. Strain throughout cross section depth

Fig. 5.21. Comparison of service test results of Specimens 2 and 3.

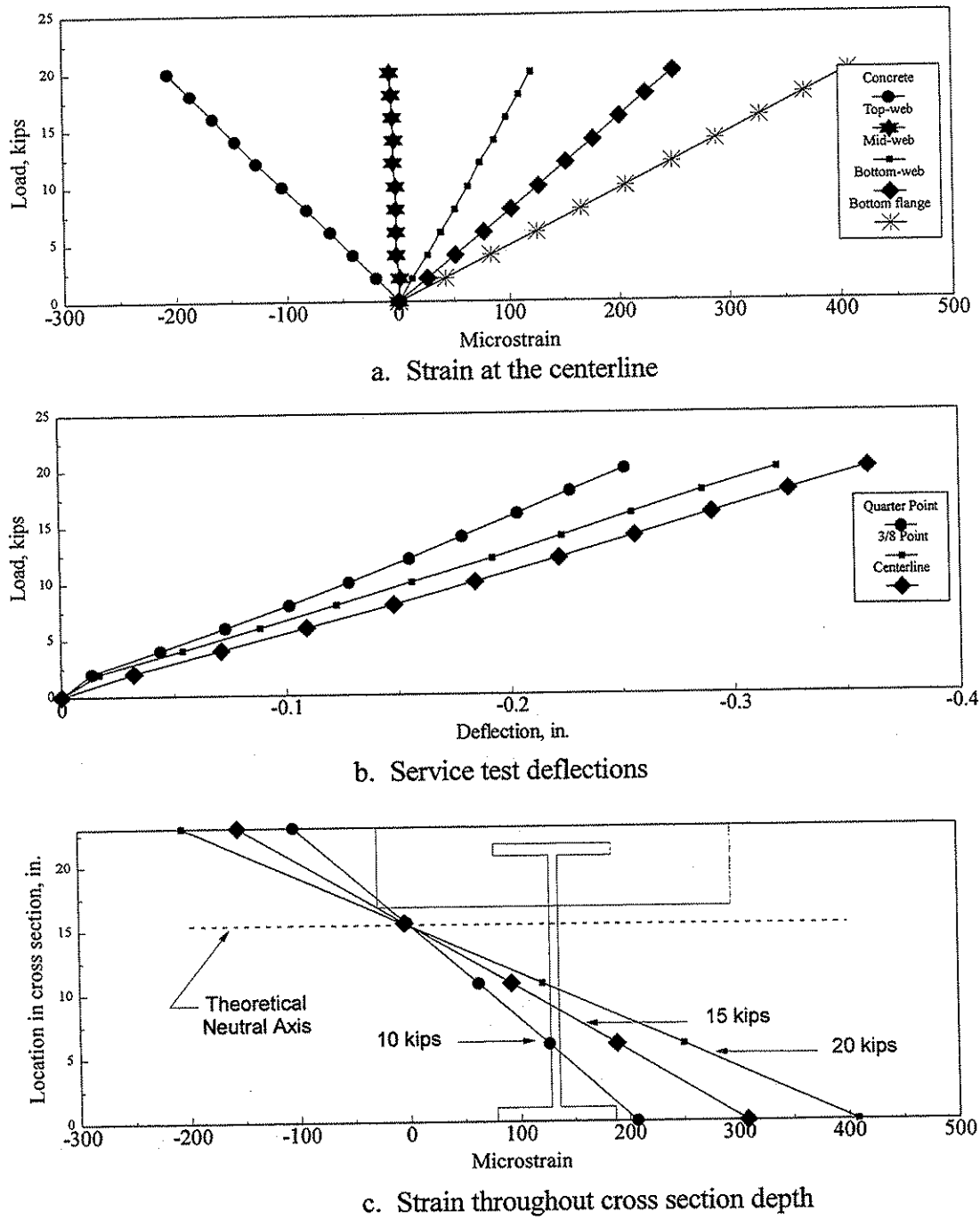


Fig. 5.22. Specimen 3 service test results.

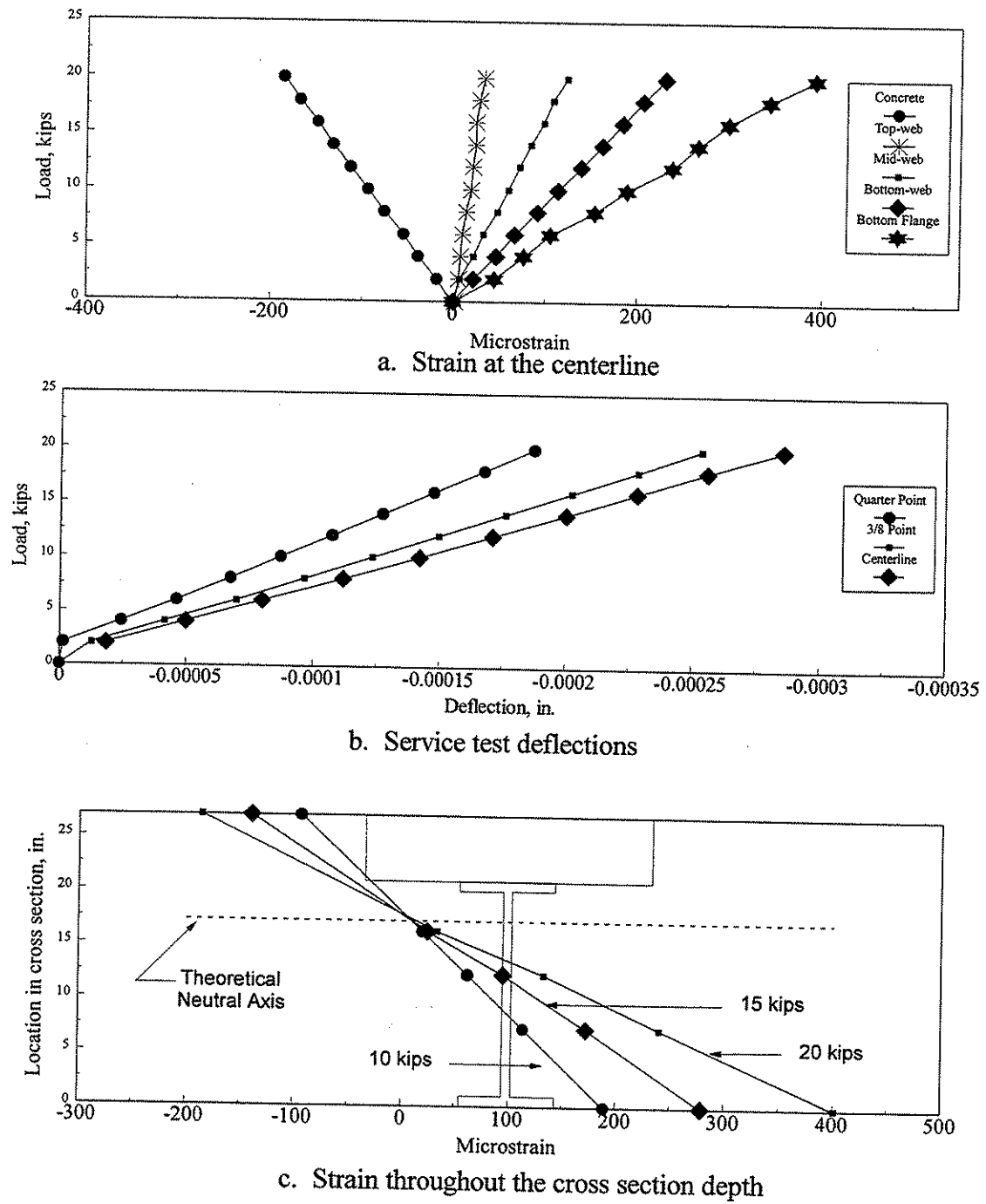
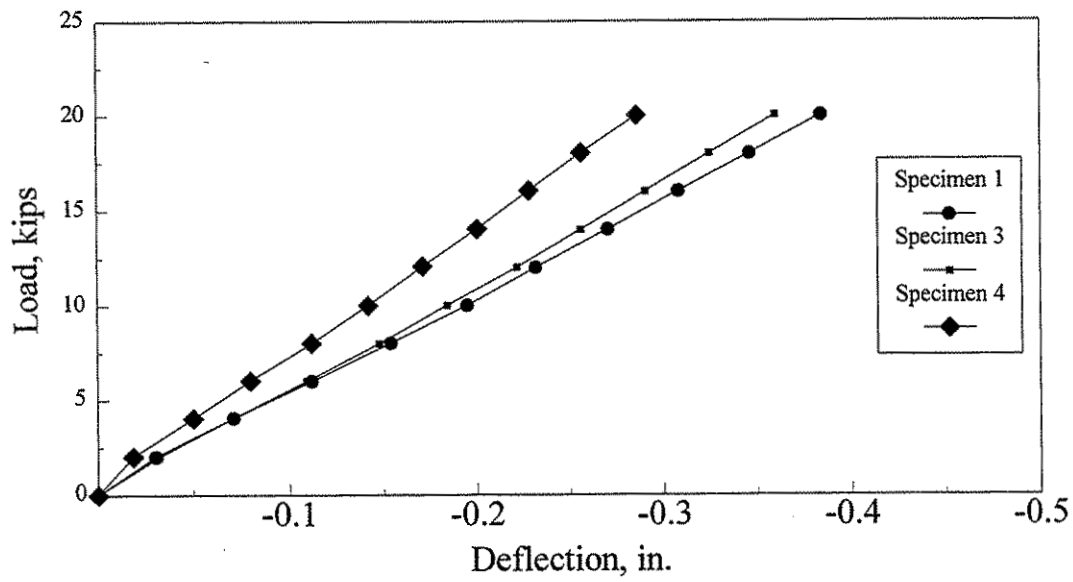
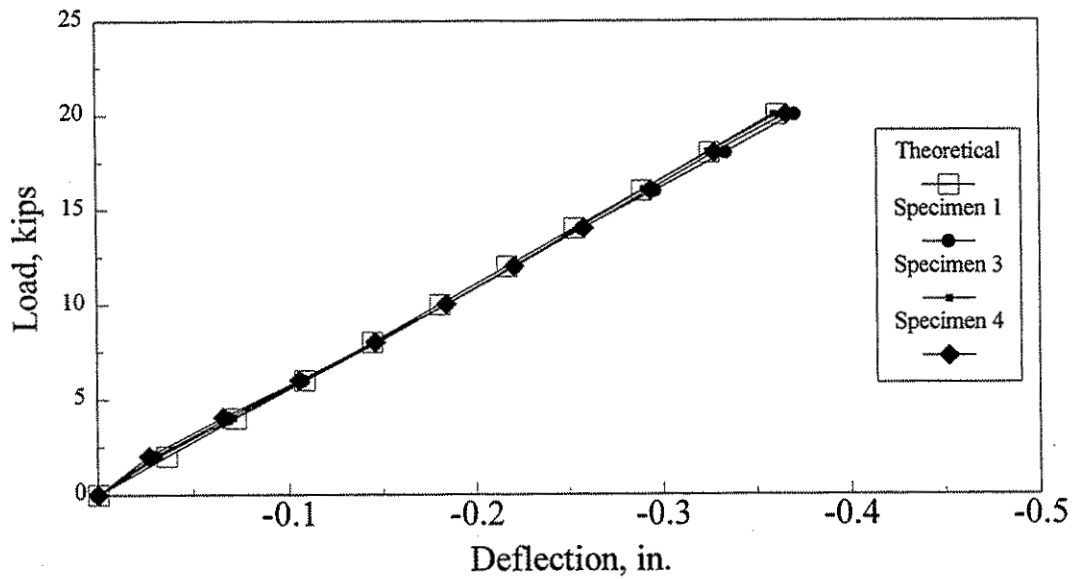


Fig. 5.23. Specimen 4 service test results.



a. As tested



b. Modified to account for differences in longitudinal flexural stiffness between specimens

Fig. 5.24. Comparison of the composite beam deflections at the centerline.



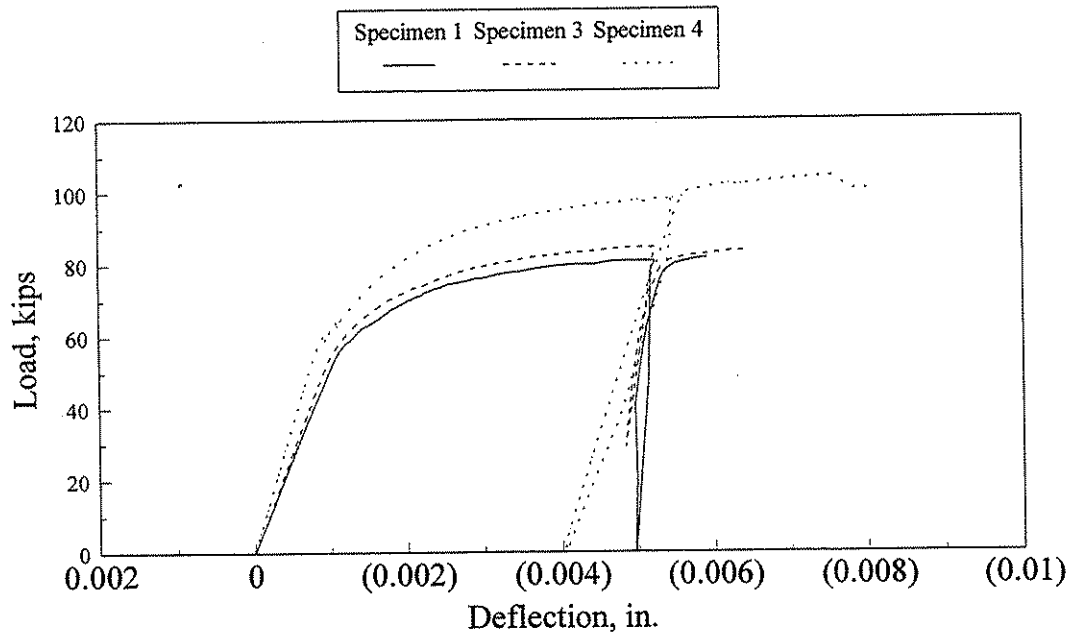
three specimens exhibit the same deflection behavior. The modifications are based upon the cross sections exhibiting complete composite behavior. Also shown in Fig 5.24b, assuming simple support conditions, is the theoretical load deflection curve for Specimen 1 based upon the calculated longitudinal flexural stiffness. The excellent agreement of these four curves (three experimental and one theoretical) indicates "complete" composite action and elastic behavior in all three specimens.

The centerline deflections in the ultimate load tests are shown in Fig. 5.25. As in Fig 5.24, "as tested" data are presented as well as adjusted data. Data in Fig 5.24b was adjusted assuming the specimens behaved elastically throughout the testing. This explains why the deflection curves in Fig. 5.25b began to diverge after approximately 267 kN (60 kips) have been applied. The specimens began to behave in a nonlinear fashion and the assumption of elastic behavior was no longer valid. As stated in Chp 2, during each of the ultimate load tests, the stroke limit of the hydraulic cylinders was reached. In order to continue loading to failure, the load was removed and the load assembly was modified in order that additional load could be applied. The ultimate load and corresponding deflection at the centerline for each specimen was: 363 kN (81.7 kips) and 150 mm (5.92 in.) for Specimen 1, 372 kN (83.5 kips) and 159 mm (6.27 in.) for Specimen 3, and 447 kN (100.5 kips) and 198 mm (7.79 in.) for Specimen 4. Ultimate failure of each specimen occurred when the concrete failed in compression.

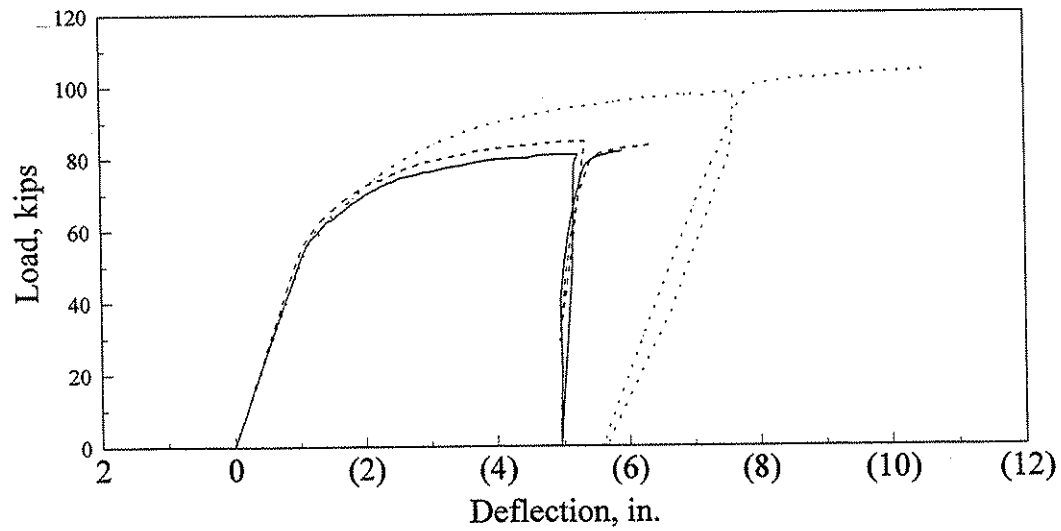
## **5.4 Field Bridge Test Results and Analysis**

### **5.4.1 Field Bridge Results**

Figures 5.26 - 5.33 present the deflection results for each of the eight tests completed, and the moment fraction based on recorded strain data. The deflection data includes readings when the rear tandem axles of the truck(s) were positioned at the quarter point, centerline, and three-quarter point of the bridge. The moment fraction is calculated based only on the eight beams in a cross-section that were instrumented for strain. As discussed previously, the actual moment fraction carried by each beam could be approximated by dividing the moment fraction in the various graphs by two. This

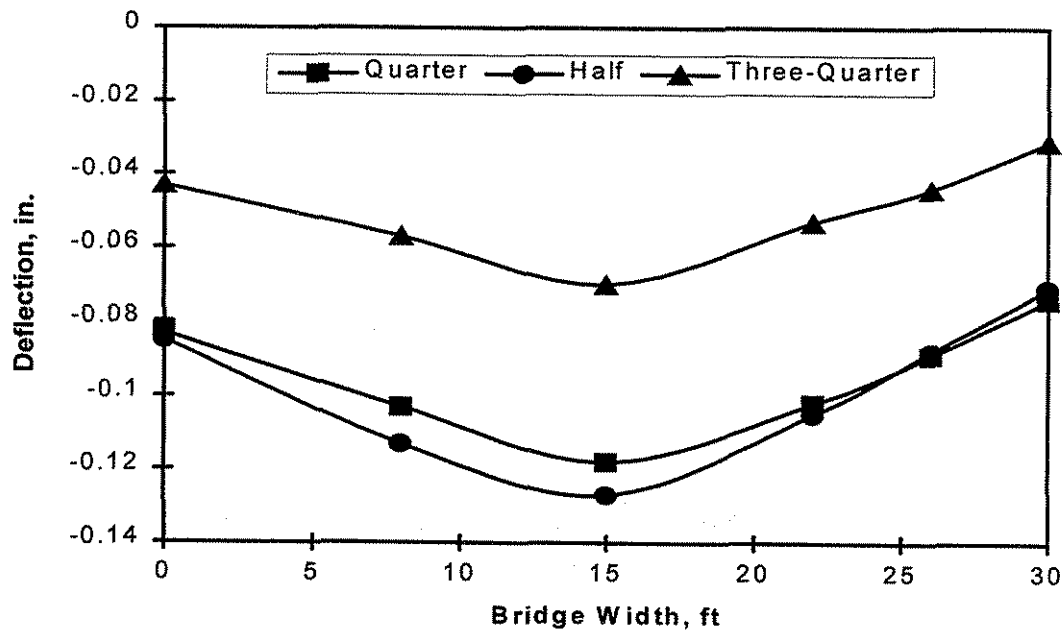


a. As tested

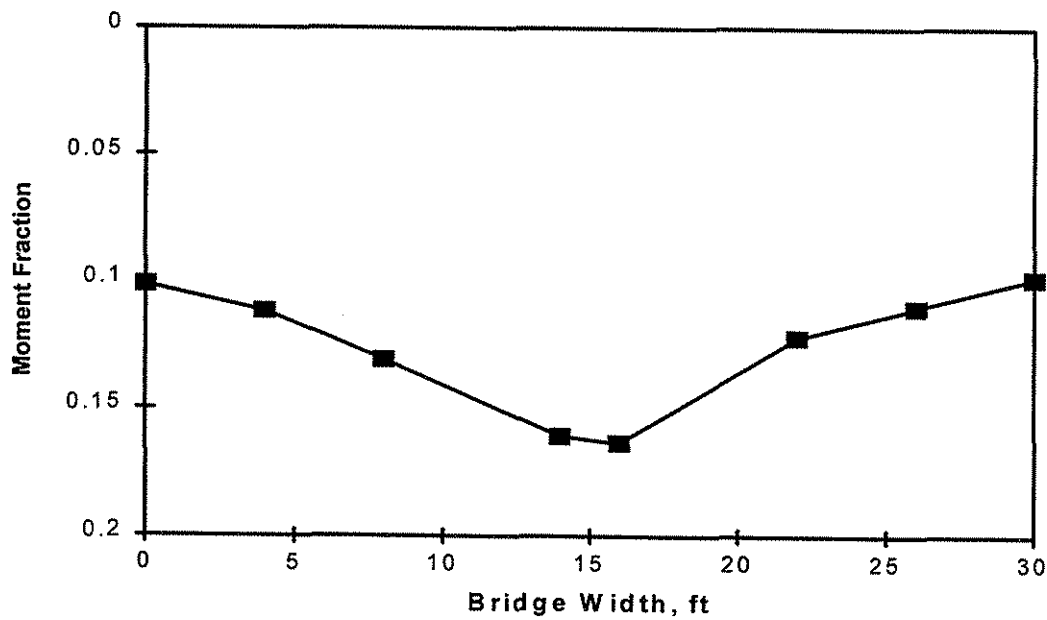


b. Modified to account for the differences in longitudinal flexural stiffness between specimens

Fig. 5.25. Ultimate load deflections

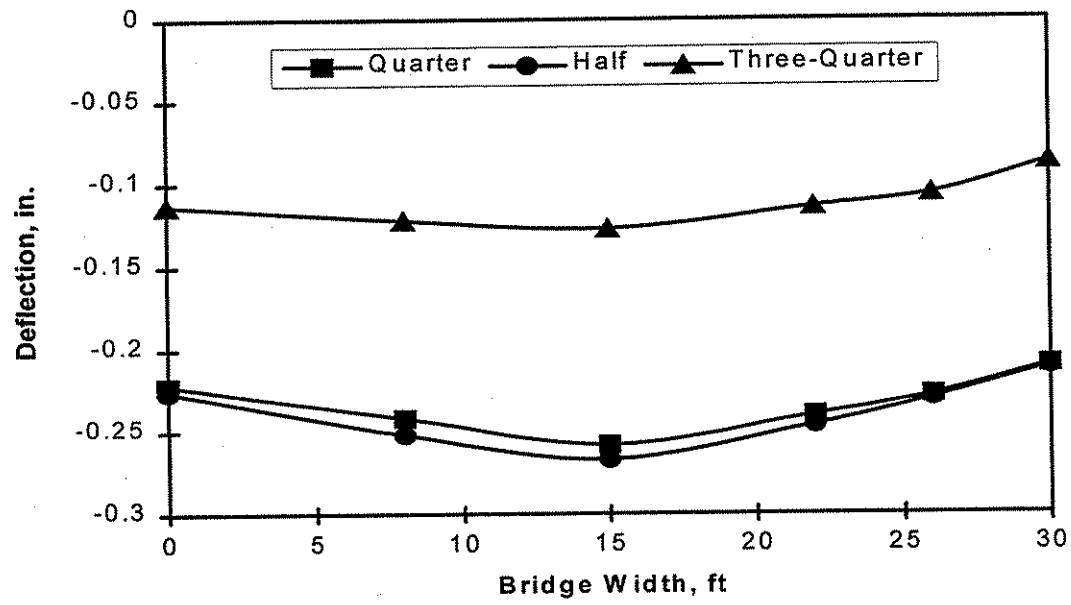


a. Centerline deflection data

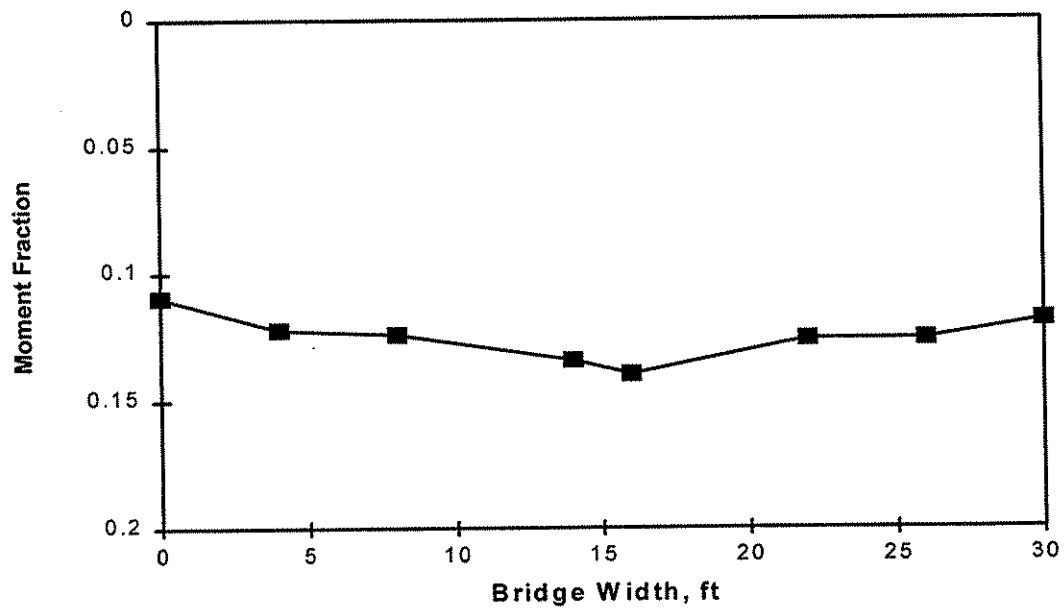


b. Moment fraction data

Fig. 5.26. Deflection and moment fraction data for Test 1.

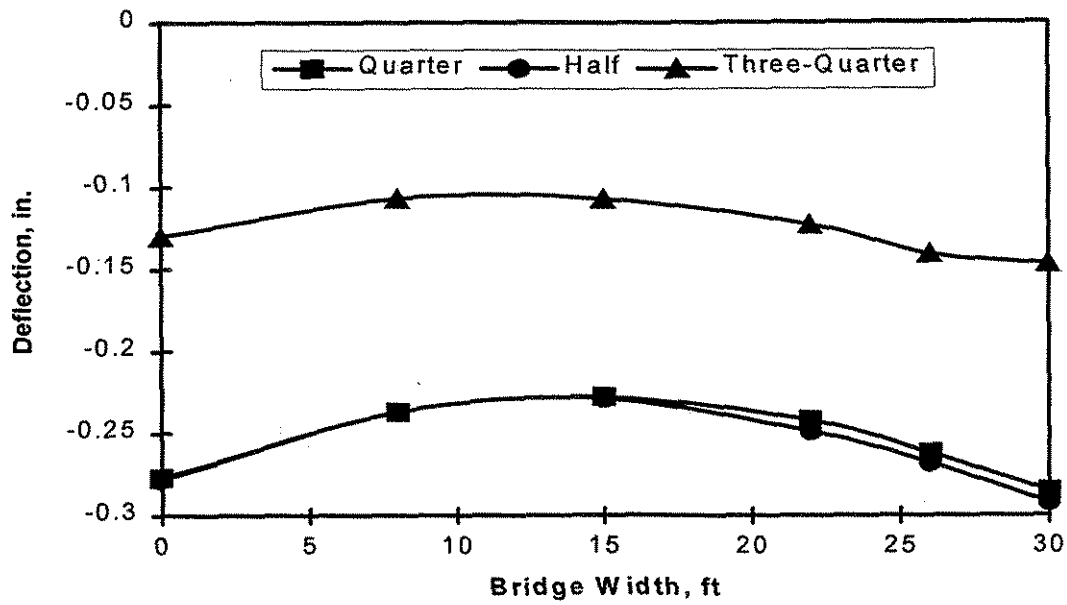


a. Centerline deflection data

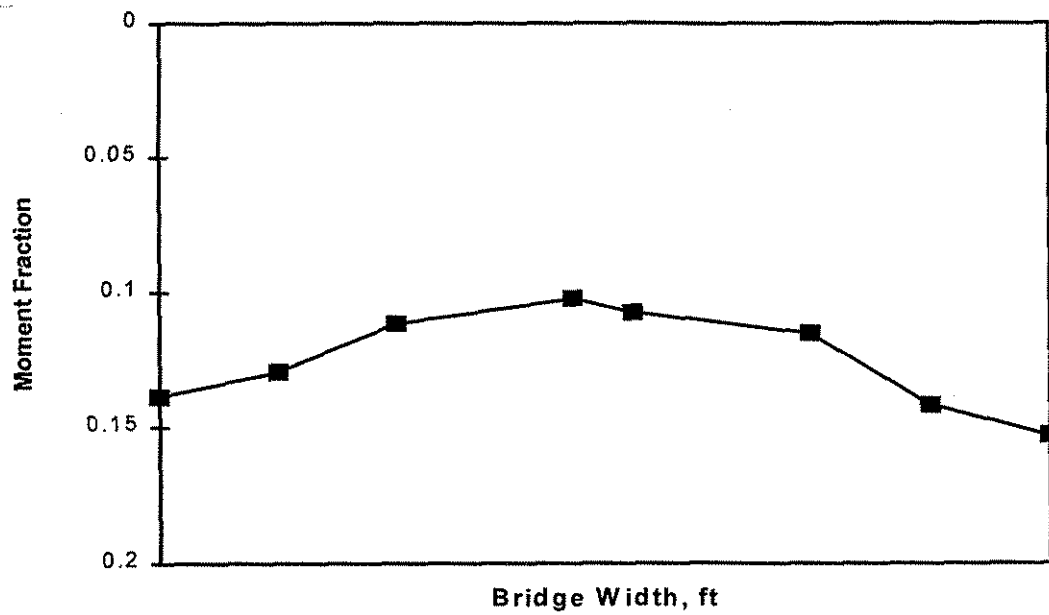


b. Moment fraction data

Fig. 5.27. Deflection and moment fraction data for Test 2.

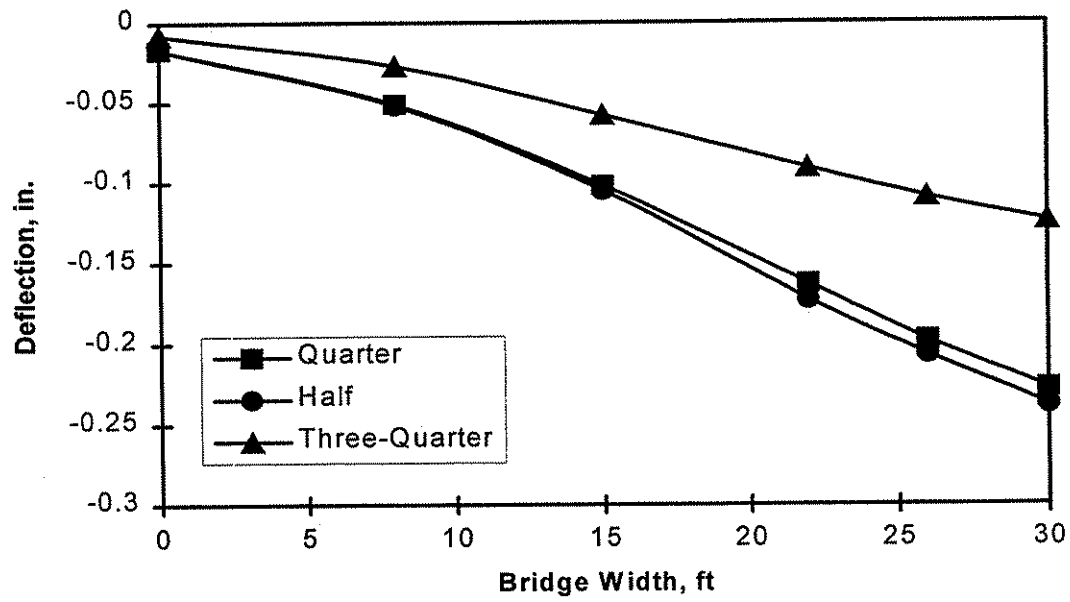


a. Centerline deflection data

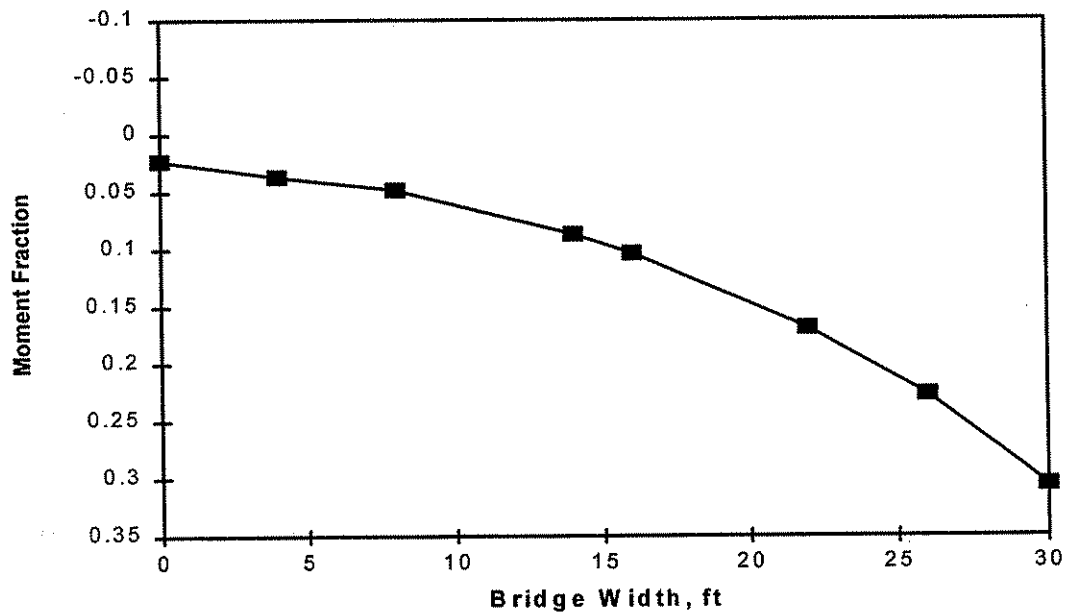


b. Moment fraction data

Fig. 5.28. Deflection and moment fraction data for Test 3.

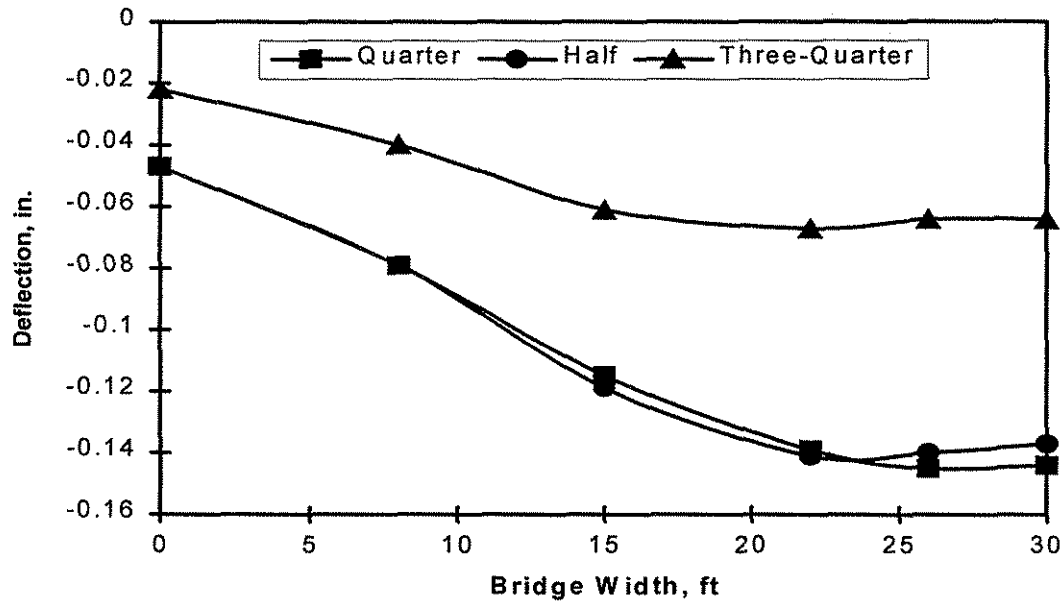


a. Centerline deflection data

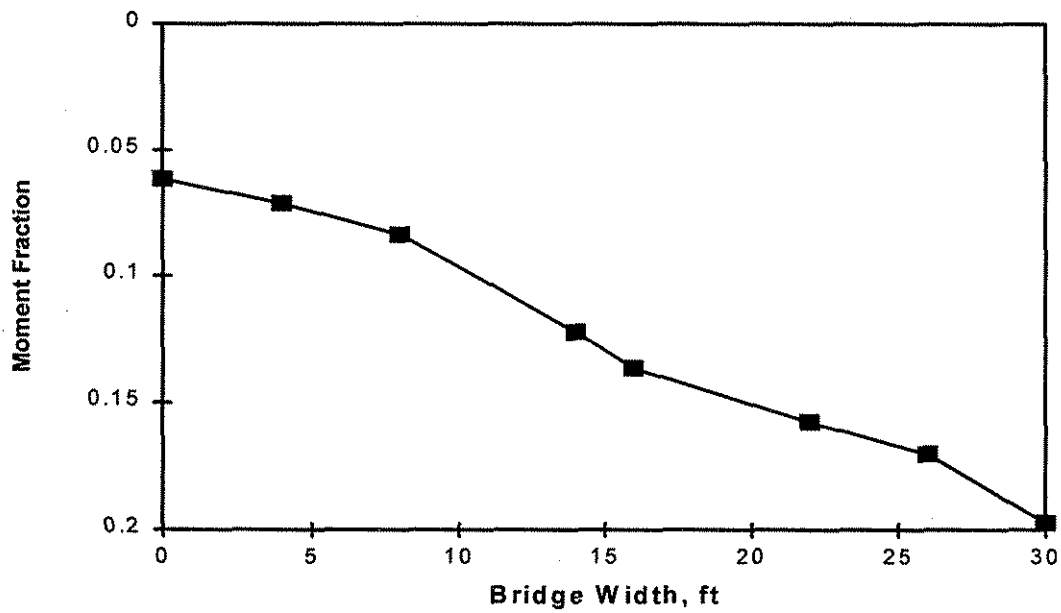


b. Moment fraction data

Fig. 5.29. Deflection and moment fraction data for Test 4.

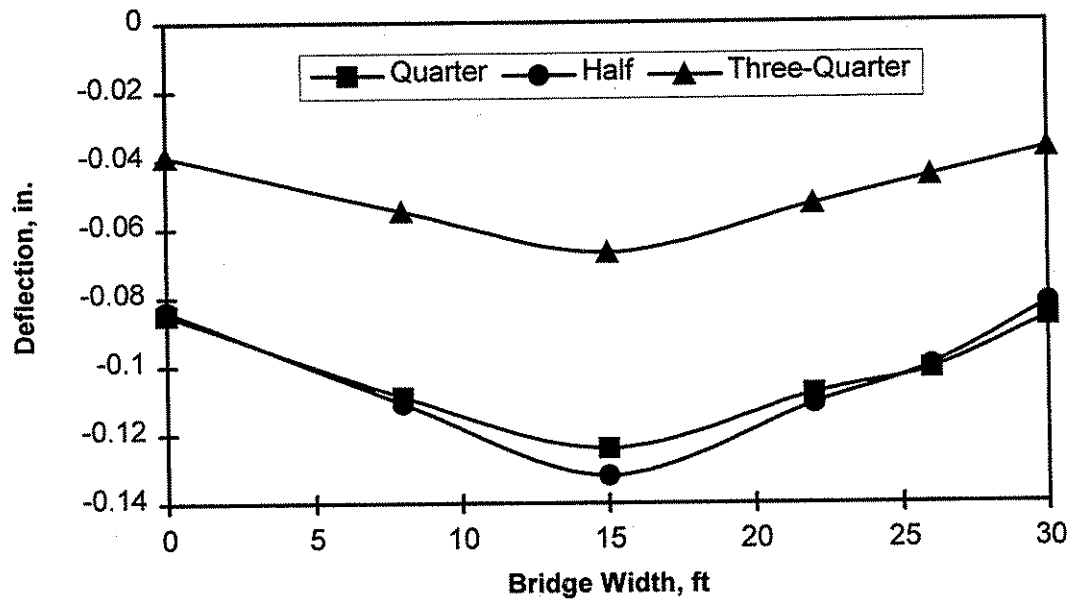


a. Centerline deflection data

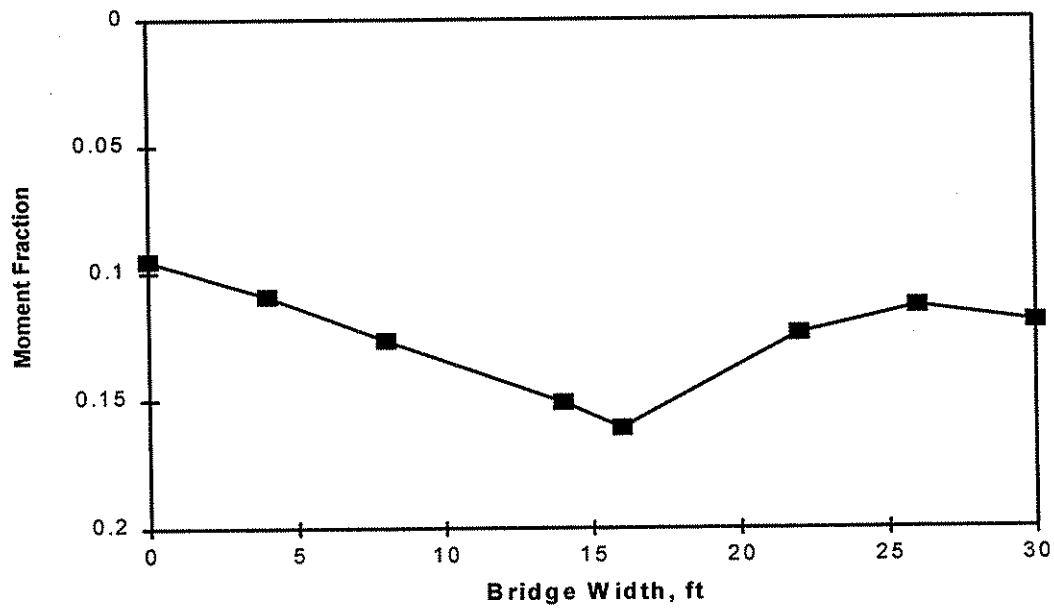


b. Moment fraction data

Fig. 5.30. Deflection and moment fraction data for Test 5.



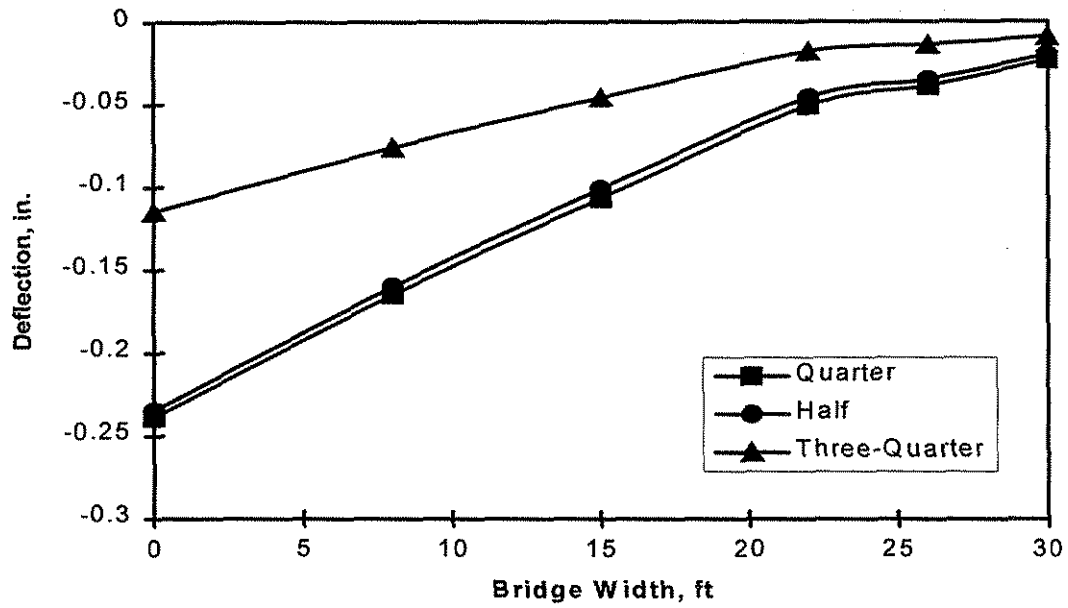
a. Centerline deflection data



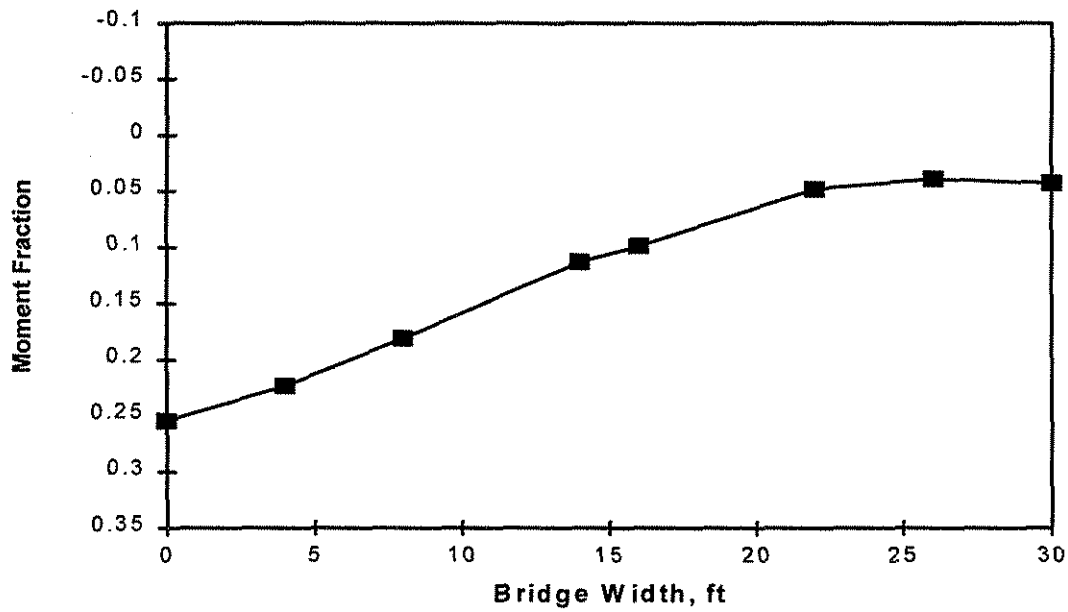
b. Moment fraction data

Fig. 5.31. Deflection and moment fraction data for Test 6.



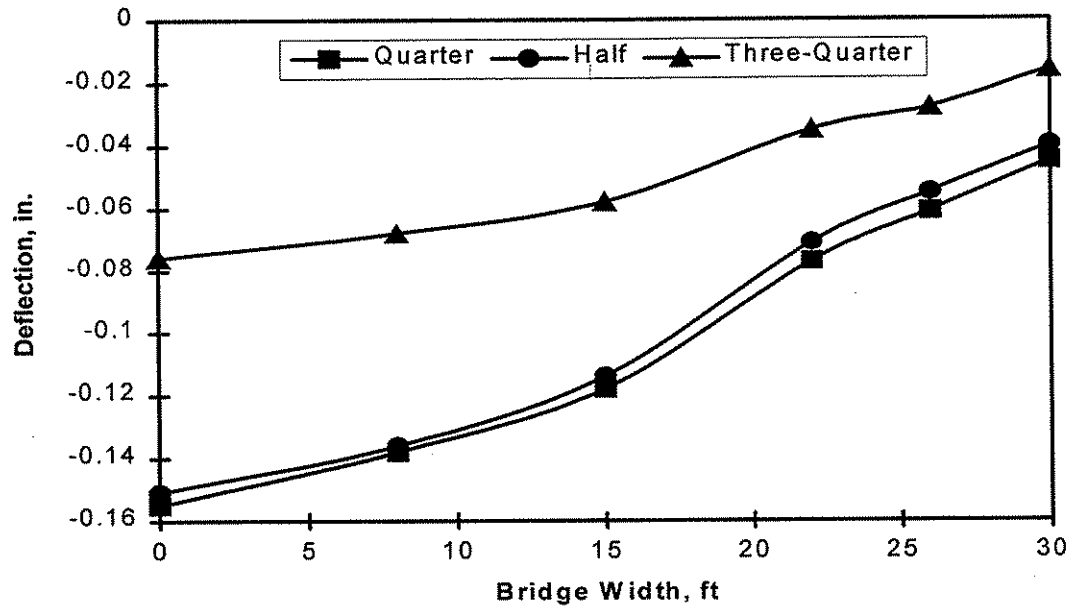


a. Centerline deflection data

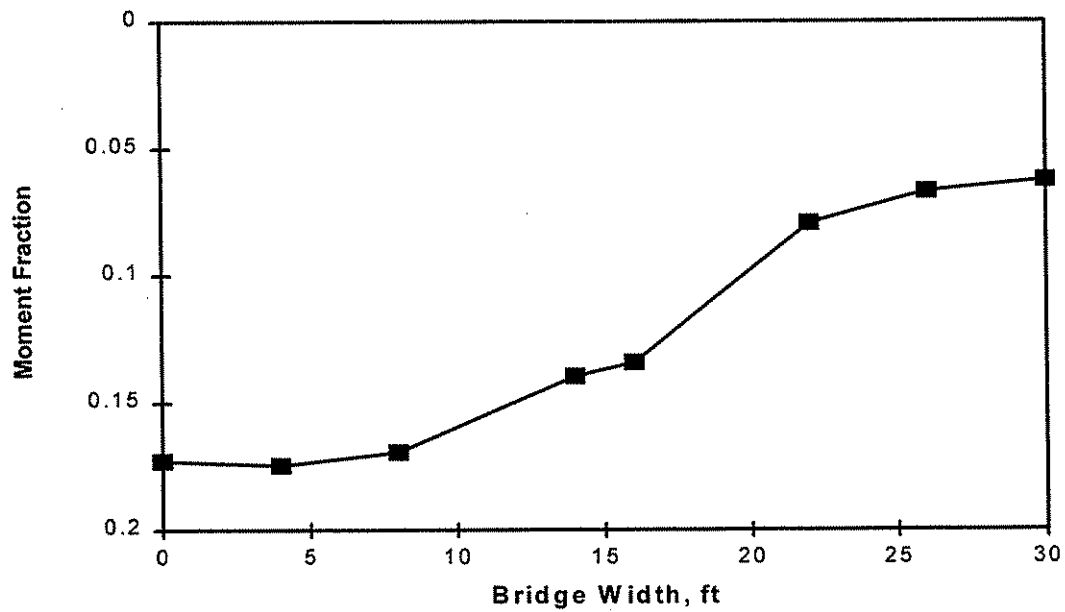


b. Moment fraction data

Fig. 5.32. Deflection and moment fraction data for Test 7.



a. Centerline deflection data



b. Moment fraction data

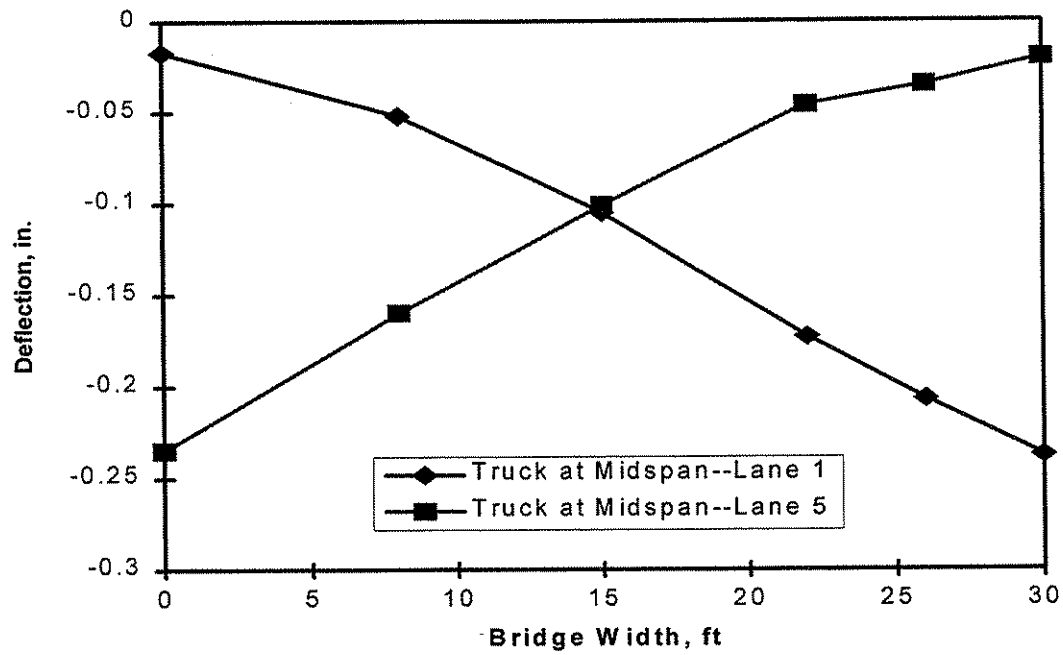
Fig. 5.33. Deflection and moment fraction data for Test 8.

would be true, assuming the strain in non-instrumented beams would be equal to an average of the strains in the adjacent instrumented beams.

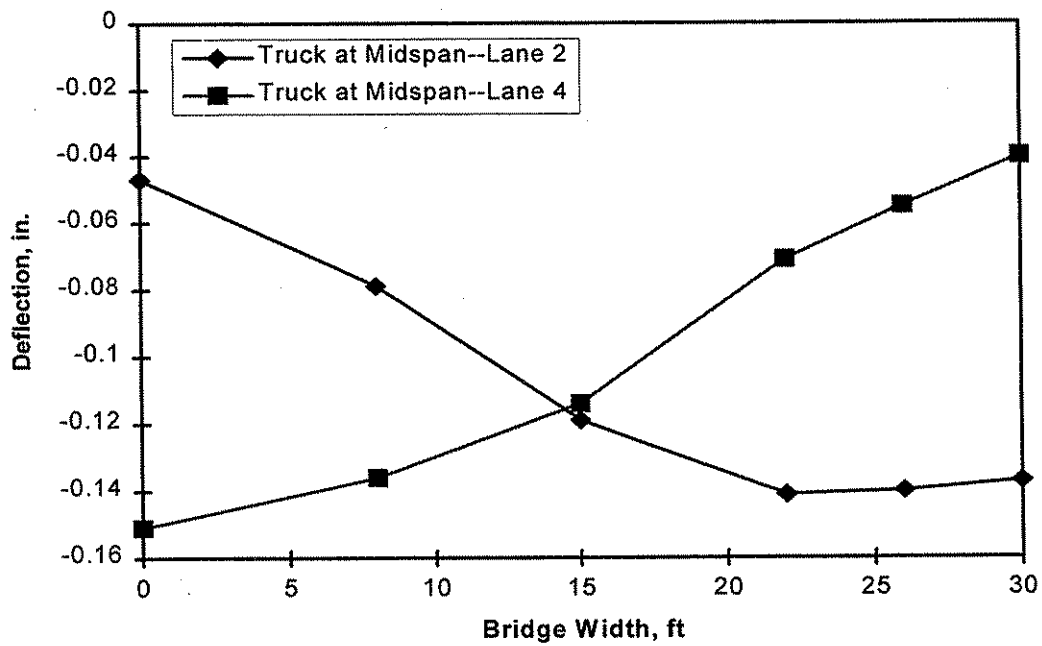
Overall, the deflection data indicated that the BISB was a very stiff structure both longitudinally and transversely. With a total load of approximately 445 kN (100 kips) (Test 2), the maximum deflection of the bridge was only 6 mm (1/4 in.). Longitudinally, there was very little difference in deflections when the truck was positioned at the quarter point or at the centerline. The maximum deflections varied by only 0.3 mm (0.01 in.). The large difference in the deflections when the trucks were at the three-quarter span can be attributed to the fact that the front axle of the truck was off of the bridge. Because approximately half of the weight of the trucks was positioned on the bridge, it would be assumed that the deflections would likewise be approximately half. This is true as can be seen in Fig. 5.26a.

Transversely, the load was very effectively distributed throughout the width of the bridge. As can be seen in Fig. 5.26b, with the load centered on the width of the bridge, the exterior beams still resisted a significant portion of the load. With 16 beams in the bridge, an even load distribution would result in 6.25% of the total load being carried by each beam. As explained earlier, the moment fraction of 0.1 for the exterior beams in Fig. 5.26b represents 0.05 (5%) of the total load. This demonstrates that the concrete between the steel beams adequately transferred the service loads to adjacent beams.

Symmetry of the field bridge was checked by comparing the deflections at midspan for Tests 4 and 7, and Tests 5 and 8. For Tests 4 and 7, the truck was positioned on the outermost lane of the bridge, on opposite sides. Although test vehicle 1 was used for Test 4 and test vehicle 2 for Test 7, the weights of the two trucks were similar; thus, a graph of the two tests should produce symmetrical results. As can be seen in Fig. 5.34a, the deflections at the center of the bridge were within 5% of each other which can be attributed to the different truck weights; thus, the bridge behaves symmetrically. Additionally, Fig. 5.34b illustrates with the trucks at midspan - one positioned in lane 2 and one positioned in lane 4 - deflections at the center are within 5%, thereby confirming the symmetry in the bridge.



a. Truck in lanes 1 and 5



b. Truck in lanes 2 and 4

Fig. 5.34 Symmetry determination on field bridge.

#### 5.4.2 Comparison of Experimental and Analytical Results

A grillage model (see Fig. 5.35) of the field BISB was developed to allow comparison of analytical and experimental data. The analytical model was developed based on principles presented earlier in Chp 4 and with consideration to the results of the sensitivity study presented in the same chapter.

The moment of inertia was calculated based on the moment of inertia of the steel beam plus the moment of inertia of the contributory area of the concrete, resulting in moment of inertia of  $3.50 \times 10^8 \text{ mm}^4$  ( $840 \text{ in}^4$ ) and  $4.25 \times 10^8 \text{ mm}^4$  ( $1020 \text{ in}^4$ ) for the exterior and interior beams, respectively. The modulus of elasticity and Poisson's ratio were assumed to be 200 GPa (29,000 ksi) and 0.3 respectively, which are common properties of structural steel.

The transverse beams were connected to the longitudinal beams by links (BEAM44). All data provided herein used a fixed connection for the link member. The links were spaced at 152 mm (6 in.) longitudinally along the entire bridge (see Fig. 5.35). The moment of inertia of the links was based on the contributory area of concrete between the steel beams, and was calculated at  $175 \times 10^8 \text{ mm}^4$  ( $420 \text{ in}^4$ ). The modulus of elasticity was input as 29 GPa (4200 ksi), an approximation based on the 28-day concrete compressive strength of the composite beam tested in the laboratory. Poisson's ratio was assumed to be 0.15.

For each truck on the bridge, six concentrated loads were placed on the finite element model to represent the six truck wheel loads. Support conditions of the longitudinal beams were then modeled assuming both pinned and fixed rotational restraint.

Figures 5.36-5.42 present the results of the theoretical analysis, along with the experimental results for each test, with the truck(s) at midspan longitudinally. Test 6 has been excluded since it was a repeat of Test 1, and the data were very similar.

As described earlier, the dowels connecting the superstructure and the abutment provide a certain amount of longitudinal beam end fixity. It can be seen by the results in Figs. 5.36-5.42 that this connection more closely resembles a fixed condition than a

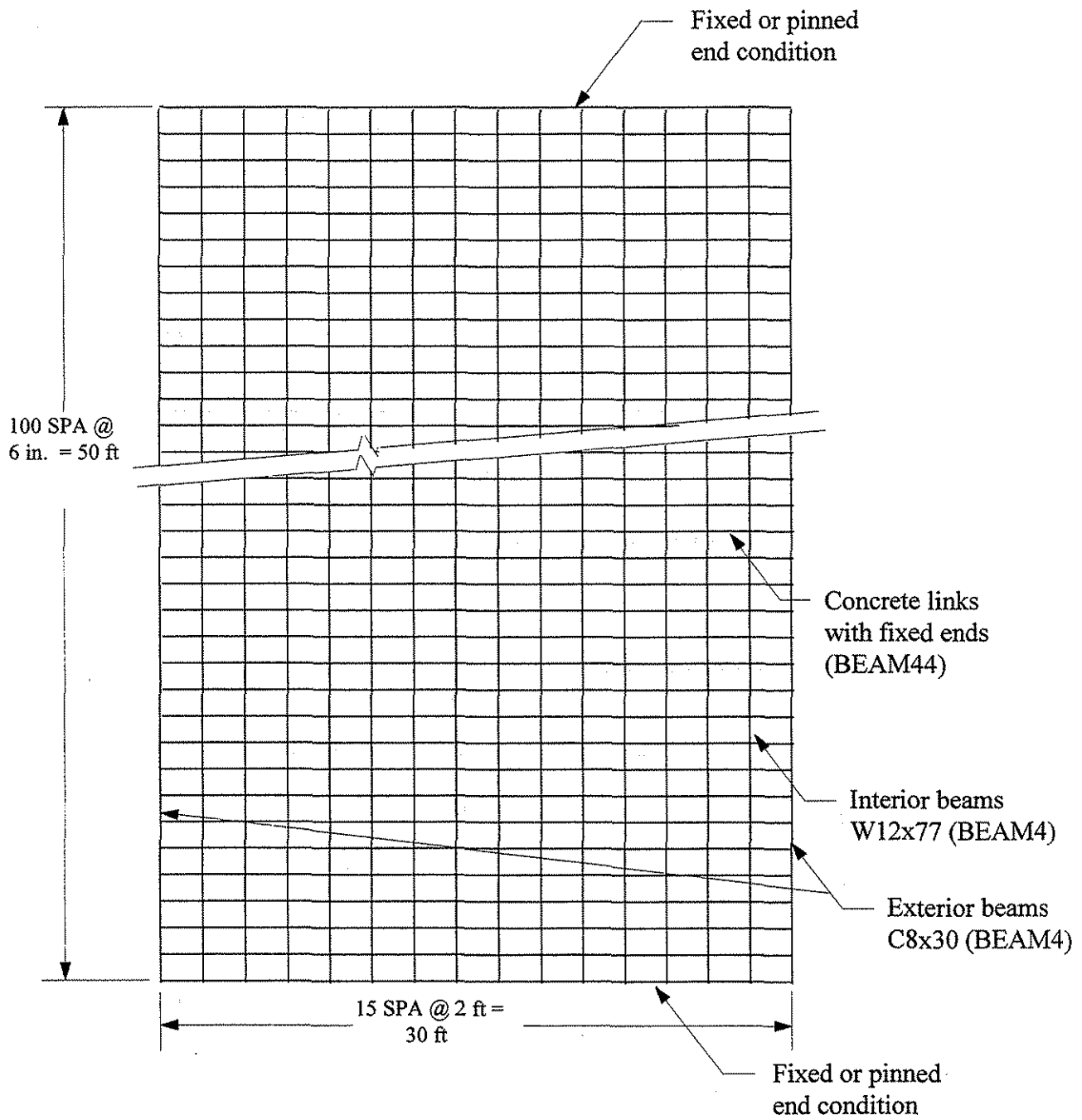


Fig. 5.35. Field bridge grillage analogy.

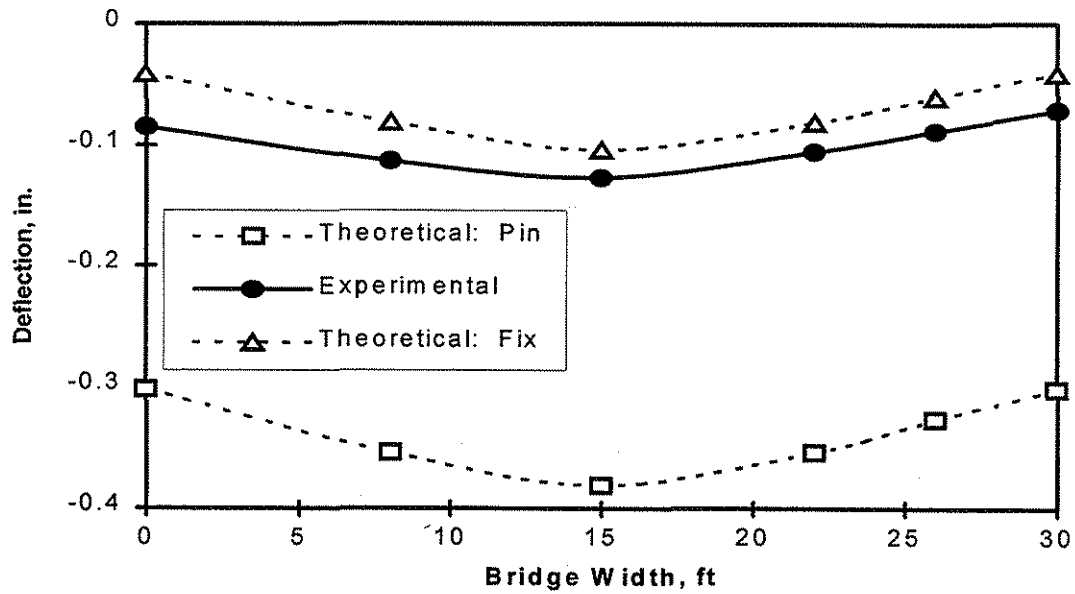


Fig. 5.36. Comparison of theoretical and experimental deflections at midspan: Test 1.

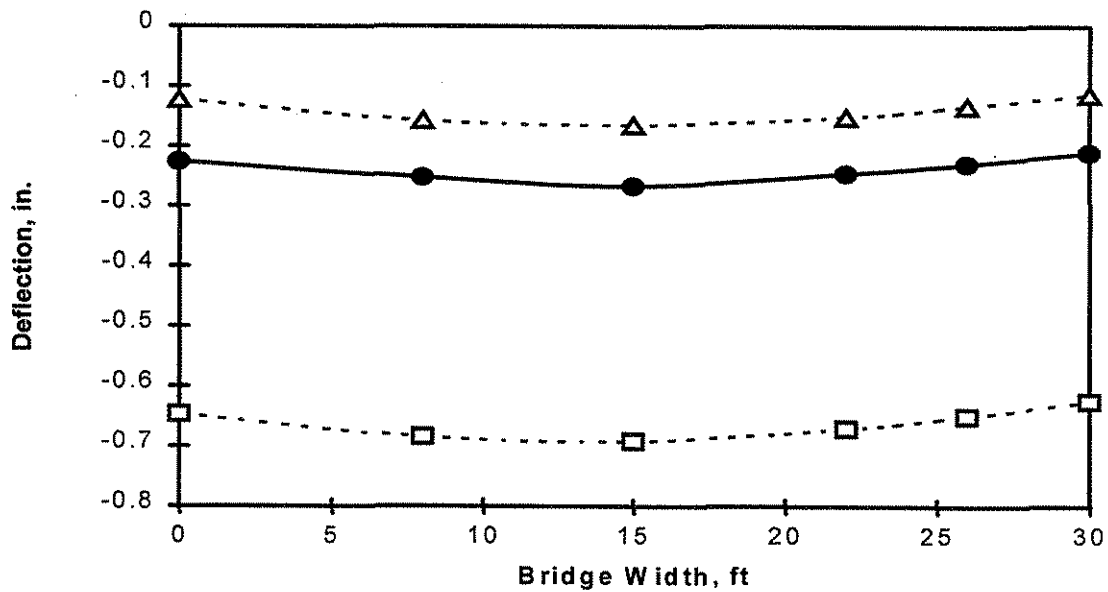


Fig. 5.37. Comparison of theoretical and experimental deflections at midspan: Test 2.

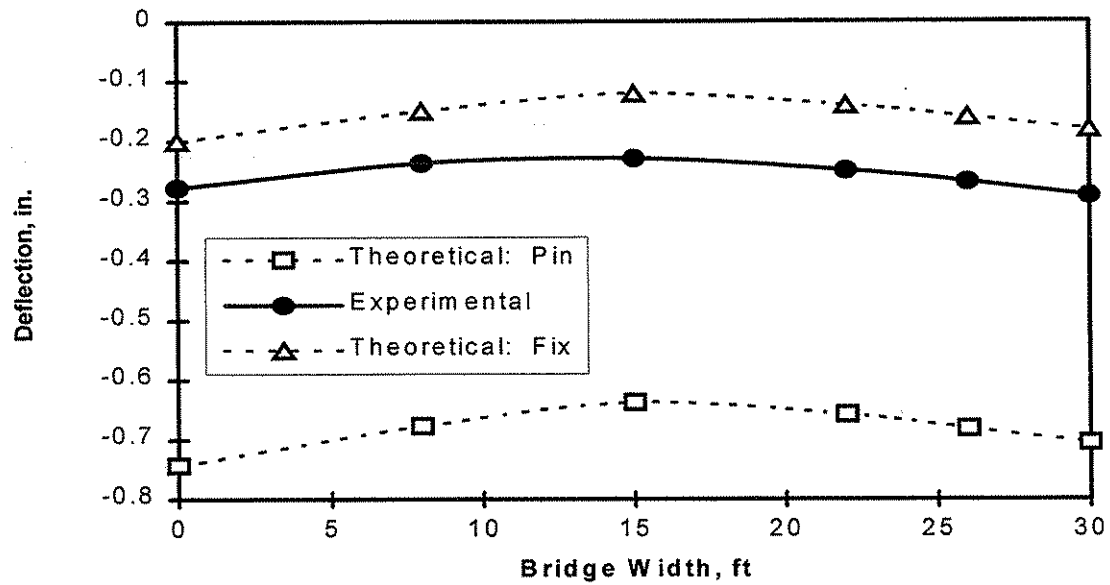


Fig. 5.38. Comparison of theoretical and experimental deflections at midspan: Test 3.

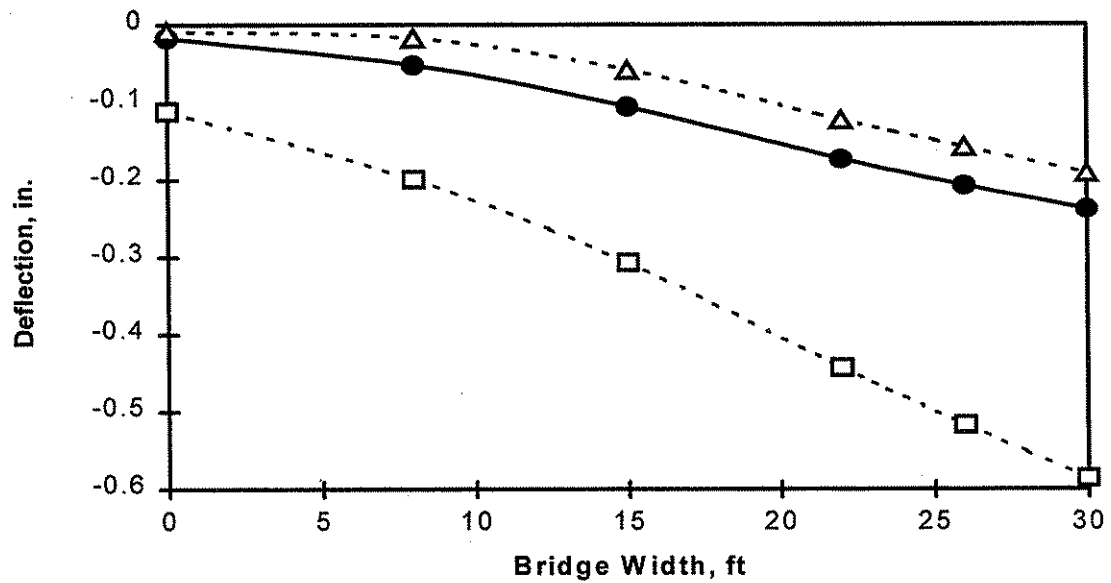


Fig. 5.39. Comparison of theoretical and experimental deflections at midspan: Test 4.



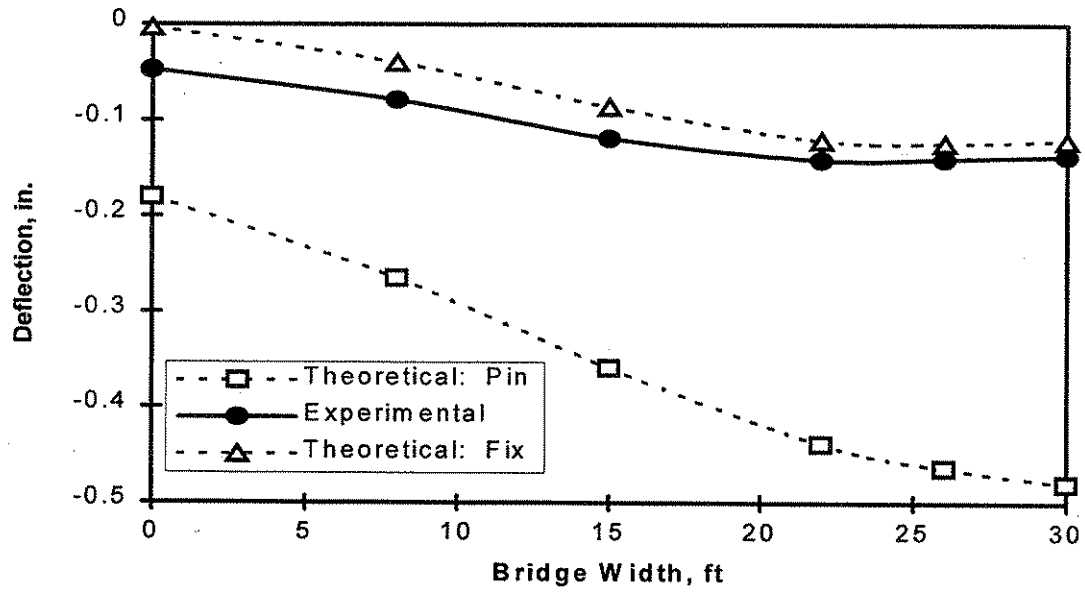


Fig. 5.40. Comparison of theoretical and experimental deflections at midspan: Test 5.

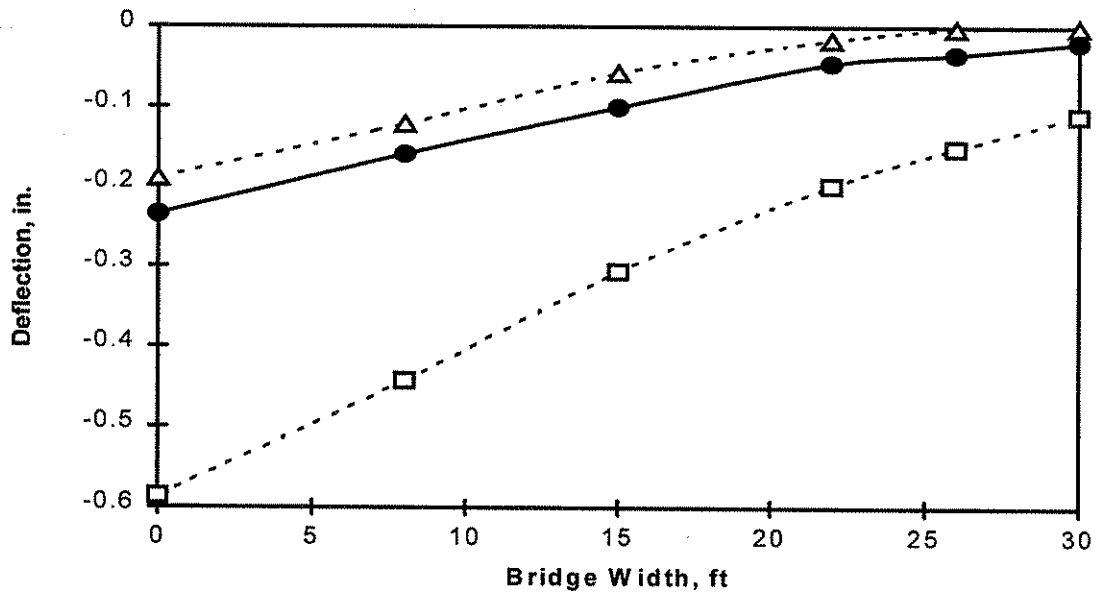


Fig. 5.41. Comparison of theoretical and experimental deflections at midspan: Test 7.

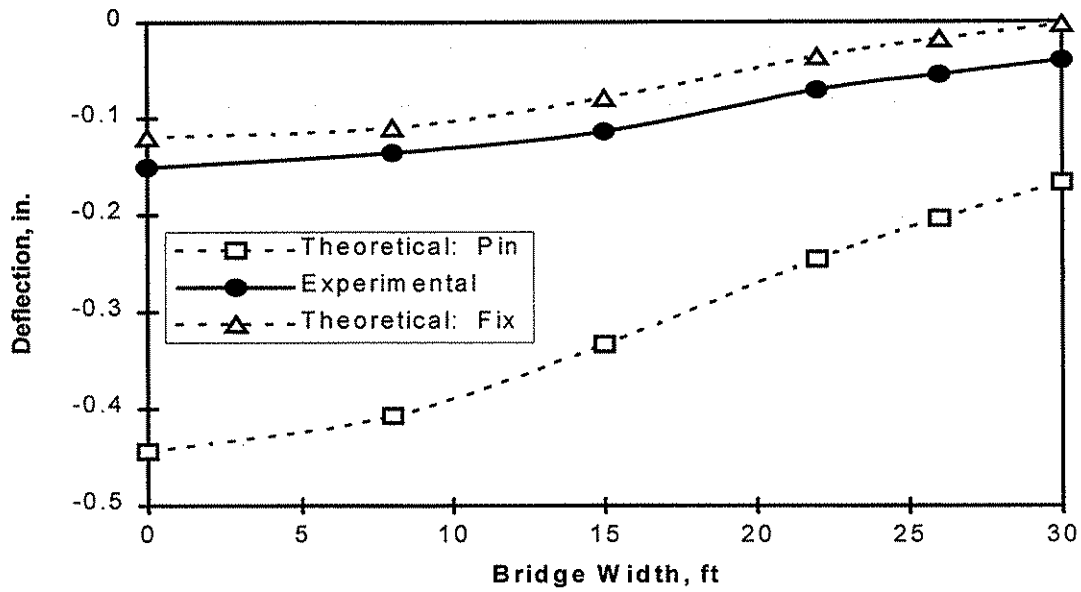


Fig. 5.42 Comparison of theoretical and experimental deflections at midspan: Test 8.

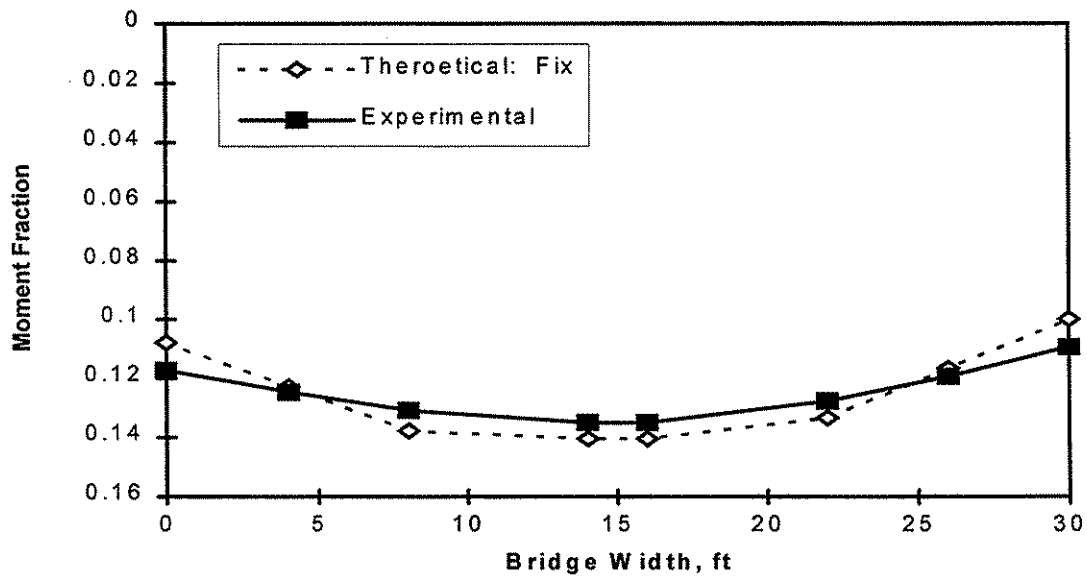


Fig. 5.43. Comparison of theoretical and experimental moment fractions at midspan: Test 2, truck at midspan.

pinned condition, thus suggesting that the connecting dowels between the abutment and superstructure provide a significant resistance to rotation.

Experimental and analytical moment fraction data are presented in Figs. 5.43 and 5.44. Two typical graphs have been shown and only the fixed end condition is depicted. Results from Figs. 5.43 and 5.44 indicate that the finite element model predicts the actual BISB deflections with reasonable accuracy.

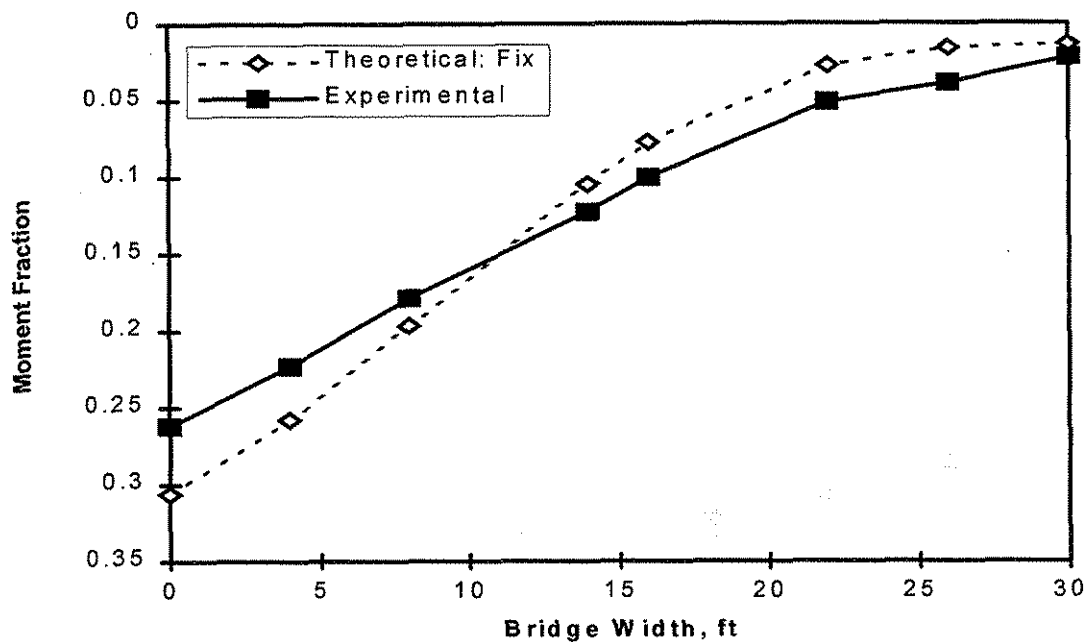


Fig. 5.44. Comparison of theoretical and experimental moment fractions at midspan: Test 7, truck at midspan.

## 6. SUMMARY AND CONCLUSIONS

In this phase of the investigation, Concept 2 - Beam-in-Slab Bridge - was investigated. The study consisted of several tasks. In the experimental part of the investigation, there were several types of static load tests: push-out tests, BISB laboratory tests, composite beam tests, and a BISB field test. In the analytical part of the study, a grillage method of analysis was used to develop analytical models of the four-beam BISB tested in the laboratory and the BISB tested in the field.

Although previous research has led to the development of a variety of design equations for the shear strength of a shear hole connector, an evaluation of those equations indicated that friction between the steel plate and the concrete was ignored, or defined in terms of unknown quantities, such as the stress at an interface, which would make use of the equation very difficult to use in design. A series of 36 push-out tests were performed considering the following: hole size, amount of reinforcing steel through the shear holes, amount of transverse slab reinforcement, concrete strength, and number of shear holes. An equation was developed relating these five variables to the design strength of a given connection.

The following conclusions are based on the results of the push-out tests:

- Separation of the concrete slabs and displacement of the steel plate were negligible factors in the strength of the connector.
- Three distinct phases were noted in the loading of an ASC: nearly linear stiffness phase, the point of maximum load, and a phase where the slip increases with a corresponding decrease in the load.
- After the maximum load was attained, generally 80-90% of the maximum load was retained at an average slip of 7.6 mm (0.3 in.). After failure of the concrete dowels, the friction between the concrete and steel plate and between cracked concrete surfaces continued to provide shear resistance.
- The fabrication method used to create the shear holes had an insignificant effect on the shear strength of the connector. Thus, torched holes can be used with very minimal decrease in shear strength.

- Spacing of the holes had an insignificant effect on the shear strength of a given ASC if a minimum spacing of 1.7 times the shear hole diameter was maintained.
- A significant strength increase, as well as an increase in the stiffness, was noted with an increase in the size of the shear hole.
- If designed correctly, the displacement between the concrete plate and the steel plate (slip) will be minimal throughout service loading conditions and failure will occur by shearing of the concrete dowels formed by concrete penetrating the shear holes.

The BISB laboratory tests of the two-beam specimen (beams spaced 610 mm (2 ft) apart) included service load tests and an ultimate load test. The model bridge ( $L = 9,150$  mm (30 ft),  $W = 915$  mm (3 ft)) was simply supported and was subjected to two-point loading. Results from the two-beam specimen tests indicated the following conclusions:

- In the early stages of loading, the specimen behaved like a composite beam. At approximately 22.25 kN (5 kips), the specimen began to behave non-compositely, indicating that the bond between the steel and concrete had been reduced. At a load of approximately 67 kN (15 kips), the specimen acted essentially like a non-composite structure, with the concrete providing minimal structural strength.
- Throughout service loading conditions, end slip was negligible. At loads exceeding 40 kips, the end slip significantly increased with increasing load.
- The specimen ultimate load capacity was approximately 890 kN (200 kips) total for the two point loading. This was the capacity of the loading system, however, for all practical purposes the beam had failed as the steel had yielded.

The BISB laboratory tests of the four-beam specimen (beams spaced 610 mm (2 ft) apart) also included both service load tests and an ultimate load test in which both deflections and strains were measured. The ultimate load test was stopped when the steel beams had yielded and the limit of the testing system had been reached. A grillage model

of the four-beam specimen was created and analytical results were compared to the experimental results of the service level load tests.

The following conclusions can be made based on the four-beam specimen tests:

- The specimen behaved nonlinearly at loads above 1.33 MN (300 kips) and 73 mm (2.87 in.) of deflection at the centerline.
- The ultimate load capacity the specimen was 1.65 MN (370 kips) and the deflection at this load was 103 mm (4.06 in.).
- The grillage analogy model provided predictions of the specimen deflections to within 15% of the experimental results.

Four composite beam specimens were tested. Specimen 1 consisted of an inverted T-section fabricated by cutting off a flange of a W21x62 steel beam. The concrete slab was cast on the top of the inverted T-section. Specimens 2 and 3 were constructed from W21x62 steel beams with their top flange imbedded into the concrete slab. The total depth (from the top of slab to the bottom flange of the beam) of the specimens was the same as Specimen 1. Specimen 4 was cast with a concrete slab cast directly on top of the top flange of a W21x62 steel beam using shear studs to attain composite action. Specimens 1, 2, and 3 were also cast to attain composite action; however, they utilized the new shear hole shear connector (ASC).

Each composite beam specimen was instrumented to measure strains and deflections. Each specimen was loaded three times at service level conditions using a two point loading arrangement, and then an ultimate load test was performed. The ultimate load test concluded when the concrete failed in compression at the midspan of the specimens.

The results from the composite beam tests indicated the following conclusions:

- The service level deflection of all three composite beam specimens was accurately predicted to within 5% by assuming complete composite action.
- No change in the neutral axis location was observed during the service level tests of all three specimens.
- The ASC shear hole shear connector is an effective shear transfer mechanism.

- The service load tests showed that the behavior of the composite beam specimen utilizing the inverted T-section can be adequately modeled using standard composite beam theory.
- The load/deflection behavior of all three types of composite beam specimens was similar.

A field bridge with a span length of 15,240 mm (50 ft) was load tested using two heavily loaded trucks. Both strain and deflections were recorded during the tests. An analytical model of the bridge using the grillage method of analysis was developed and results were compared with the experimental field bridge data.

The results from the testing indicated the following conclusions:

- The BISB system results in a very stiff structure both transversely and longitudinally (the maximum bridge deflections was approximately 6 mm (1/4 in.) with a load of 445 kN (100 kips)).
- Load is distributed effectively transversely throughout the width of the bridge.
- Theoretical analysis results from the grillage model of the bridge when compared to the experimental load test data indicated that the bridge has a significant amount of rotational fixity at each abutment.

## 7. RECOMMENDED RESEARCH

On the basis of the work completed in this phase of the investigation, the completion of the following tasks are recommended before this concept can be employed in a demonstration project:

1. Additional laboratory tests are required. In these tests the following variables should be investigated: post-tensioning of the steel beams to create camber so that the system can be used on longer spans, T-sections fabricated from W-shaped sections, and structural plates. In all the tests, the ASC should be fabricated with torched holes.
2. A limited number of cyclic tests are needed. The majority of these should be performed on push-out specimens; however, some should be performed on full-scale composite beam specimens.
3. Using the results of the previous two tasks and the results from the Phase I research, two and four beam composite specimens with fabricated T-sections, ASC, and various profiles of tension concrete should be fabricated and tested. The tests should be service load tests as well as ultimate load tests.

Assuming successful completion of these recommended three tasks, the next step should be to use the modified BISB in a demonstration project.



## 8. ACKNOWLEDGEMENTS

The study presented in this report was conducted by the Bridge Engineering Center under the auspices of the Engineering Research Institute of Iowa State University. The research was sponsored by the Project Development Division of the Iowa Department of Transportation and Iowa Highway Research Board under Research Project 382.

The authors wish to thank the various Iowa DOT and county engineers who helped with this project and provided their input and support. In particular, we would like to thank the project advisory committee:

- Dennis J. Edgar, Assistant County Engineer, Blackhawk County
- Robert L. Gumbert, County Engineer, Tama County
- Mark J. Nahra, County Engineer, Cedar County
- Gerald D. Petermeier, County Engineer, Benton County
- Wallace C. Mook, Director of Public Works , City of Bettendorf
- Jim Witt, County Engineer, Cerro Gordo County

Appreciation is also extended to Bruce L. Brakke and Vernon Marks of the Iowa DOT for their assistance in obtaining the surplus steel beams used in this investigation. Gerald D. Petermeier is also thanked for providing the field bridge for load testing and the loaded trucks used in the testing.

Special thanks are accorded to the following Civil Engineering graduate and undergraduate students and Construction Engineering undergraduate students for their assistance in various aspects of the project: Andrea Heller, Trevor Brown, Matthew Fagen, David Oxenford, Brett Conard, Matt Smith, Chris Kruse, Mary Walz, Penny Moore, Dave Kepler, Ryan Paradis, Hillary Isebrands, Ted Willis, and Kevin Lex. Brent Phares, graduate student in Civil Engineering is also thanked for his special efforts in organizing this report. The authors also wish to thank Elaine Wipf for editing the report and Denise Wood for typing the final manuscript.

## 9. REFERENCES

1. "Ninth Annual report to Congress-Highway Bridge Replacement and Rehabilitation Program", FHWA, Washington, D.C., 1989.
2. "Rural Bridges: An Assessment Based Upon the National Bridge Inventory". Transportation Report, United States Department of Agriculture, Office of Transportation, April 1989.
3. Wipf, T.J., Klaiber, F.W., Prabhakaran, A., "Evaluation of Bridge Replacement Alternatives for the County Bridge System". Iowa Department of Transportation Project HR-365, ISU-ERI-Ames 95403, Iowa State University, Ames, Iowa, 1994.
4. Leonhardt, E.F., Andra, W., Andra, H-P., Harre, W., "New Improved Shear Connector With High Fatigue Strength for Composite Structures (Neues, vorteilhaftes Verbundmittel für Stahlverbund--Tragwerke mit hoher Dauerfestigkeit)". Beton--Und Stahlbetonbau, Vol. 12, pp. 325-331, 1987.
5. Roberts, W.S., and Heywood, R.J., "An Innovation to Increase the Competitiveness of Short Span Steel Concrete Composite Bridges". Proceedings, Fourth International Conference on Short and Medium Span Bridges. Developments in Short and Medium Span Bridge Engineering '94, Halifax, Nova Scotia, Canada, pp. 1160-1171, 1994.
6. Antunes, P.J., Behavior of Perfobond Rib Connectors in Composite Beams. B.Sc. Thesis, University of Saskatchewan, Saskatoon, Canada, 1988.
7. Veldanda, M.R., and Hosain, M.U., "Behavior of Perfobond Rib Shear Connectors in Composite Beams: Push-out Tests". Canadian Journal of Civil Engineering, Vol. 19, pp. 1-10, 1992.
8. Oguejiofor, E.C., and Hosain, M.U., "Behavior of Perfobond Rib Shear Connectors in Composite Beams: Full Size Tests". Canadian Journal of Civil Engineering, Vol. 19, pp. 224-235, 1992.
9. Oguejiofor, E.C., and Hosain, M.U., "Perfobond Rib Connectors For Composite Beams". Proceedings, Engineering Foundation Conference on Composite Construction in Steel and Concrete II, Potosi, Mo. 1992, pp. 883-898.
10. Davies, C. Tests on half-scale steel-concrete composite beams with welded stud connectors. Structural Engineering, 47(1), pp. 29-40, 1969.

11. Slutter, R.G., and Driscoll, G.C. "Flexural Strength of Steel-Concrete Beams". American Society of Civil Engineers, Journal of the Structural Division, Vol. 91, No. ST2, April 1965. pp. 71-99.
12. Roberts, W.S., and Heywood, R.J., "Development and Testing of a New Shear Connector for Steel Concrete Composite Bridges". Proceedings, Fourth International Bridge Engineering Conference, 1994, pp. 137-145.
13. Standard Specification for Highway Bridges, American Association of State Highway and Transportation Officials (AASHTO), Sixteenth Edition, Washington, D.C., 1996.
14. Siess, C.P., Newmark, N.M., and Viest, I.M., "Small Scale Tests of Shear Connectors and Composite T-Beams". Studies of Slab and Beam Highway Bridges, Part III. University of Illinois Bulletin, Vol. 49, No. 45, Bulletin Series No. 396, February 1952.
15. Ollgard, Jorgan G., The Strength of Stud Shear Connectors in Normal and Lightweight Concrete. M.S. Thesis, Lehigh University, Bethlehem, Pennsylvania, 1970.
16. Jaeger, L.G., and Bakht, B., Bridge Analysis by Microcomputer. McGraw-Hill, New York, 1989.
17. ANSYS User's Manual for Revision 5.1. Swanson Analysis Systems, Inc., Houston, PA, 1992.
18. Yan, L.C.P., Design of Composite Steel-Concrete Structures, London: Surrey University Press, 1981.